Anni Cao

FSI Analysis of Abnormal Wave Slamming Events

Master's thesis in Marine Technology
Supervisor: Jørgen Amdahl, Zhaolong Yu, Bjørn Christian Abrahamsen
July 2020

Master's thesis

NTNU
Norwegian University of
Science and Technology

Anni Cao

FSI Analysis of Abnormal Wave Slamming Events

Master's thesis in Marine Technology
Supervisor: Jørgen Amdahl, Zhaolong Yu, Bjørn Christian Abrahamsen
July 2020

Norwegian University of Science and Technology
Faculty of Engineering
Department of Marine Technology

NTNU
Norwegian University of
Science and Technology

MASTER THESIS 2020

For

Stud. Anni Cao

FSI Analysis of Abnormal Wave Slamming Events

Koplet væske-konstruksjonsresponsanalyse av abnormale bølgeslagshendelser

Background:

Following the COSL Innovator accident on the 30th of December 2015, the current industry practises for calculating air gaps and slamming loads on deck box in the case of negative air gap have been put under review. Platforms with negative air gap, i.e. the distance between wave crest and bottom of steel, may experience large loads due to wave impacts. Common practise is to use linear diffraction analysis combined with model tests in order to determine the loads.

Recent model tests have revealed that also the impact loads on the columns from breaking, or near breaking, waves are significant and possible considerably higher than what is indicated in the relevant rules and regulations. The loads are characterized by short durations, large spatial variations and high values, which put the measurement system at a considerable stress. Further, the interpretation of the test results is challenging for several reasons: - Froude scaling may not be appropriate - Large fluctuations in the measurements may indicate a dynamic load (possibly entrapped air), or unforeseen dynamic responses in the measurement system - The statistical distributions of the extreme loads are not well behaved or do possibly not follow a Gumbel distribution - The measurement systems used in experiments have so far have only been representative for and elastic structural response with small deformations. Are they also relevant for abnormal slamming actions, where the response will be elasto-plastic with large

deformations? In spite of the challenges above, the model test results are at this stage the best there is. Currently there is a push from both the industry and the academia to resolve the uncertainties, but it is likely that any results will not be available in the short term.

Traditional design, accompanied with traditional analyses, will not be sufficient to prove that the semi columns will be able to withstand the measured wave impact loads. As such, the work should focus on local structural integrity/capacity of the column designs for a semi-submersible subject to slamming loads from breaking waves. Non-linear structural analyses shall be performed in order to investigate the structural capacity for different slamming loads with different horizontal and vertical extent, duration and slamming pressure. Variations to the global design (column width, square vs. round), as well as local design (girder spacing, plate thickness etc) may be studied.

The purpose of the project thesis is to investigate the theory and established engineering practise for how to conduct dynamic response of a stiffened plated vertical surface on a floating platform and to familiarize with nonlinear finite element analysis the response to slamming loads.

The aim of the project and master thesis work is to obtain more knowledge of the fluid structure interaction (FSI) during slamming through the detailed study of drop test, where the structure impacts a calm free surface. The structure can be a cylindrical structure with a circular cross section. This is a relevant structural shape for many offshore structures. One option is to study these simplified problems using commercial FSI softwares like LS-Dyna. The student may then carry out heavy fluid structure interaction calculations (FSI) using super computers.

The present master theses will be written in connection with the SLADE project, which is a 4 year joint SINTEF Ocean and NTNU project. The student will hence be part of a project which is ongoing. This means that the student will get supervision and input from NTNU and SINTEF Ocean.

The project work is proposed carried out in the following steps:

1. Establish a finite element model of the column of a semi-submerisble platform for slamming analysis with LS-DYNA. The extent of the model that is needed to get satisfactory results shall be discussed taking into consideration the size of the slamming exposed area. Describe the choice of boundary conditions based on evaluation how they represent physical conditions. The

finite elment model should preferably be parameterized, allowing for changing plate thicknesses, stiffener size and spacing, frame spacing, size of free girders or bulkhead representation in column top.

2. Perform nonlinear analysis of the column based on given pressure time histories that may vary spatially. Document the development an degree of plastic deformations, and modify the structure if needed.

3. Compare results from nonlinear analysis with SDOF analysis based on ideelized equivalent displacement fields. Bigg's charts with triangular pressure pulses may be employed, alternatively numerical analysis with more arbitrary pressure-time histories and resistance functions may be adopted.

4. Conduct ALE analysis of drop tests with the same finite element model. Compare the results with those obtained with pressure time histories. Compare the pressure-time histories and explain the differences. Compare results from ALE analysis with those based on plastic theory.

5. If possible and time allows, conduct nonlinear analysis with pressure based on CFD analysis where fluid structure interaction is taken into account.

6. Conclusions and recommendations for further work.

Yu, Zhaolong; Amdahl, Jørgen; Greco, Marilena; Xu, Hui-li.(2019) Hydro-plastic response of beams and stiffened panels subjected to extreme water slamming at small impact angles, Part I: An analytical solution. Marine Structures 2019 ;Volum 65. pp 53-74, , Part II: Numerical verification and analysis. pp. 114-133

Literature studies of specific topics relevant to the thesis work may be included.

The work scope may prove to be larger than initially anticipated. Subject to approval from the supervisor, topics may be deleted from the list above or reduced in extent.

In the thesis the candidate shall present his personal contribution to the resolution of problems within the scope of the thesis work.

Theories and conclusions should be based on mathematical derivations and/or logic reasoning identifying the various steps in the deduction.

The candidate should utilise the existing possibilities for obtaining relevant literature.

The thesis should be organised in a rational manner to give a clear exposition of results, assessments, and conclusions. The text should be brief and to the point, with a clear language. Telegraphic language should be avoided.

The thesis shall contain the following elements: A text defining the scope, preface, list of contents, summary, main body of thesis, conclusions with recommendations for further work, list of symbols and acronyms, references and (optional) appendices. All figures, tables and equations shall be numerated.

The supervisor may require that the candidate, in an early stage of the work, presents a written plan for the completion of the work. The plan should include a budget for the use of computer and laboratory resources, which will be charged to the department. Overruns shall be reported to the supervisor.

The original contribution of the candidate and material taken from other sources shall be clearly defined. Work from other sources shall be properly referenced using an acknowledged referencing system.

The report shall be submitted in two copies: - Signed by the candidate - The text defining the scope included - In bound volume(s) - Drawings and/or computer prints which cannot be bound should be organised in a separate folder.

Supervisor: Prof. Jørgen Amdahl Postdoc Zhaolong Yu

Co-supervisor SINTEF OCEANS: Bjørn Christian Abrahamsen

Deadline: June, 2020

Trondheim, January 15, 20120

Jørgen Amdahl

Preface

The following work is a master thesis in marine structures as a part of the MSc in Marine Technology at NTNU during the spring semester of 2020, which continues the work of the project thesis on the same topic written during the autumn semester in 2019.

The present master thesis is written in connection with SLADE project with Sintef Ocean: Slamming Loads in Structural Design Project. Almost all work-related with this thesis is the numerical calculation which gives me an excellent opportunity to get familiar with FEM and other numerical methods. The topic is fascinating. From the modelling to the simulation, great efforts are paid into it. Even sometimes many problems would occur like the problem of extremely high pressure. Keep calculating, and there is always a way to find the reason. Especially when the calculating results have consistent trends or values with the analytical model in other papers, these kinds of things encourage me to dive deeper into this thesis.

Trondheim 20.06.2020

Anni Cao

Anni Cao

Acknowledgement

Abstract

Slamming impact is a hazardous phenomenon to ships and offshore structures, which is characterised by a highly nonlinear coupling interaction between the structure and the fluid. To evaluate it correctly and accurately is a fundamental task for marine engineers. There are several methods to simulate this phenomenon. One is the model test by experiments. But the disadvantage of the experiment is expensive and time-consuming, which makes the model test more challenging to handle in daily time. Other methods alternatively, like simplified calculation and numerical calculation in commercial codes also have their advantages and disadvantages. However, compared to the experiments, these methods could be convenient to access for the engineer.

As the development of commercial software these years, some representative software, e.g. LS-Dyna, ADyna could already give more accurate results than before. The solver could use less time to solve the problems with complex geometry. In this report, the slamming impact has been modelled as drop tests of a stiffened plate with a constant velocity. The drop tests were simulated in the finite element software LS-Dyna, where the fluid-structure interaction was modelled by ALE formulation. The primary purpose of this thesis is to explore the slamming phenomenon in numerical way, experience the procedure to proofread the structure and calculate the response under the slamming loads and find a more convenient method to approximate the impact response.

In this thesis, the steel column model is established first. For the FEM model in LS-Dyna, static analysis is conducted following. The boundary effects on the resistance curve of the steel column would be analysed. It is proved that the rear end boundary conditions does not affect the resistance curve of the steel column. Different resistance curves are plotted in models with different plate thickness. SDOF parameters could be found from these plots. In ALE drop test, the detailed process of slamming events have been analysed. The displacement curve shows excellent consistency with the analytical model. From the section plots in the Appendix, the stiffeners deform first and the bulkhead following, the side plate girders give the plate and stiffeners robust support and almost unreformed during the whole impact process. Three groups of parametric study have been made to evaluate the effect of material properties, velocities, and plate thickness on the response of the structures. SDOF method has also been established by using the parameters from static analysis. Comparison between the SDOF method and ALE methods shows a feasible approximation by using the SDOF method to predict ALE

results. Finally, dynamic tests are made trying to find the possibility to use the elastic material result to predict the response of elasto-plastic material. Even though the effect is not impressive, it provides a new way of thinking.

Nomenclature

Abbreviations and symbols:

ULS	Ultimate limit state	β	Impact angle
ALS	Accidental limit state	σ_y	Yield stress
RP	Recommended practice	ξ	Non-dimensional hydroelasticity parameter
FE	Finite element	EI	Bending stiffness
FEM	Finite element method	F_{max}	Equivalent load amplitude of specific shape pulse
SDOF	Single degree of freedom	k_1	Elastic stiffness
MDOF	Multiple degree of freedom	M_p	Plastic moment capacity in pure bending
DLF	Dynamic load factor	K, np	Power-law model parameters
EOS	Equation of state	R_0, R_{el}	Plastic collapse load in pure bending
FSI	Fluid structure interaction	T_n	Eigen period
OTG	Offshore technical guidelines	t_d	Duration of the impact
E	Young's modulus	V	Impact velocity
PR	Poisson's ratio	c, p	Strain rate hardening parameters

Contents

List of Figures

List of Tables

1 Introduction

1.1 Background

The common practice to predict loads of the slamming events is to use the linear diffraction analysis combined with the model tests. This practice starts to use since the COSL Innovator accident on the 30th of December 2015. However, recent model tests revealed the common practice is not conservative in the load prediction. Traditional linear structural analysis is proved to be not sufficient to evaluate the slamming load. Because the slamming phenomenon is a fully non-linear problem, which is characterised with extremely high peak pressure and low duration of the impact process. In that situation, the non-linear structural analysis shall be applied to predict if the structure has enough integrity and capacity to withstand the slamming loads. Even if the most reliable methods in this domain is still the model tests, the numerical calculation could also be performed to prove the results from the experiment. Furthermore, different from the experiment method, the numerical methods are very flexible to change the information in the models and to modify the geometry. And one of the numerical method, the ALE method is famous for the ability to evaluate the response in the Fluid structural interaction process. For this reason, several drop tests are conducted in this thesis in order to study the slamming phenomenon in detail.

1.2 Objectives

The thesis focuses mainly on the modelling of the steel column and numerical calculation to predict the dynamic response. The simulations are grouped into three parts by using different method. The static part, ALE drop test part, and the dynamic parts. The main purpose of this thesis is to explore the slamming phenomenon in numerical way, experience the procedure to proofread the structure and calculate the response under the slamming loads and find a more convenient method to approximate the impact response for elasto-plastic material. The objectives in detail are introduced following:

1. Discuss the boundary condition of the steel column.

2. Obtain the resistance curve of the steel column.

3. Obtain the SDOF parameters from the resistance curve.

4. Analyse the process of the impact process in detail.

5. A Parametric study to evaluate the effect of different parameters on the structural response in ALE drop tests.

6. A comparison study of the structural response between the SDOF method and ALE method.

7. Calculate the dynamic response of the structure under the pressure variation load from ALE drop tests.

8. Analyse the possibility to use the dynamic results under the impulse from ALE elastic drop tests to approximate ALE elasto-plastic drop test results.

1.3 Literature Review

In 1929, Von Kármán [9], for the first time, raised the formula for the process of water entry. A 2D wedge model was established in the derivation. After three years, Wagner [10] tried to solve the slamming problem analytically in both inner and outer domain for the same 2D model. From then on, the water entry phenomenon opened the window for the simplified analytical 2D model. More and more researchers recognised the water entry event might become a severe problem to the structure with the increasing of the entry velocity. Also, the pressure around the object would change with different structure geometry. The two-way interaction between the structure and fluid was noticed in the 90s. This strong interaction can not be neglected when discussing the response of the structure. Researches start to develop in hydroelasticity problem, included Faltinsen. In 1999, the hydroelastic orthotropic plate theory for a stiffened plate was used to discuss the water entry events [11].

After 2000, the invention of the computer changes the methods of scientific calculation. The numerical calculation was developed. The different numerical method started to be established by the researchers. The advantage for the numerical calculation is the repeatability of the test and the simulation for the model with a significant dimension. The arbitrary Lagrangian-Eulerian

method is one of the most famous methods for calculating FSI problems.

Before the numerical methods, engineers had started to establish the rules and guidelines in the design. Until now, there is a sound system in the guidelines regarding both the design procedure and the numerical simulations. [3] and [12] shows several simplified methods to calculate the response of structures in the extreme situation by hand calculation by cheeking the charts and the tables. The technical guidelines in OTG-14 [13] provides guidelines for calculation of impact loads for ULS design of vertical structures. The report includes guidelines for estimation of the design pressure and guidelines for how large critical horizontal impact loads that must be considered in the design. The OTG only addresses ULS design condition, which means that the guidelines consider the elastic structural response of waves with an annual probability of 10^{-2}.

With the full development of the numerical methods, more researchers come back to the analytical model and try to find the formula behind the phenomenon. In 2019, zhaolong Y. derived the analytical model to describe the response of the stiffened plate in extreme water slamming events [8].

1.4   Limitations of the Report

At the beginning of the master thesis, the steel column needs to be modelled parametrized, allowing for changing the dimension of all the components. Due to different software has been used in the modelling process and the dimension of model is so huge, it is hard to change the geometry of the components, e.g. the stiffener and girder size when it has been generated in the FEM model. So it was decided not to build a parameterized FEM steel column. Nevertheless, the thickness of each component of the model could still be changed. Non-linear analysis based on CFD analysis was also decided not to perform due to the time limit. However, many topics out of the tasks have investigated, e.g. A parametric study of the ALE tests, using fourth-order Runge-Kutta integration methods to calculate the response under the equivalent load, and Calculating the dynamic response of the structure under the pressure variation load from ALE drop tests.

1.5   Structure of the Report

The thesis is structured as:

- Chapter 2 Theories behind the calculation is introduced.
- Chapter 3 Methods including the modelling information, material types, calculation methods, and the used keywords in LS-Dyna are presented.
- Chapter 4 Four parts results (static analysis, ALE drop tests, dynamic analysis and SDOF response calculation) are illustrated with tables and figures.
- Chapter 5 Discussion of the report.
- Chapter 6 Conclusion of the report.

2 Theory

In this chapter, the different theories behind the calculation are demonstrated. The whole theory part would be divided into three sections to introduce. The first part gives a small review of the wave theory. Following this, the characteristic of slamming phenomenon would be introduced. After that, a summary of structural analysis is provided . Simplified method and analytical model would also be explained. Finally, the theory of LS-Dyna offers the basis for the software.

2.1 Wave Theory

2.1.1 Perturbation Method

Wave-body interaction problem is always a challenging thing for marine technology researchers to deal with more accurately. In order to solve this problem in a more accessible scheme, in both [14] and [1], perturbation method is brought out. For a typical wave-body interaction problem, nonlinearities could be depicted by using the parameter ϵ which is small enough to make this method valid in both the expression of the velocity potential (eq: 2.1) and the wave elevation (eq: 2.2). Then these two crucial variables can be expanded into several sub-terms. More terms are involved in the analysis; more accurate results could be accessed.

$$\phi = \tilde{\phi}_1 \epsilon + \tilde{\phi}_2 \epsilon^2 + \tilde{\phi}_3 \epsilon^3 + ... \tag{2.1}$$

$$\zeta = \tilde{\zeta}_1 \epsilon + \tilde{\zeta}_2 \epsilon^2 + \tilde{\zeta}_3 \epsilon^3 + ... \tag{2.2}$$

When the target frequency is wave-frequency, this wave-body interaction problem could be simplified by the using linearisation assumption. All the expression above should be abridged and reserve only the first term on the right-hand side. By the linear assumption, the response (output) will be proportional to the excitation (input). Even though the slamming phenomenon is a kind of problem with higher non-linearities, we can still make a linear assumption in some specific situations.

2.1.2 Linear Wave Theory

By using linear theory, equation (eq: 2.3) gives the velocity potential solution when wave propagates in the positive x-direction with finite water depth h. Note that $\omega^2 = gk \tanh(kh)$.

$$\phi = \zeta_a \frac{g}{\omega} \frac{\cosh\big(k(h+z)\big)}{\cosh(kh)} cos(\omega t - kx) \tag{2.3}$$

After knowing the velocity potential, the hydrodynamic pressure (eq: 2.6) around the body surface could be calculated in order to capture the hydrodynamic force. Moreover, the wave velocity components in the x and z direction (eq: 2.4, 2.5) could be adopted as a velocity input in the impact simulation with different wave impact direction, e.g. ALE test.

$$u = \zeta_a \omega \frac{\cosh\big(k(h+z)\big)}{\sinh(kh)} \sin(\omega t - kx) \tag{2.4}$$

$$w = \zeta_a \omega \frac{\sinh\big(k(h+z)\big)}{\sinh(kh)} \cos(\omega t - kx) \tag{2.5}$$

$$P_{dynamic} = \rho g \zeta_a \frac{\cosh\big(k(h+z)\big)}{\cosh(kh)} \sin(\omega t - kx) \tag{2.6}$$

2.2 Slamming Phenomenon

2.2.1 Characteristic of Slamming Phenomenon

The slamming phenomenon is referred to as the liquid impact on the structures with high nonlinearity. It will lead to a significant effect on structural integrity, fatigue strength, operations. Furthermore, it could also arouse other dangerous events like sloshing and whipping, which are introduced in [2]. Even so, slamming is a localized phenomenon as well, which highly depends on the local geometry, kinematic and dynamic conditions around the impact region. In general, two kinds of domain around the impact region of slamming phenomenon are offered in figure 2.1. One is called the jet domain or outer domain, which has a small effect on slamming load. The other is named as the spray domain, or inner domain. In this domain, pressure varies

notably in space as well as in short time duration (e.g. the order of milliseconds). It may cause a tremendous crooked free surface shape which is hard to track. Sometimes, a little bit perturbation on the boundary or initial condition will give rise to an enormous slamming pressure change. Given this reason, slamming is a localized, transient, irregular and sensitive phenomenon with a significant effect on structures.
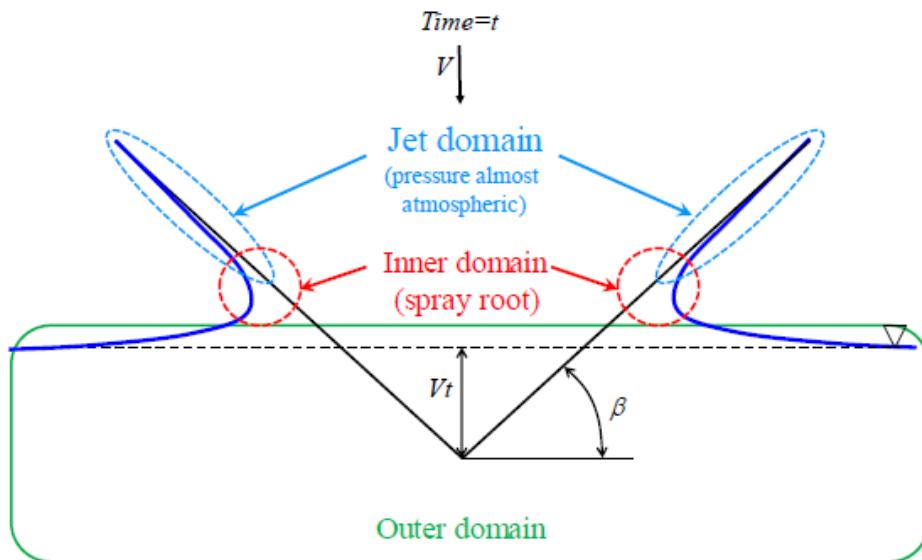
Figure 2.1: Introduction of domain in slamming (Referenced from [1])

In 1932, wagner solved this slamming problem in both inner and outer domain for a 2D blunt body in [10]. From his solution, two parameters (initial conditions) below are crucial for slamming load:

1. Relative impact angle (β)

2. Relative impact velocity(V)

In short, the smaller impact will bring about higher peak pressure locally; this kind of impact could be named as blunt impact. Also, more significant impact velocity will cause severer consequence on structures. In fact, the most significant pressure to the structure is not the peak pressure but the following steady pressure following. Because in the dynamic analysis of the structure, the most decisive parameter is not the pressure value itself, but the integration of the pressure series with time, in other words, impulse.

2.2.2 Analytical Model of Slamming Phenomenon

For the purpose to obtain the slamming load on the structure, the pressure is the primary thing that needs to be known. Usually, fluid pressure could be calculated by (eq: 2.7).

$$P = -\rho g z - \rho \frac{\partial \phi}{\partial t} - \frac{1}{2}\rho |\nabla \phi|^2 \tag{2.7}$$

According to [14], the pressure equation of slamming could be simplified as (eq: 2.8) due to the variations in time are far greater than that in space:

$$P \approx -\rho \frac{\partial \phi}{\partial t} \tag{2.8}$$

In the boundary value problem, the Laplace equation needs to be solved with three boundary conditions: Free surface boundary condition, far-field condition and body boundary condition. On the free surface of the fluid, the pressure is equal to the atmospheric pressure, which means the velocity potential variation against time should be equal to zero. Only $\omega \to \infty$ could satisfy this condition. That means slamming phenomenon cannot generate the wave. Damping is not such essential when dealing with the slamming problem.

When the structure could be simplified by an equivalent flat-plate. The corresponding velocity potential (eq: 2.9) on the body is found by Newman in [15]. $c(t)$ and V is the half-length of the wetted plate and the impact velocity at the time t respectively.

$$\phi = -V\sqrt{c(t)^2 - x^2} \qquad |x| < c(t) \tag{2.9}$$

The vertical velocity on the free surface can be accessed by calculating the partial derivative of the velocity potential with respect to variable z in equation (eq: 2.10).

$$\frac{\partial \phi}{\partial z} = V|x|/\sqrt{x^2 - c(t)^2} - V \quad z = 0, x < -c(t) \quad and \quad x > c(t) \tag{2.10}$$

In line with the equation (eq: 2.8), the hydrodynamic pressure can be derived in (eq: 2.11).The

hydrodynamic pressure could be divided into two parts. One is from the variation of wetted surface, and the other is from the change of the velocity. The last term is also named by added mass pressure due to this pressure is proportional to the acceleration of the impact.

$$P \approx -\rho\frac{\partial \phi}{\partial t} = \rho V \frac{c}{\sqrt{c^2 - x^2}}\frac{dc}{dt} + \rho\frac{dV_r}{dt}\sqrt{c^2 - x^2} \qquad (2.11)$$

By integrating the pressure along the body wetted surface, the vertical force could be gained:

$$F = -\int_{-c}^{c} pn_3 dx \qquad (2.12)$$

2.2.3 Slamming Induced Physical Phenomenon

The slamming can cause several physical phenomena based on the book [2]. In figure 2.2, there are several stages to describe slamming:
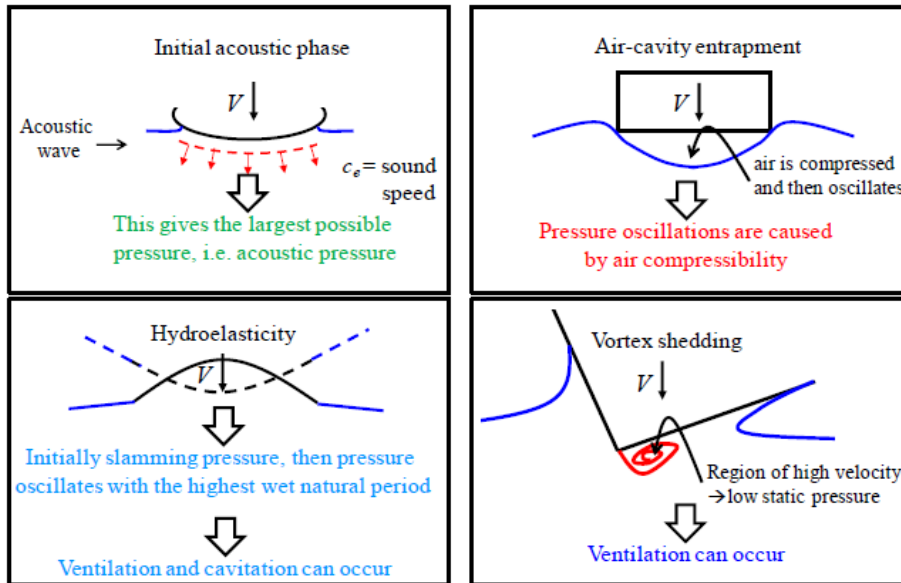
Figure 2.2: Stages of slamming(Referenced from [2])

The first stage is the acoustic phase; in that stage, the acoustic wave will develop with the sound speed, the peak pressure in (eq: 2.13) will be given, where c_s is the sound speed, ρ_w is the water density and V_0 is the initial impact velocity. The similar pressure plot could be seen in the simulation. In that stage, the pressure is tough to capture exactly in both numerical

9

method and the experimental method. After the stage, oscillated air will generate an air pocket around the free surface. The cushioning effect will reduce the pressure on the structure. The last stage, pressure on the structure will oscillate with the highest wet natural period [14]. The coupling effect (Hydroelasticity effect) will rise between the fluid and structure.

$$p_a = \rho_w V_0 c_s \tag{2.13}$$

However, the coupling effect does not need to be considered all the time. A non-dimensional parameter ξ will be introduced to judge if the hydroelasticity effect will be crucial to the slamming phenomenon in [11], which is $tan\beta$ divided by the non-dimensional velocity. Specifically, hydroelasticity occurs when $\xi < 0.25$. If hydroelasticity is excited, the hydrodynamic problem and the structural problem should be considered together, which need a solver to transfer the data between hydrodynamic and structural analysis. If the hydroelasticity is not excited, the quasi-static approach could be used. The structure would be assumed to be a rigid body.

$$\xi = tan\beta/[V(\rho L^3/EI)^{1/2}] \tag{2.14}$$

2.3 Structural Analysis

2.3.1 Material Behavior

Slamming is an accidental phenomenon in the marine technology field, which means the deformation will extend to the elastic-plastic or pure plastic range. Once the structure enters into the plastic domain, a portion of deformation can not be eliminated even if the loading disappears. The response of ductile material can be described in several stages:

1. Elastic Behaviour

In this stage, small deformation will be assumed. Most elastic materials behave as a linear relation in the strain-stress curve shown in figure 2.3. The linear relationship is called Hooke's law. The slope of this straight line is named as the elastic modulus. In that stage, the elastic strain which is caused by resizing and reshaping the crystalline cells of the lattice [16] would be wiped out when the external load is no longer present.
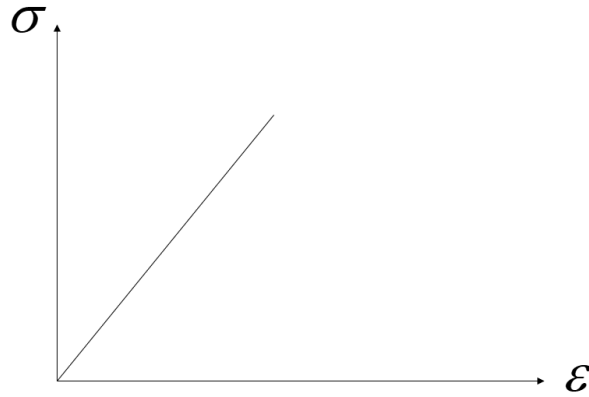
Figure 2.3: Linear behaviour of material

2. Elastic-plastic Behaviour without Much Hardening

After the elastic limit. The material comes into the second stage, which is the elastic-plastic behaviour. In that stage, the material behaves the non-linear relationship between stress and strain. Also, the material may reach a critical level in this stage. This critical level is defined as the yield criterion. According to 2.4, The yield criterion states that when:

$$f = \sigma_R(\sigma_x, ..., \tau_{xy}, ..., \epsilon_x, ..., \gamma_{xy}) - \sigma_Y = 0 \tag{2.15}$$

11
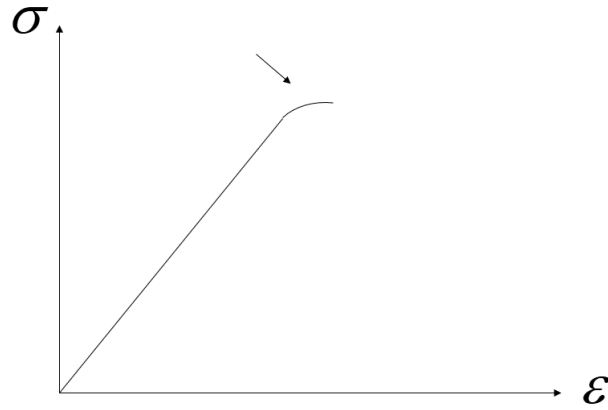
Figure 2.4: Material behaviour without much hardening

In (eq: 2.15), f describes a surface, which is called the yield surface. σ_R is called the reference stress. Stress points on a surface represent the stress state at the yield limit. This surface is a general expression, which can be used in both the perfectly plastic material and the hardening situation. The only difference between these is the reference stress of perfectly plastic material depends only on the stress state, while the reference stress for material with hardening depends on both the stress and strain state. For the perfectly plastic material, the yield surface is, therefore, a fixed surface in six-dimensional space. It can undergo unlimited plastic deformation when constant reference stress is equal to the yield stress. Outside the yield surface, the stress-strain points can not be reached. Initially, the plastic strain increment should be parallel to the normal direction of the yield surface. Then the plastic deformation starts to occur by this increment.

3. Pure Plastic Behaviour with Plastic Hardening

In figure 2.5, the hardening rule could be referred, which governs the strengthening of this material [17]. In that stage, the yield stress increases with the development of plastic strain. Between the plastic strain and stress, the relation read in (eq: 2.16):

$$\sigma_p = H' \epsilon_p \qquad (2.16)$$

The hardening rule describes how the yielding changes by the historical plastic flow in (eq: 2.17). If the material is not failed, stress-strain points should always be on the yield surface, *df* should
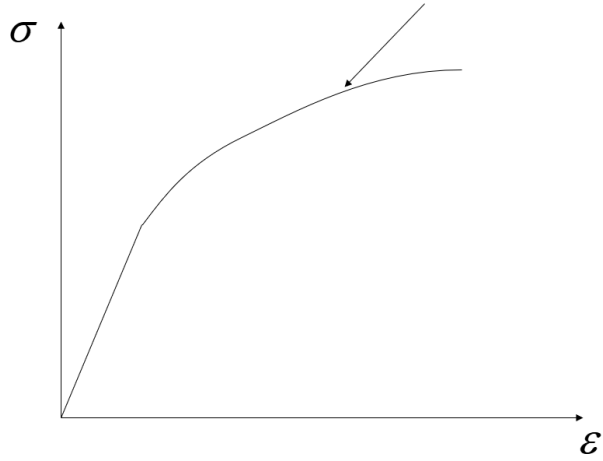
Figure 2.5: Material behaviour with hardening

be zero. Then $\sigma = \sigma_p$

$$df = \frac{\partial f}{\partial \sigma}\partial\sigma - \frac{\partial f}{\partial \epsilon_p}\partial\epsilon_p \tag{2.17}$$

2.3.2 Strain Hardening and Power-Law Model

In [18], true stress σ_{true} and true strain ϵ_{true} curve in the strain hardening part could be defined as the power-law model (eq: 2.18) which is close to the parabolic relation [19]. K and n are the power-law parameters. Theoretically, the true stress and strain have the relation with engineering stress and strain in equations (eq: 2.19, 2.20).

$$\sigma_{true} = K\epsilon_{true}^{np} \tag{2.18}$$

$$\epsilon_{true} = ln(1 + \epsilon_{eng}) \tag{2.19}$$

$$\sigma_{true} = ln(1 + \sigma_{eng}) \tag{2.20}$$

13

2.3.3   Strain Rate Hardening

The slamming phenomenon is famous for its low duration and high peak pressure in the initial stage. This kind of short loading time may cause the strain rate exceeds $0.1[s^{-1}]$. In such high strain rate situation, the strain rate hardening phenomenon will be induced. A model developed by Cowper and Symonds [20] solved this problem by introducing an equation (eq: 2.21) to represent the dynamic stress. Due to the high strain rate, the stress state changes from static type to the dynamic type. In [18], a set of strain rate parameters are provided when there is no information to be refereed. In this parameters, $C = 4000[s^{-1}]$ and $p = 5$ are proposed for steel material in offshore structure.

$$\sigma_{dynamic} = \sigma_{static}[1 + (\frac{\dot{\epsilon}}{C})^{\frac{1}{p}}] \tag{2.21}$$

2.3.4   Static Analysis Method

1. Linear Static Analysis

The linear static analysis is an analysis where the elastic relation between stress and strain holds. In practice, the small deflection would be assumed. The structural stiffness matrix is constant during solving process. The response can be calculated by using the inverse stiffness matrix times the external load. Compared to a non-linear analysis of the same model, the solving process of linear analysis is relatively short. For a continuous system, discretization needs to be done to apply in the solving procedure. This is called the finite element method, which includes four steps.

1. Geometry (CAD model)

2. Material properties

3. Applied loading

4. Boundary conditions

The equation solved by this method in structural analysis is called virtual work method or

principle of virtual displacement method, for example, the beam form PVD reads:

$$\int_0^l \tilde{\epsilon}\sigma A dx = \int_0^l \tilde{u}q dx + \tilde{v}_1 S_1 + \tilde{v}_2 S_2 \tag{2.22}$$

Where $\tilde{\epsilon}, \tilde{u}, \tilde{v}$ is the test strain, field displacement and nodal displacement, which can be described by an assumed polynomial shape function and its derivatives. By using this way, the PVD has a straightforward form:

$$Kr = R \tag{2.23}$$

K represents a constant stiffness matrix of the system in figure 2.3, R is the external load and r is the response that we would like to know. By calculating the inverse of the K matrix by the numerical method in the computer, the solution can be obtained.

2. Non-linear Static Analysis

In [21] and [22], The non-linear analysis is an analysis where a non-linear relation holds between the strain and stress. The non-linear effects can originate from geometrical non-linearity (stiffness change due to the change of structure), material non-linearity and contact non-linearity. In contrast, linear analysis has a constant stiffness matrix, while the non-linear analysis has the stiffness matrix, which is the function of time. Due to the dependence on time, the stiffness matrix would change during the loading increasing. The stiffness in the equation above has relation with time, and the equation will change as:

$$K(t) \cdot r(t) = R(t) \tag{2.24}$$

or

$$K(t) \cdot \Delta r(t) = \Delta R(t) \tag{2.25}$$

Different techniques can handle geometry non-linearity, one is called the Updated Lagrange method, and the other is Total Lagrange method. The difference is that different methods

choose a different reference frame to simulate. For each time point, the stiffness matrix is unique. The solution strategies have several kinds.

1. Incremental or step-wise procedures

2. Iterative procedures

3. Combined methods

2.3.5 Dynamic Analysis Method

In dynamic analysis, equations of motion usually like this:

$$M\ddot{x} + C\dot{x} + Kx = F(t) \tag{2.26}$$

The solution for this equation can be divided by two parts: one is the homogeneous solution which corresponds to the free oscillation solution, the other part is called particular solution, which is induced by the forced oscillation. Free oscillation response depends highly on the initial condition. The solution will be a harmonic oscillation function. While for the forced oscillation, the solution usually is the static response amplified with the DLF factor. The free oscillation would decay by the time elapsed, while the forced oscillation will not. Then there is no need to consider the homogeneous solution. The most significant solution is external load. The load can be divided into a short time load and a long time load.

2.3.6 Dynamic Loading Domain

The response of structure could be classified into three categories according to the relative ratio between the duration of the explosion pressure pulse, t_d and the natural period of the structure, T in [4] and [23].

1. Impulsive domain - $t_d/T < 0.3$

2. Quasi-static domain - $3 < t_d/T$

3. Dynamic domain - $0.3 < t_d/T < 3$

1. Impulsive Domain:

The response is governed by the impulse $I = \int_0^{t_d} F(t)dt$. Structure could resist a very high peak and extremely low duration pressure. The maximum deformation, ω_{max} can be calculated iteratively in (eq: 2.27).

$$\int_0^{t_d} F(t)dt = \sqrt{2m_{eq} \int_0^{\omega_{max}} R(\omega)d\omega} \tag{2.27}$$

Where $R(\omega)$ = force-deformation relationship for the structure m_{eq} = equivalent mass for the structure

2. Quasi-static Domain:

When the rise time is relatively small, the maximum deformation of the component can be solved iteratively from the equation (eq: 2.28):

$$\omega_{max} = \frac{1}{F_{max}} \int_0^{\omega_{max}} R(\omega)d\omega \tag{2.28}$$

When the rise time is large, the maximum deformation could be solved as equation (eq: 2.29).

$$F_{max} = R(\omega_{max}) \tag{2.29}$$

3. Dynamic Domain:

Response in this domain should be solved numerically.

2.3.7 Failure Modes of Stiffened Plate

When the failure occurs, different failure modes on the structure are often the crucial thing that needs to be evaluated. For a stiffened plate, the failure will be demonstrated in various way. In figure 2.6 from [3], there are two main kinds of collapse, one is the beam collapse (stiffener collapse), the other is girder collapse. In both the two main kinds collapse layouts, deformation in remaining supporting structure may be elastic or plastic. SOF analogy can only be used when only one component of the stiffened panel gets failure so that the dynamic interaction between the plate flange and the profile can be neglected.
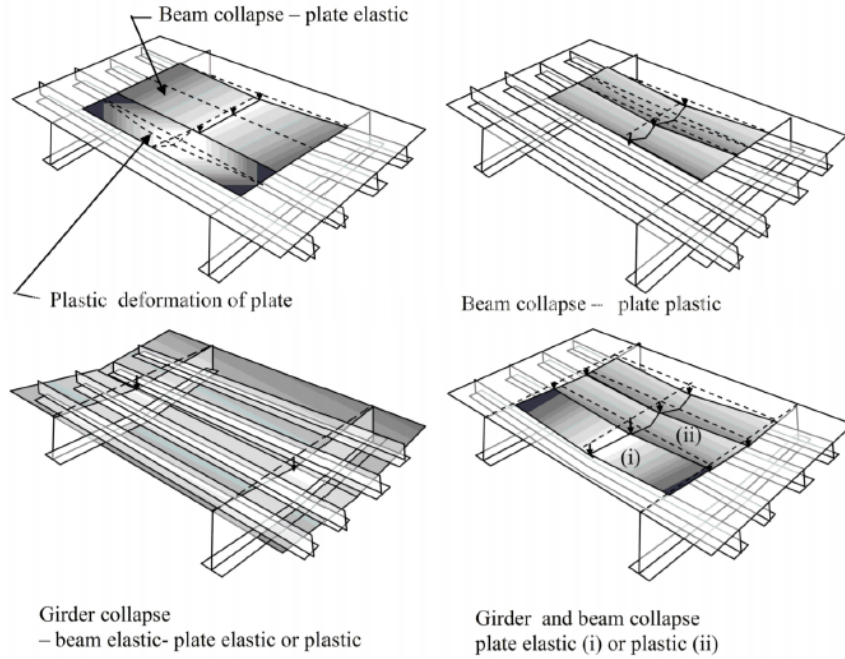
Figure 2.6: Different failure modes of stiffened plate (Referenced from [3])

2.3.8 Resistance Model of the Stiffened Plate in Lateral Loads

Resistance curve of a structure can represent the static response in a developing linear load in both the elastic and plastic range. According to [4] and [3], the plastic resistance curve for the stiffened plate in lateral loads with SDOF analogy is demonstrated in figure 2.7. The different stiffened plate could be simplified by the beam with various dimensions, boundary conditions(c), flexibility(α). In uniform pressure loading, the beam plastic resistance can be represented by the equation (eq: 2.30), where c is a parameter which has the relation with boundary condition ($c_1 = 2$ for clamped beams and $c_1 = 1$ for pinned beams), W_p is the plastic section modulus of the beam which could be calculated by equation (eq: 2.31) in the assumption that plastic neutral axis is close to the web toe of the stiffener, A_s is the area of the stiffener. The axial displacement will affect the generation of membrane force inside the beam under large deformation. The stiffness can be calculated by equation (eq: 2.32).

$$R_0 = \frac{8c_1\sigma_y W_p}{l} \tag{2.30}$$

18

$$W_P = z_g A_s \tag{2.31}$$

$$\frac{1}{k_1} = \frac{1}{k_{node}} + \frac{l}{2EA} \tag{2.32}$$
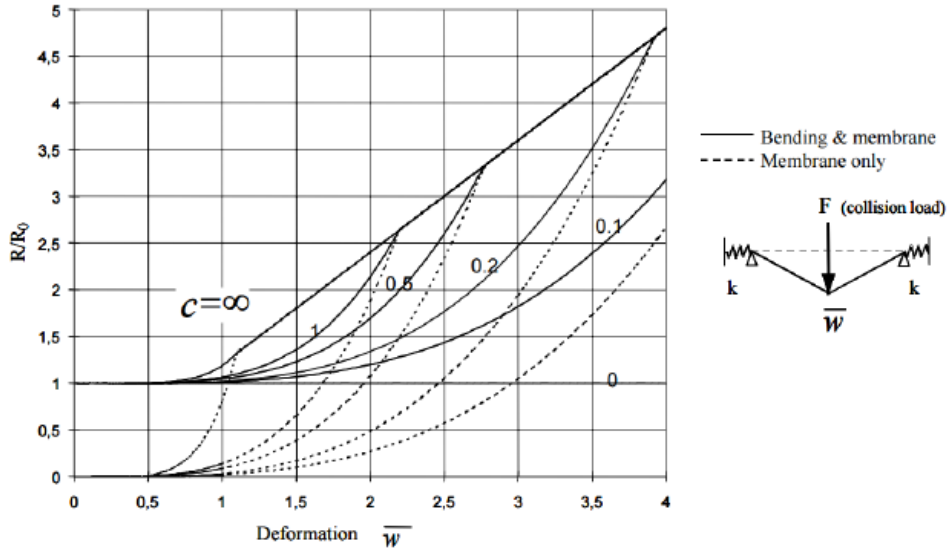
Figure 2.7: Resistance curve (Referenced from [4])

2.3.9 SDOF Analogy

1. SDOF Method in the Guideline

Slamming load, like an explosion load, is characterised by temporal and spatial pressure distribution. Based on the DNV-RP-C204 [3] and NORSOK standard N-004 [4], two methods could be used to calculate the response to the explosion loads. One is the non-linear dynamic finite element analysis, and the other is a simple calculation based on SDOF analogies and elastic-plastic methods of analysis. Simple calculation model would transform the model in reality into a single degree of freedom spring-mass system subjected to an equivalent load pulse employing suitable shape functions for the displacements in the elastic and elastic-plastic range. In order to simplify the problem, the temporal variation of the pressure profile could be assumed to be triangular, the maximum displacement of the structure can be calculated from design charts for the SDOF system as a function of period ratio td/T and load ratio R_{el}/F_{max} in the

figure 2.8.
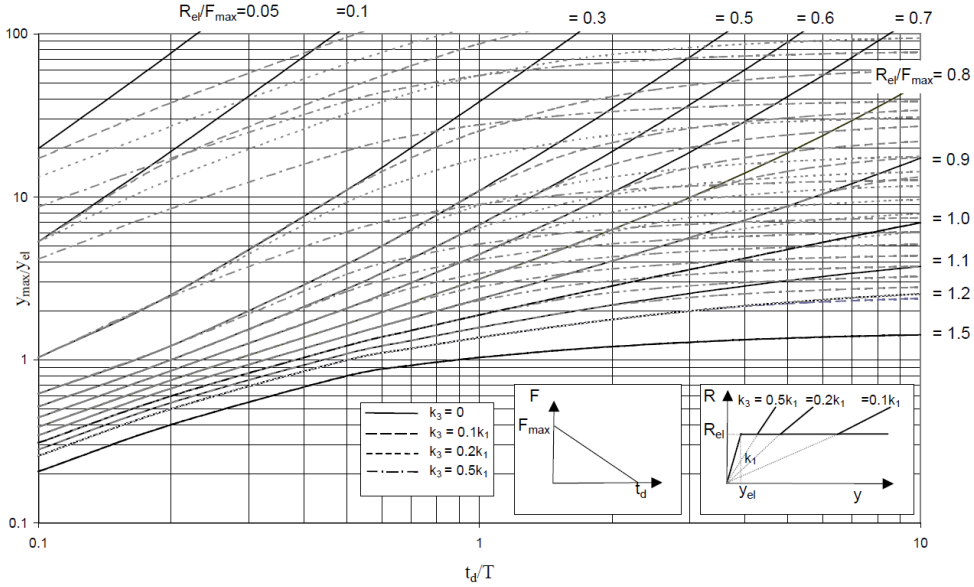
Figure 2.8: Dynamic response of a SDOF system to a triangular load (rise time=0s) (Referenced from [3])

The SDOF system can be established from the modal superposition method of the original continuous system by application of generalised coordinates. The deformation shape $\omega(x,t)$ can be expressed by the time-scaled shape function given in the equation below:

$$\omega(x,t) = \phi(x)Y(t) \tag{2.33}$$

The accuracy of the method depends on how well the shape function $\phi(x)$ is able to describe the actual deformations of the system. A common method for finding a sufficiently accurate shape function is to perform a static analysis with a load pattern comparable to the dynamical one, and then to use the result deformation as a shape function $\phi(x)$. The parameter $Y(t)$ represents the displacement magnitude varying through time. The dynamic equilibrium equation is expressed in a generalised form:

$$\overline{m}\ddot{y} + \overline{k}y = \overline{f}(t) \tag{2.34}$$

20

Generalized mass:

$$\overline{m} = \int_l m\phi(x)^2 dx + \sum_i M_i \phi_i^2 \tag{2.35}$$

Generalized load:

$$\overline{f}(t) = \int_l q(t)\phi(x)dx + \sum_i F_i \phi_i \tag{2.36}$$

2. Fourth-order Runge-Kutta Integration Method

Fourth-order Runge-Kutta method could be used for calculating the response by integration. The meaning of the integration is because the velocity in the dynamic system could be calculated by the integration of the acceleration or external force, and the displacement could be calculated from the velocity as well. By using the integration twice at each time point, the displacement field could be obtained from the load field. In equation (eq: 2.37) , f means the function of this integration which corresponds to the dynamic equilibrium equation of the system. In each time step, the velocity for the next step could be calculated first by using the linear combination of the coefficient k_1 to k_4. Then by using the velocity and the displacement from step now, the displacement for the next time step could be accessed.

$$k1 = hf(x_n, y_n) \tag{2.37}$$
$$k2 = hf(x_n + \frac{h}{2}, y_n + \frac{k_1}{2})$$
$$k3 = hf(x_n + \frac{h}{2}, y_n + \frac{k_2}{2})$$
$$k4 = hf(x_n + h, y_n + k_3)$$
$$y_{n+1} = y_n + \frac{k_1}{6} + \frac{k_2}{3} + \frac{k_3}{3} + \frac{k_4}{6} + O(h^5)$$

3. Eigen Period of the SDOF System

The eigen period for a SDOF system could be calculated by equation (eq: 2.38, where the $\overline{m}$ and $\overline{k}$ are the generalized mass and stiffness of the system).

$$T_n = 2\pi \sqrt{\frac{\overline{m}}{\overline{k}}} \tag{2.38}$$

2.3.10 Added Mass

In the radiation problem, the fluid will be oscillated because of the motion of the immersed structure. The pressure field around the object will change due to the interaction of the fluid and structure. A portion of pressure change has the same phase with the acceleration of the object, which is called added mass term due to it looks like the additional mass of the structure. In dynamic analysis, inertia term is the most important term in the equilibrium, that means added mass can not be negligible in the analysis. In figure 2.9, added mass for a fully submerged rectangular plates could be referred from [3].

The added mass can be calculated by:

$$M_a = C_A M \tag{2.39}$$
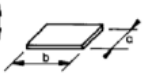
Body shape	Direction of motion	C_A				V_R
Rectangular plates	Vertical	b/a	C_A	b/a	C_A	$\dfrac{\pi}{4} a^2 b$
		1.00	0.579	3.17	0.840	
		1.25	0.642	4.00	0.872	
		1.50	0.690	5.00	0.897	
		1.59	0.704	6.25	0.917	
		2.00	0.757	8.00	0.934	
		2.50	0.801	10.00	0.947	
		3.00	0.830	∞	1.000	

Figure 2.9: Added mass of 2D plate (Referenced from [3])

2.4 Simplified Method

In [8], a simplified method for prediction of large inelastic deformation resistance of stiffened panels subjected to lateral loading is presented. Depending on how much the axial force would occupy the cross-section, the response of the stiffened panel can be classified into four stages.

Stage 1: Tension force in the plate flange only

$$0 \leq \frac{N}{N_p} \leq 2\frac{A_p}{A_e} - 1 \tag{2.40}$$

$$F = \frac{M}{M_p} + (\frac{N}{N_p})^n - 1 = 0 \tag{2.41}$$

Stage 2: Tension force in the plate flange and web

$$2\frac{A_p}{A_e} - 1 \leq \frac{N}{N_p} \leq 1 - 2\frac{A_t}{A_e} \tag{2.42}$$

$$F = \frac{M}{M_p} + \frac{1}{1 + \frac{A_t}{A_w}}(\frac{A_e}{2A_w})^2(\frac{N - N^*}{N_p})^2 - 1 = 0 \tag{2.43}$$

Stage 3: Tension force in the plate flange, web and top flange

$$1 - 2\frac{A_t}{A_e} \leq \frac{N}{N_p} \leq 1 \tag{2.44}$$

$$F = \frac{M}{M_p} + \frac{N - N^{**}}{N_p - N^{**}} - 1 = 0 \tag{2.45}$$

Stage 4: Pure tension force

$$\frac{N}{N_p} = 1 \tag{2.46}$$

In the final stage, only the tension force exist in the cross-section, and the bending moment M

has vanished completely. For each of the stages, with increasing tension force N and decreasing bending moment M, an expression for the plastic interaction function F is deduced. The function F describes the plastic interaction relationship in the cross-section.

2.5 Theory of LS-Dyna

2.5.1 ALE method

FSI problems often require high distortion mesh during the interaction. According to [24], it is crucial to choose a correct formulation of the solid and fluid when the large deflection occurs in simulation. Also, solving the FSI problem needs to deal with the boundaries between the fluid and the structure to make the data transform. The most common descriptions of motions in continuum mechanics are the Lagrangian, Eulerian and Arbitrary Lagrange Eulerian, denoted ALE, formulations.

In the Lagrangian description, the computational mesh follows the material deformation, which is usually used in solid mechanics. One of the benefits of the Lagrangian description is to track of free surfaces and interfaces between different materials conveniently. A significant weakness of the Lagrangian formulation is that the mesh will deform with the material. The Lagrangian method is, therefore, unable to follow substantial distortions of the elements without frequent re-meshing operations, and as a consequence of this, the computation becomes unstable.

In the Eulerian description, which is widely used in fluid mechanics, the computational mesh is fixed, and the continuum moves concerning the grid. The Eulerian formulation can manage significant distortions in the domain, but often at the expense of the precision of the interface and resolution of flow details.

Due to the shortcomings of the Lagrangian or Eulerian formulations, a better method has been invented, which is called in the Arbitrary Lagrangian-Eulerian, ALE, method. According to [25], the ALE method consists of a physical domain that changes with time, i.e. the Lagrangian, and a reference domain that is constant with time, i.e. the Eulerian. The computational grids can move with velocity as a moving reference frame. The mesh inside the domains is allowed to move arbitrarily for the purpose to reduce element distortion. In comparison, the movement of the mesh on the boundaries is to delineate the interfaces between fluid and solid.

In ALE formulation [26], The solid structure is often modelled as a Lagrangian material. The water and air are modelled with the Null material type. The water is represented by a solid material which is allowed to deform into a surrounding void space.

2.5.2 Penalty Algorithm

The coupling forces in LS-Dyna are often calculated based on a penalty method. The penalty algorithms require that the node sets in the FSI problem must either be assigned the role of master or slave. The moving part of the impact problem is assigned as a slave,e.g. the structure, while component in the stationary would be assigned as master in [26]. For an FSI impact problem where a plate hits the water, the nodes in the plate will be slave nodes, while the nodes in the fluid mesh will be assigned the role of master nodes.

2.5.3 EOS

In [26], the help manual provides a introduction of EOS. The EOS (Equation of state) provides the relations between the fluid pressure and the volume change. Only the solid type and a few particular shell element could be applied with EOS. There are two main kinds of type EOS. One is 'Gruneisen EOS', the other is 'Linear Polynomial EOS' whose equation of state is linear in internal energy. They are adapted with two different deformation situations. 'Gruneisen EOS' is good at dealing with the more extensive deformation in the fluid, while the 'Linear Polynomial EOS' can be applied in the relatively small deformation situation.

The pressure for 'Linear Polynomial EOS' is expressed by, where from C_1 to C_6 are the polynomial equation coefficient, E is the internal energy in equation (eq: 2.47).

$$P = C_0 + C_1\mu + C_2\mu^2 + C_3\mu^3 + (C_4 + C_5\mu + C_6\mu^2)E \tag{2.47}$$

The pressure for 'Gruneisen EOS' is given in equation (eq: 2.48), where S_1 to S_3 are non-dimensional coefficients, C represents the bulk sound speed, γ_0 is the unit-less Gruneisen gamma, a is the correction to γ_0:

$$P = \frac{\rho_0 C^2 \mu [1 + (1 - \frac{\gamma_0}{2})\mu - \frac{a}{2}\mu^2]}{[1 - (S_1 - 1)\mu - S_2\frac{\mu^2}{\mu+1} - S_3\frac{\mu^3}{(\mu+1)^2}]^2} + (\gamma_0 + a\mu)E \tag{2.48}$$

3 Method

In this chapter, methods applied in the calculation are investigated in detail. First of all, the analysis model would be illustrated with the dimensions, material types and other considerations. After that, the numerical methods used in the calculation part are also introduced later.

3.1 Modelling

The model of the steel column in this thesis was built based on the information from AkerSolutions company and SINTEF OCEAN in SLADE project. Professor Jørgen Amdahl and post-doc Zhaolong Yu also gave a lot of useful and practical experience with the dimension of the steel column during the modelling. Great efforts were paid in the modelling process so that it takes a relatively important role in the whole thesis except the simulation. The model consists of the stiffened side panel, decks, bulkheads and brackets. The response of this steel column is evaluated for the horizontal slamming wave impacts on the side panel.

3.1.1 Geometry Model

The original model in figure 3.10a of the platform comes from the slides of AkerSolutions which is a semi hull column with four legs in the SLADE project. The outline contour, cross-section plot and the shell expansion plot with water elevation marks are provided. From the outline picture, many engineering equipment could be seen on the first deck. However, the deck is not the most vulnerable area against slamming in the platform due to the high position. When slamming impact occurs, the most critical area of impact focuses on the leg of this semi-submersible platform. Due to all four legs are the same in the platform, only the area of the red circle in figure 3.10a are investigated in this thesis. Figure 3.10b is the cross-section plot of one leg of the platform. In order to save the cost of numerical calculation in the analysis, only the green blocked area in figure 3.10b was modelled in the thesis considering the symmetry property in the cross-section plot. Thus the analysis model contains:

1. Side plate.

2. Stiffeners and girders on the side plate.

3. Bulkheads.

4. Stiffeners and girders on the bulkhead.

5. Decks.

6. Brackets.
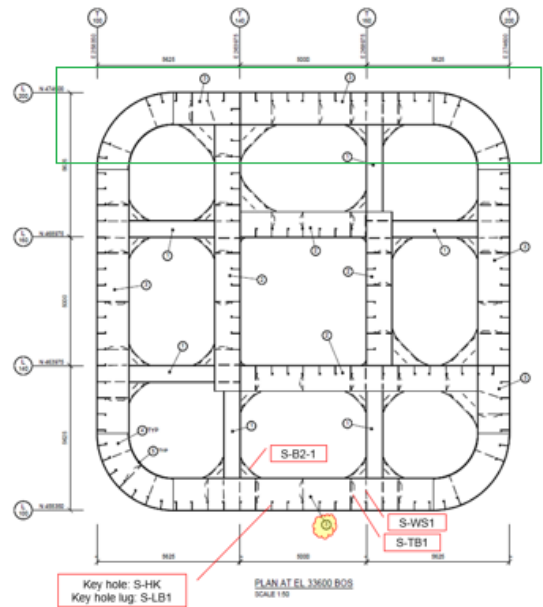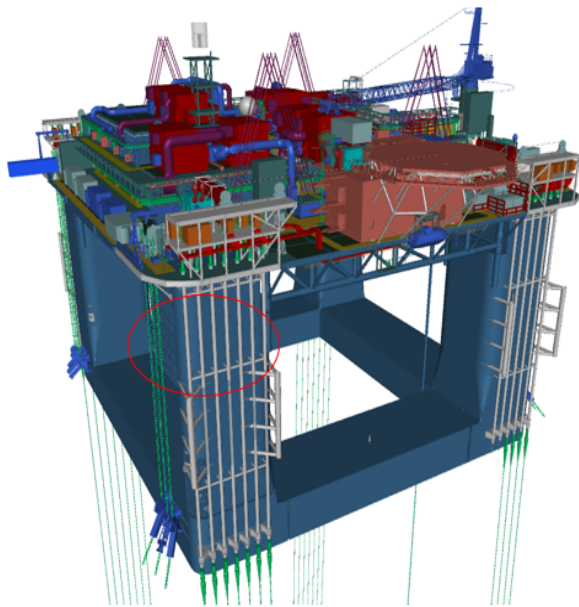
(a) The platform model from AkerSolutions (Referenced from [5])

(b) The cross-section of the platform model AkerSolutions (Referenced from [5])

Figure 3.10: The outline contour and cross-section plot of the platform from AkerSolutions

Along the vertical direction, the analysis model was framed from the top deck (first deck) to the third deck, which is inside the red circle in the figure 3.11. In the figure below, the deck is drawn with the bold red line. There are three decks modelled in the analysis model, one is the top deck around EL.51000mm level, the secondary deck is around EL.31500mm level, and the third one is at EL.20000mm level. The slamming impact area is vertically around the second deck, which is in the middle of the model. The model was built with substantial length in vertical direction because it could provide the deformation and stress state in a broad scope, which could tell more information than a $3 \times 3 m^2$ stiffened plate model in [13].
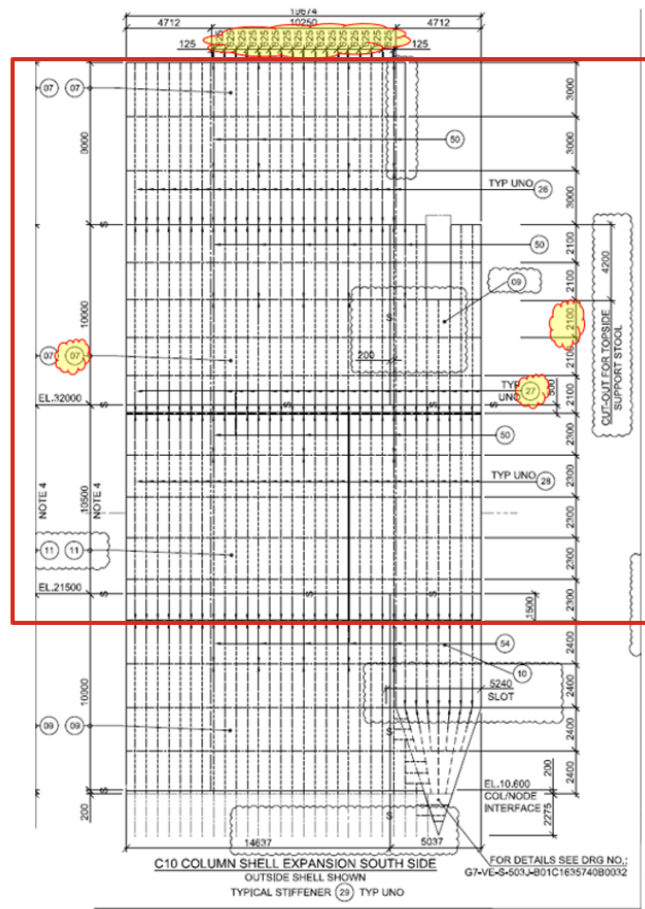
Figure 3.11: The shell expansion plot with water elevation marks (Referenced from [5])

Detailed dimensions of the analysis model could be found below. In order to represent it clearly, different parts with corresponding numbers are illustrated in figure 3.12a. Part number 1 and 5 represent the side plate and bulkhead, respectively, while the deck components are not drawn in this figure. Then those deck components part number in the table 3.1 and 3.2 below use 'NULL'. Part 2, 7 and 8 are referred to the stiffener on the side plate and two bulkheads. There are two kinds of stiffeners in the analysis model, and one is on the straight edge of the side plate, the other is on the curved edge of the side plate. For a different design, each kind may have a different size. Because of this, it is set a different part number for different kinds of stiffeners. Part 3 and 4 are the girder on the two kinds of plates. Part 6 represents the supporting bracket between girders on the side plate and bulkhead.

In table 3.1 and 3.2, dimensions of all components in detail are demonstrated. According to [5], the side plate and the deck plate are assigned with $16mm$ and $12mm$ thickness respectively. The Bulkhead has the same thickness as the side plate. The side plate is relatively more important against the slamming impact than the deck plate. That is the reason why the side plate is thicker than the deck plate. Further, the bulkhead can take the responsibility to give support for the side plate. So it is easy to understand that they share the same thickness. Based on the recommendations from [7], the minimum thickness for the stiffened panel in the offshore structure is $8mm$. The choice of the thickness of the side plate and deck plate could satisfy this requirement. 16mm side plate thickness is a default value. In section 4.2.4, 12mm and 20mm side plate thickness are also chosen to evaluate the effect of side plate thickness in the ALE calculation. All the stiffener in the model except the deck stiffener has the section profile HP260x10. The deck stiffener will be smaller than others, which is HP220x10 in profile. Both of them could meet the requirement of minimal section modulus is around $1.5e^{-5}m^3$. For all HP section, the bulb profile, the stiffener flange has the irregular shape which will add difficulty in modelling and calculation process. For this reason, the bulb profile will be substituted by a rectangular profile. The requirement for this transformation is to ensure the same moment of inertia to both of the profiles.

Table 3.1: Plate components dimensions in detail

Part number	Part	Type	Thickneess
1	Side plate	PL16	16mm(default)/12mm/20mm
NULL	Deck plate	PL12	12mm
5	Bulkhead	PL16	16mm(default)/12mm/20mm

Table 3.2: Other components dimensions in detail

Part number	Part	Type	Web height	Flange width	Web thickness	Flange thickness
2	Side plate stiffener	HP	260mm	37mm	10mm	27.3mm
3	Side plate girder	TGA	1000mm	300mm	16mm	20mm
4	Bulkhead girder	TGA	1000mm	300mm	16mm	20mm
7	Bulkhead stiffener	HP	260mm	37mm	10mm	27.3mm
8	Curved side plate stiffener	HP	260mm	37mm	10mm	27.3mm
6	Bracket	S-B2-1				
NULL	Stiffener on the deck	HP	220mm	20mm	35mm	10mm
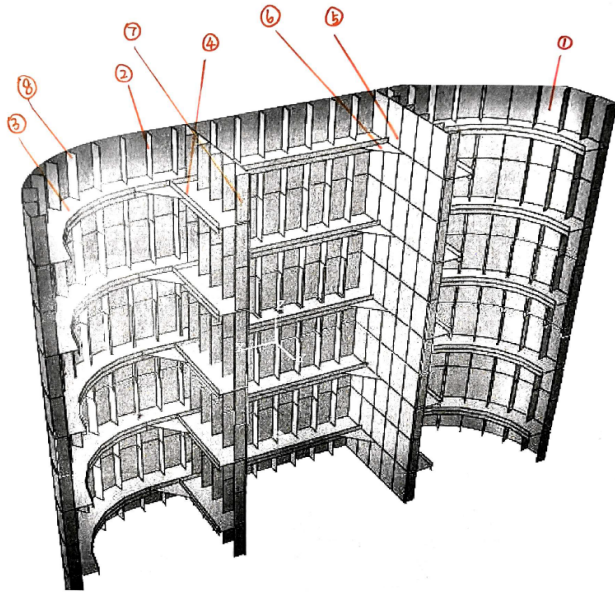
(a) Illustration for the components of the analysis model with part numbers
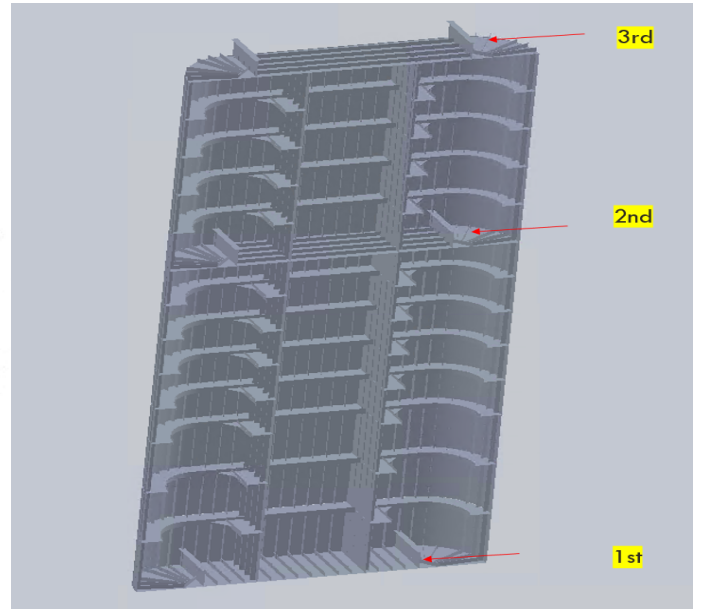
(b) The steel column model built in SolidWorks

Figure 3.12: Illustrations of the geometry model

Whole geometry model was built in software SolidWorks as figure 3.12b shows. Following this, the geometry model in '.iges' format from SolidWorks was imported into ANSYS for the meshing work in the next section. In the SolidWorks geometry model plot, three decks are marked in order. The detailed modelling for the first deck and the decks in the middle are different. The direction of stiffeners on the first deck follows with the short edge of the bulkhead, while the direction of the stiffeners on the second and third deck is perpendicular to the short edge of the bulkhead. They will give the deck and side plate support for a different direction.

3.1.2 FEM Model

For the FEM model of the steel column, all girders are continuous, and stiffeners stop at the girders. Only one intersecting edge between the girder and the stiffener should exist so that the force could be transferred two ways in both components. Meshing work was done in ANSYS-LS-Dyna solver Prepost. Shell element 163 in ANSYS-LS-Dyna solver Prepost was adopted as the element type. The meshing requirement for this structure is at least four elements should be divided along with the stiffener web height (260mm for the side plate stiffener and 220mm for the deck stiffener). Then the local element size for the stiffener and girder should be at most 60mm. Although larger element size could be applied in the side plate and bulkhead, it will lead to the irregular shape of elements on the boundary between components which will give inaccurate results in the following calculation. Given this, 60mm global size per element was chosen to ensure the rectangular shape of each element in the FEM model. In the master thesis [27], convergence test for the drop test of a stiffened plate was done. It is proved that 60mm is a right choice for the element size both in the structure and fluid. The final meshing plot could be seen in figure 3.13a. Keyword file for LS-Dyna with all information of nodes and elements could be outputted directly from ANSYS. The model in LS-Dyna shows in figure 3.13b with the coordinate system. The vertical direction of the steel column is with the y-axis. The deck plane is on the x-z plane. It is easy to construct the fluid element used in ALE calculation in the LS-Dyna directly with the function 'Element Block', which is shown in figure 3.13b with the red block. The element size of the fluid element is the same as the global size of the structural element, 60mm. The dimension of the fluid element block is 9000mm x 9000mm in x and y direction for each kind of fluid (the water and the air). The thickness along z-direction for each of the fluid block has the same width as the bulkhead in the z-direction. Because of the interaction components with the fluid is only the part of the side plate, one bulkhead length of the fluid block in the z-direction is enough for the ALE calculation.
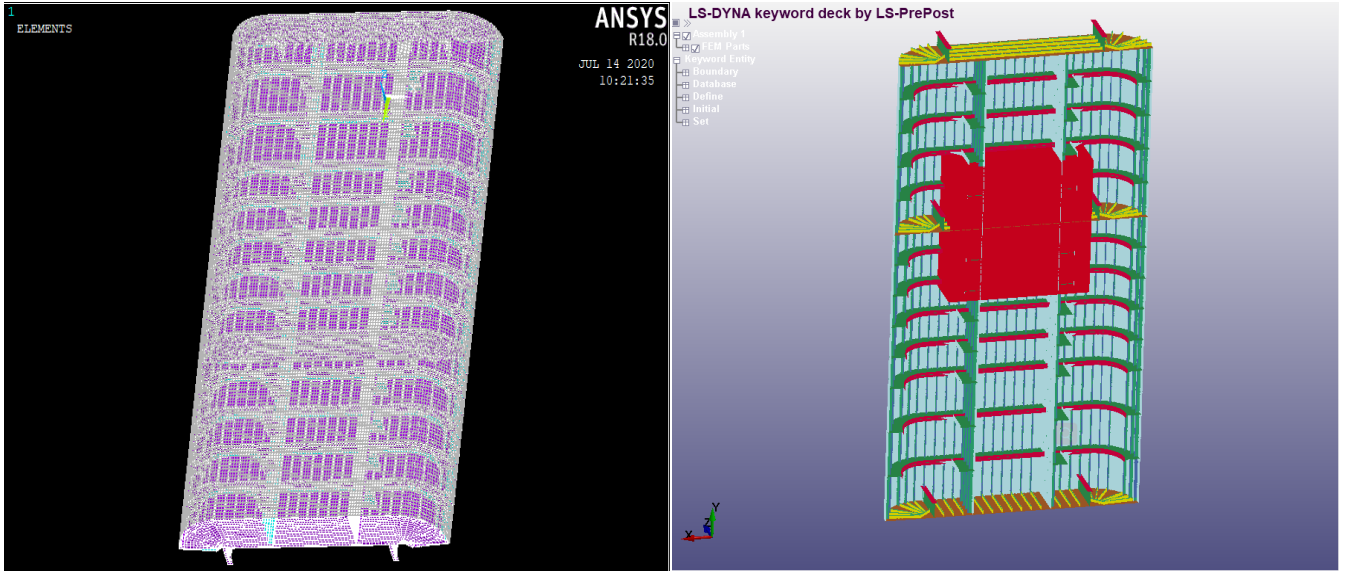
(a) FEM model in ANSYS for meshing work   (b) FEM model in LS-Dyna with fluid element

Figure 3.13: Illustration of the FEM model

Although the SI unit is the most frequent unit system for the analysis to use, it is not convenient for some physical quantity, e.g. pressure in [pa] is a too-small unit for the slamming phenomenon in the figure. For this reason, the unit of the physical quantity in the calculation was chosen as [mm-t-Mpa] system, which is demonstrated in the table 3.3. The advantage for this unit system is that the pressure could be obtained directly in [Mpa] not [pa] in the calculation.

Table 3.3: Physical quantity used in analysis

Physical quantity	Unit
Length	mm
Force	N
Pressure	Mpa
Mass	t
Density	t/mm^3
Time	s

3.2 Material in the Analysis

3.2.1 Mass of the Structure

In LS-Dyna, the fluid will be formed with material NULL, while the structure material could be various. All components in the steel column including the plate, deck plate, all kinds of stiffeners, girders and the brackets are made of S355 steel. The density for S355 is around $7.8e^{-9}t/mm^3$, which gives the total mass of the steel column $187.35t$ with side plate thickness 16mm (section 4.2.4 may change the thickness of the side plate for comparison reason).

Table 3.4: The structural mass data from LS-Dyna

Structure	Total mass in the air
16mm plate	$187.35t$
20mm plate	$212.2\ t$
12mm plate	$162.4\ t$

3.2.2 Elastic Material Formation

The elastic material model in table 3.5 is used in the elastic analysis. In LS-Dyna, keyword *MAT_ELASTIC (001) is applied to input the parameters in the table.

Table 3.5: Elastic material properties

Material	Type	Density	E	PR
1	Elastic	7.8e-9 t/mm^3	2.03e5 Mpa	0.3

3.2.3 Elasto-plastic Material Formation

1. Power-law Parameters Calibration

The engineering stress-strain curve of S355 steel could be found in [6], in figure 3.14. From the stress-strain curve above and the data in [19], calibration for the power law parameter could be made by using the fitting procedure below:

STEP1: Find two points from the engineering strain stress curve (two red dots in figure 3.14. One is the last point in the elastic range (σ_e, ϵ_e), the other is the max stress point (σ_m, ϵ_m). See the table 3.6 below:

STEP2: Use the equation2.19 and 2.20 in theory part to calculate the true stress, true strain from engineering one.
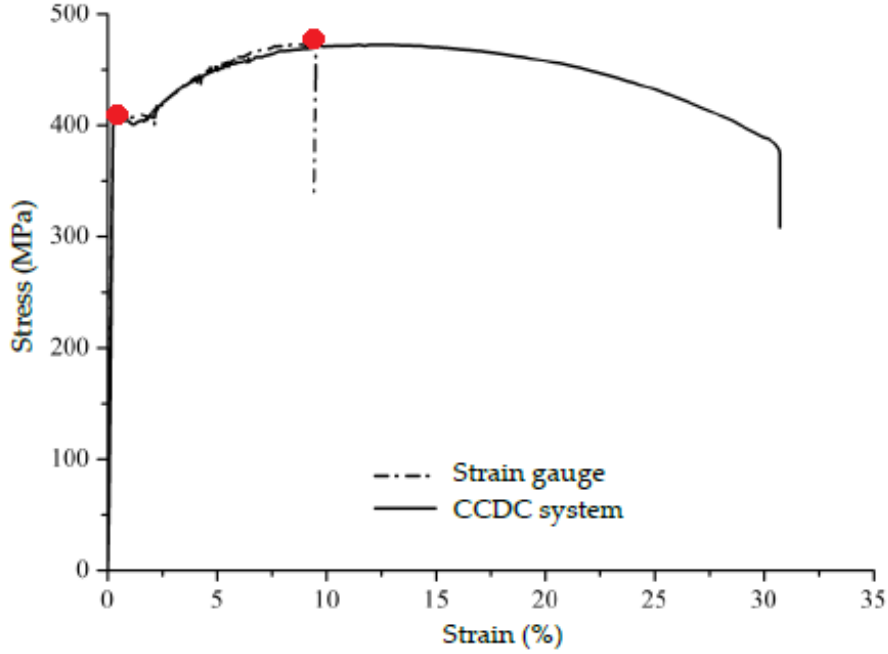
Figure 3.14: Engineering stress strain curve with DIC test (Referenced from [6])

STEP3: Fitting the two sets of true stress, strain data with equation 2.18, then the power-law parameters K, np could be accessed.

Table 3.7 shows the whole calculation results:

Table 3.6: Strain stress data for the sampling point

	Enginnering	True
σ_e	400.5Mpa	401.3Mpa
ϵ_e	0.002	1.998e-3
σ_m	503Mpa	553.2Mpa
ϵ_m	0.107	0.0998

Table 3.7: Fitting results of power law parameters

Material	type	K	np	C	p
2	Elasto-plastic power law model	755.2	0.102	4000 s^{-1}	5
3	Elasto-plastic power law model	755.2	0.102	0	0

2. Material Model from Guidelines

In the guidelines [18] and the paper from [28], several non-linear material model for the S355 are proposed in table 3.8, which is very close to the calculated model above in table 3.7. Material

35

properties from the guideline neglect the strain rate hardening effects. The strain rate hardening parameters in table 3.8 are zero.

Table 3.8: Power law model parameters from other sources

Material	Type	Source	K	np	σ_{yield}	C	p
4	Power law model	Paper [28]	780	0.22	357Mpa	4000 s^{-1}	5
5	Power law model	Guidelines [18]	740	0.166	366.1Mpa	0	0

3. Strain Rate Hardening

In the section 2.3.3, the strain rate hardening has been discussed. Following this, the material model with strain rate hardening in the analysis would use the parameters below which are already occur in table above:

Table 3.9: Strain rate hardening parameters

C	p
4000 s^{-1}	5

3.3 Staic Analysis Formulation in LS-Dyna

In static analysis, the uniform pressure load will exert in the red circled segment area in figure 3.15, which is realized by the keyword DEFINE_CURVE and LOAD_SEGMENT_SET. The area is the same as the interaction area in ALE calculation. The dimension for this area is $2100mm$(vertically) x $5000mm$(horizontally), which is corresponding to $10.5m^2$. The pressure should be defined as a linear increasing load, and the steel column will deform with different boundary conditions which will discuss in section 4.1.1 and 4.1.2.

The numerical calculation could be divided into the implicit one and the explicit one. The static analysis will be conducted with the explicit method in LS-Dyna. Compared with the explicit method, the implicit method is conditionally stable. In LS-Dyna, implicit time integration assumes the acceleration varies linearly over the time step, while the explicit time integration assumes constant acceleration over the time step. Also, the implicit method uses the information from the previous time step and the unknown time step, but the explicit method only adopts the information from the previous step. Although the results of static analysis in the implicit method may be more accurate than the explicit method, there is often a converge problem occurs in the implicit method. Further, the cost of the numerical calculation will be immensely higher than the explicit method. The analysis for slamming impact has several characteristics. The first one is that the structure in the analysis is enormous, which means more nodes and elements need to be involved in the calculation. The other one is that the calculation time is short due to the feature of slamming events. Usually, for a long time calculation, the implicit method should be adopted because the time step length is not essential in the implicit analysis. Equilibrium can always get in each step. Thus for a long time calculation, a more significant time step length could be set. While for the explicit method, due to equilibrium is not checked in each step. Then the best way to get an accurate result is to decrease the time step length. The advantage is also evident due to this. There is no converge problem in each step. The calculation time for each step will be much lower than the implicit method. That is why, for a short time analysis, even if the small time step length is chosen in the explicit analysis, the total calculation time will not be so considerable. In this thesis, efforts were paid for the static analysis in the implicit method. However, due to the converge problem, the explicit method was chosen finally to conduct the static analysis. The reason for the converge problems may

come from the vast dimensions of the analysis model.

Several keywords in LS-Dyna are connected with the explicit method which will control the time step, solver type and termination time. Initially, DT=1e-6s will be used as the time step length. Hourglass parameters are set to avoid the zero energy deformation mode.
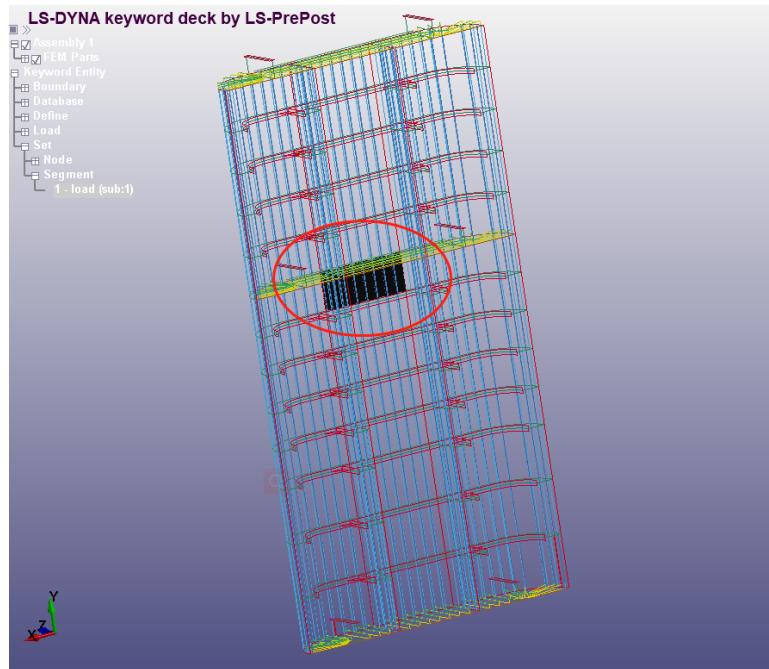
Figure 3.15: Static analysis loading model

3.4   ALE Formulation in LS-Dyna

As the introduction in theory part, the ALE method is often used for the fluid interaction problem. In LS-Dyna, there are several keywords in ALE formulation which are worthy of discussing.

1. EOS

In section 2.5.3, different formulation in EOS are described. The 'Gruneisen EOS' is suitable for the larger deformation of the fluid, which corresponds to the water. Because during the slamming impact, the water particle will experience great deformation. The 'Gruneisen EOS' will be used with the water. On the other hand, the air will use the 'Linear Polynomial EOS' due to smaller deformation. The parameters in detail are illustrated in table3.10 and 3.11.

Table 3.10: The parameters used in Linear Polynomial EOS model

Source	Fluid type	C_0	C_1	C_2	C_3	C_4	C_5	C_6	E_0	V_0
[26]	air	0	0	0	0	0.4	0.4	0	0.25	1

Table 3.11: The parameters used in Gruneisen EOS model

Source	Fluid type	C(mm/s)	S_1	S_2	S_3	$GAMAO$	A	E_0	V_0
[26]	water	1.480e+0060	1.9210000	-0.0960000	0	0.3500000	0	0.2895000	1

2. Prescribed Velocity

Only part of the cross-section of the whole platform leg is built, the mass of part discarded in the geometry need to be considered in ALE test. One method is to add the mass element on the boundaries (red highlight in figure 3.16). Alternatively, by prescribing a constant velocity on these boundaries can have the same effect due to the discarded part has a huge mass which could be seen as a rigid body without the velocity change during the impact. The constant velocity during impact means no displacement on these boundaries.
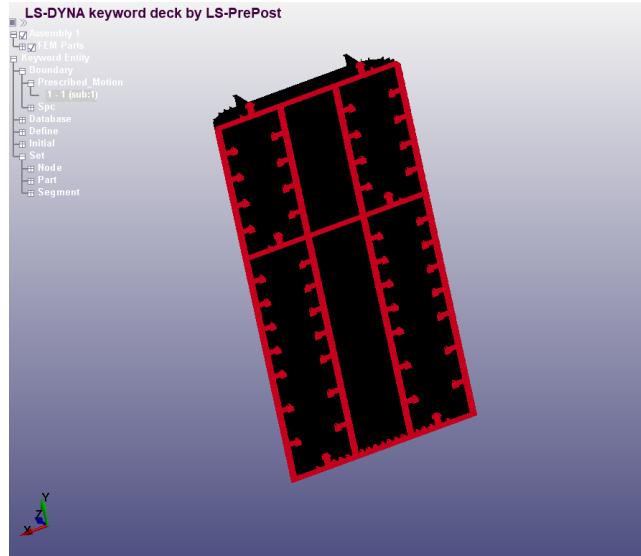
Figure 3.16: Boundary between the modelled part and discarded part

3. Boundary Condition

Since the slamming is a local phenomenon whose impact focusing on the interaction area, the rear end boundary conditions are not crucial. All of the dofs excepted the z-direction on the boundaries in figure 3.16 are fixed in all ALE tests.

4. Formulation of the Element

For fluid, the solid element with ALE multi-material element formulation is used. In order to keep numerical calculation stable, fully integrated shell element is chosen for the structural element formulation.

5. Mass Scaling and Termination

Mass scaling is a kind of effective way to speed up the ALE calculation. For ALE simulation, LS-Dyna will calculate the time step length inside automatically. This time step length may be so small that would increase the calculation time cost. The mechanism for mass scaling is to add a virtual mass to the structure to keep a constant times step length in the whole calculation. While the requirement for the virtual mass should be small enough compared with the total structural mass, which could be checked in the message file each time to ensure the results are valid. Duration of calculating time should ensure the displacement amplitude is relatively stable in the history plot. Termination time 0.06s is set for satisfying this requirement.

40

6. Impact Area and Location of Largest Displacement

The impact area around the secondary deck is illustrated in figure 3.17a. Within the area, the fluid could have an interaction with the structure. Outside the area, the fluid could be free to move. It spans from one bulkhead to the other, which is around 5000mm horizontally and from the second deck to the next side plate girder, which is around 2100mm vertically. Usually, the max displacement occurs in the middle of the side plate between two continuous side stiffeners shown in figure 3.17b.
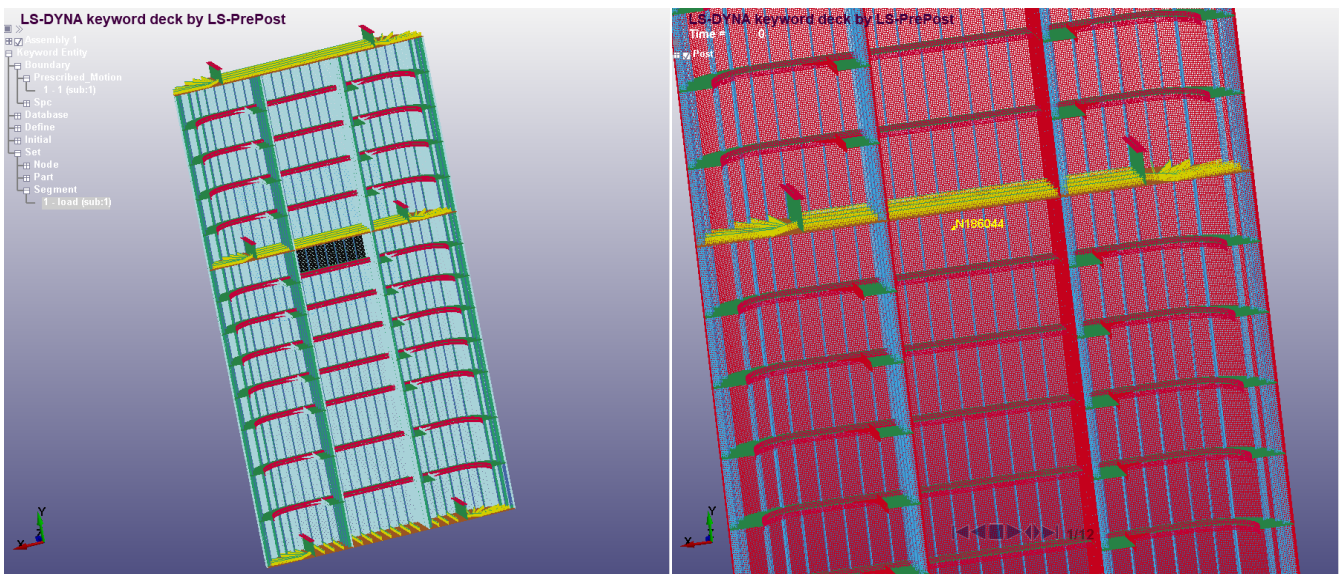
(a) Impact area of the structure (b) Location of max displacement in ALE calculation

Figure 3.17: Illustration for the impact area and max displacement location

6. The Initial Gap from the Structure and the Water

The purpose of the initial gap from the structure and the water is to avoid the considerable acceleration shock of the water. The structure will possess a velocity immediately when the drop test starts. If there is no gap between the water and structure, the water will experience a big acceleration shock, which may cause a vast pressure peak initially. In view of this, the 0.5mm initial gap was chosen in the analysis. In the results plot following, this gap in the maximal lateral deflection plots is cut by Matlab for the comparison purpose.

3.5 Dynamic analysis Formulation in LS-Dyna

Same as the static analysis, the pressure loads could be set on the structures in the dynamic analysis. This pressure variation load may come from the ALE test. It will use the same boundary conditions, BC-2 in the discussion of longitudinal BC. Due to the explicit method is adopted in dynamic analysis, small step length should be assumed to obtain more accurate results. Because of this, DT=9e-7s will be used as the time step length. Same loading method will be used with the static analysis in figure 3.15.

4 Results

In this chapter, three kinds of numerical calculations are conducted for different purposes. Due to the significant dimension of the analysis model, all of numerical simulations are calculated on the cluster of NTNU's supercomputer "Vilje".

4.1 Static Tests of Steel Columns in Explicit Method

The objective of static analysis in this thesis:

1. Discuss the boundary condition of the steel column.

2. Obtain the resistance curve of the steel column.

3. Obtain the SDOF parameters from the resistance curve.

Two main kinds of boundary conditions are discussed in this section in order to evaluate the boundary conditions effect on the structure. One is the longitudinal boundaries which are discussed in section 4.1.1, and the other is deck boundary in section 4.1.2. After that, resistance curves for models with different plate thickness could be obtained for the purpose of SDOF parameters calculation. Equivalent beam analogy and tri-linearisation resistance curve comparison in SDOF method are discussed following. These parameters provide the information for the SDOF calculation in section 4.2.5 to calculate the dynamic response of the structure. For the input, only material 2 in table 3.7 is adopted in all static analysis. All geometry information has been introduced in table 3.1. The calculation methods in detail have been illustrated in section 3.3.

4.1.1 Effects of Different Longitudinal BCs

1. Introduction of Different Longitudinal BCs

In figure 4.18a boundaries are the interface between the modelled part and discarded part due to simplification. The discarded part has an enormous mass which gives full support of the modelled part. For this reason, to assume the boundary can not deform in the z-direction is a good idea. According to [3] and [28], the boundaries on the longitudinal end (figure 4.18b) are very crucial for the stiffened panel. In this section, four different longitudinal boundary

conditions are argued:

1. BC-1: Fix all dofs on longitudinal boundaries.

2. BC-2: Fix translational dof in the z-direction on longitudinal boundaries.

3. BC-3: Fix all translational dofs on longitudinal boundaries.

4. BC-4: Set free all dofs on longitudinal boundaries.

(a) Boundaries with all dofs fixed   (b) Longitudinal boundaries
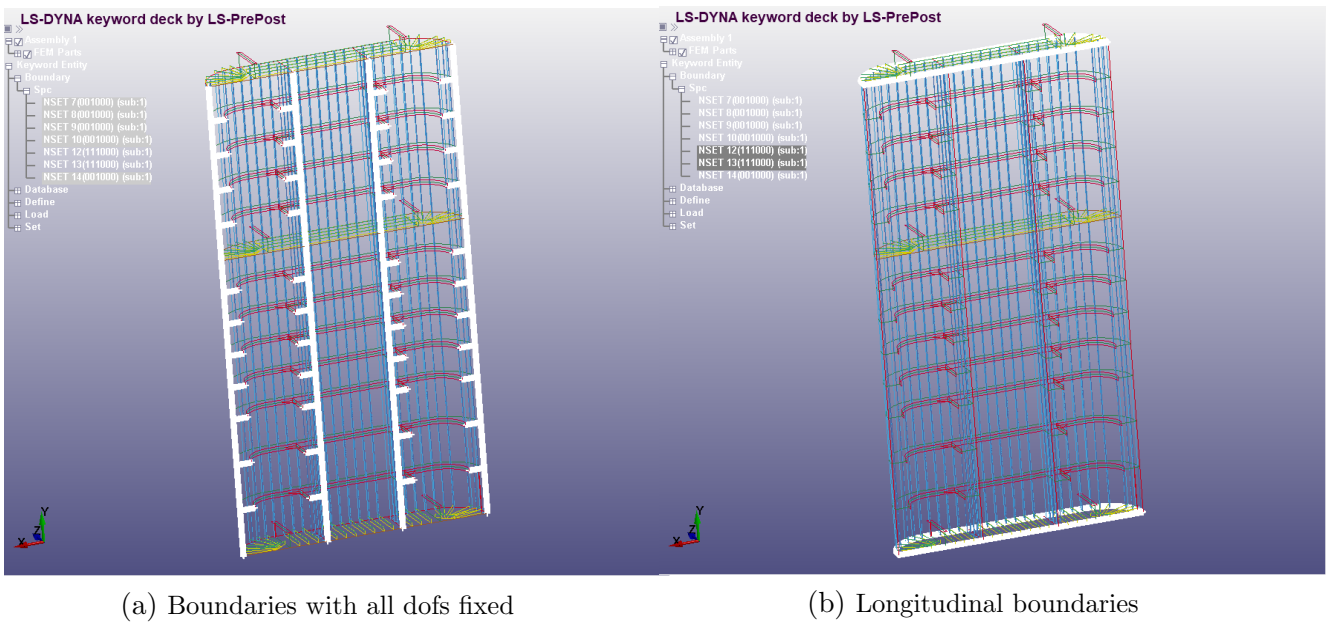
Figure 4.18: Longitudinal boundaries illustration

2. Comparison of Resistance Curves Between Different Longitudinal BCs

From figure 4.19a, four BCs give almost the same resistance curve. Only BC-1 (Fix all dofs on longitudinal boundaries) and BC-3 (Fix all translational dofs on longitudinal boundaries) give a little higher load at the same displacement level compared with the other two kinds of BCs. Moreover, the results from BC-1 and BC-3 is very similar, which means the resistance curve is very sensitive with the translational boundary conditions on the longitudinal end, not the rotational boundary conditions on the same edge. However, the difference among all BCs results on the longitudinal end is tiny in general, which is because the boundary is too far from the loading area. In other words, the rear end boundary conditions have a relatively small effect on the slamming area. The slamming phenomenon is a very local one to some extent. Then in the ALE calculation, all dofs excepted z-direction on the rear end and deck could be fixed for

44

the convenience reasons, which seems to be reasonable (z-direction is the moving direction).

The figure 4.19b gives the non-dimensional results of the resistance curve. From the curve, it is non-dimensioned by the plastic collapse force in pure bending R_0 and the stiffener web height h_w. It is easy to see R_0 for all BCs is around 0.143 Mpa, which is equal to 1.5 MN (the area of the loading area is $10.5m^2$). The max elastic deformation ω_{el} is around $12.5mm$ which is about $\frac{1}{20}$ of the stiffener web height. The elastic stiffness is around $120MN/m$. After the elastic range, the membrane force is developed in the structure. These parameters will be concluded in section 4.1.4.
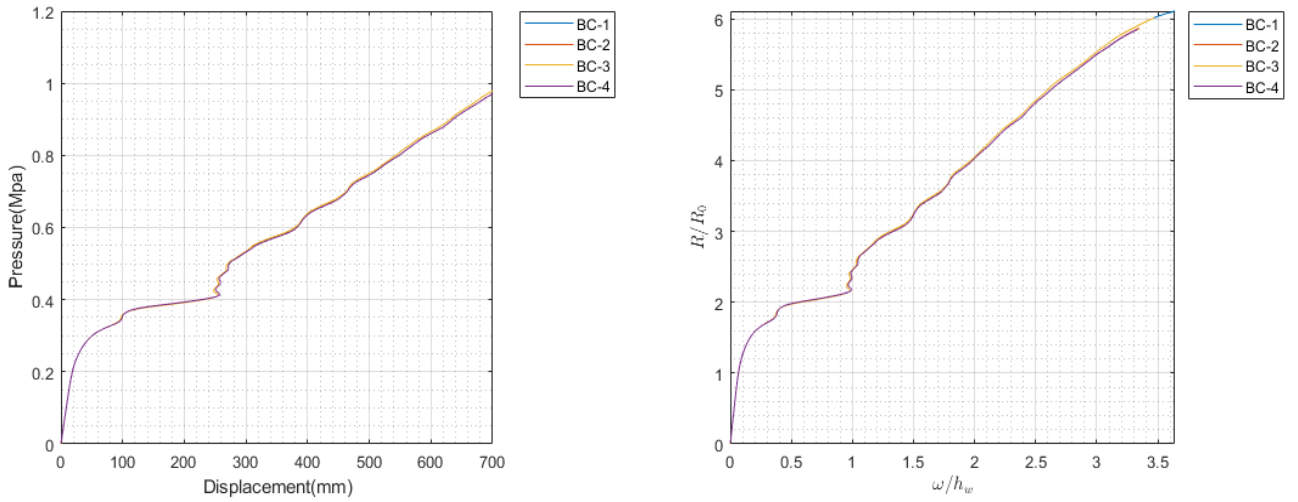
(a) Resistance curve comparison between four longitudinal BCs

(b) Non-dimensional resistance curve comparison between four longitudinal BCs

Figure 4.19: Resistance comparison for longitudinal BCs

4.1.2 Effects of Different Deck BCs

1. Introduction of Different Deck BCs

Figure 4.20b shows the location of the deck boundary, which is very close to the loading area. The objective of this section is to evaluate if the boundary on the deck will affect the resistance curve of the structure. In section 4.1.1, it is proved that rear-end boundary conditions have not so much effect on the resistance curve of the structure. Then for the longitudinal boundaries, only z-direction translational dof is fixed. Other boundaries in figure 4.20a except the longitudinal one fix all of dofs. Four-deck boundaries are discussed in this section:

1. BC-1: Fix translational dof in the z-direction on the deck boundary.

2. BC-2: Fix all dofs on the deck boundary.

3. BC-3: Fix all translational dofs on the deck boundary.

4. BC-4: Set free all dofs on the deck boundary.
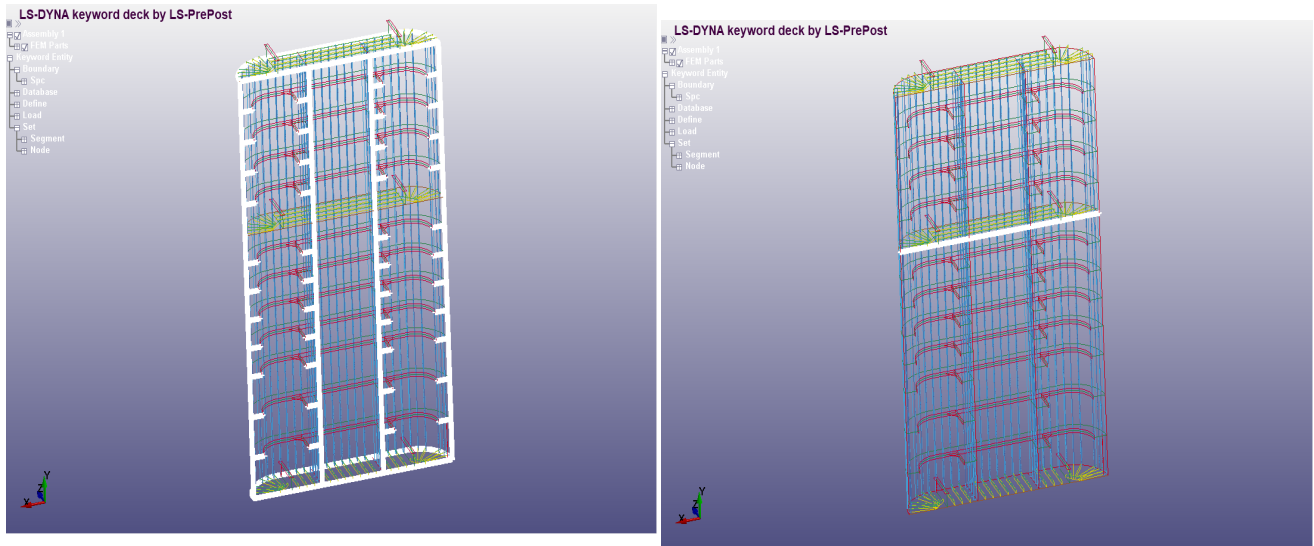
(a) Fixed z dof on longitudinal end and fixed all dofs on other boundaries

(b) Deck boundary

Figure 4.20: Deck boundaries illustration

2. Comparison of Resistance Curves Between Different Deck BCs

Deck BC has a similar result with the longitudinal BCs. For BC-2 (Fix all dofs on the deck boundary) and BC-3 (Fix all translational dofs on the deck boundary), all translational dofs on the deck boundary are fixed in common. Higher loads at the same displacement level are expected in these two cases compared with other BCs. BC-4 (Set free all dofs on the deck boundary) gives the lowest load level in high displacement domain (2-3 stiffer web height) but gives highest load level in middle displacement domain (0.5-1 stiffer web height). Furthermore, there is a lag phenomenon occurs in BC-4 compared with other BCs. While in the elastic range, those resistance curves behave very similar, which means the boundary conditions will not affect the elastic behaviour of the structure. Globally, the difference between the results of all BCs is not very large. Due to the similarity of the resistance curve, the deck boundary could also be seen as a rear-end boundary. The SDOF parameters from the last section are still valid to some

46

extent.
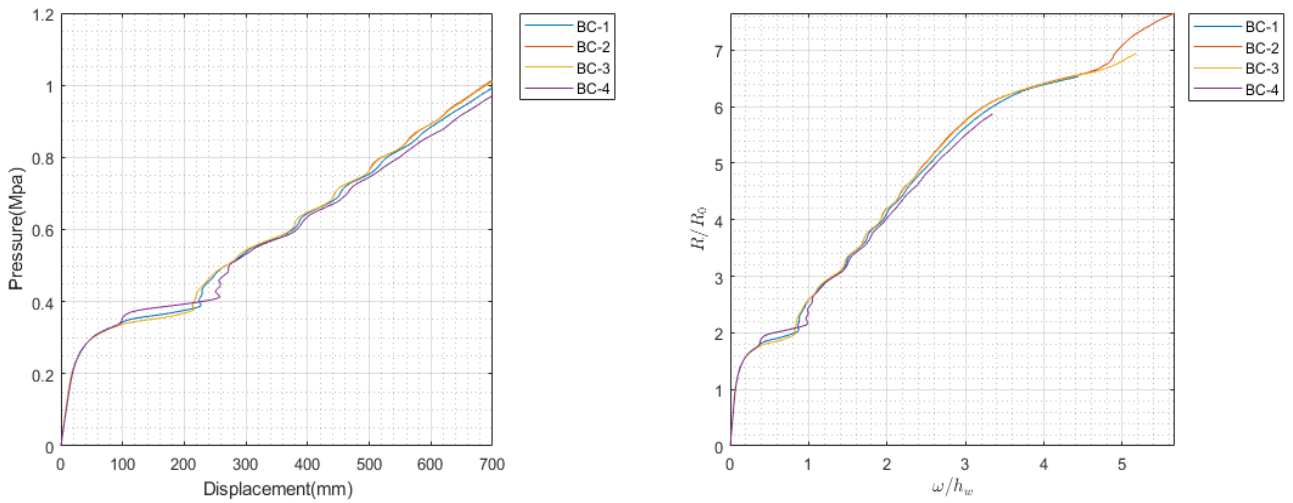
(a) Resistance curve comparison between four the deck BC

(b) Non-dimensional resistance curve comparison between four the deck BC

Figure 4.21: Resistance comparison for the deck BC

4.1.3 Resistance Curves of Models with Different Plate Thickness

In figure 4.22, three resistance curves of 3 different plate thickness models are plotted. With the increase of the plate thickness, the elastic and elasto-plastic stiffness of the structure would also increase. The stiffness for the 20mm plate thickness model is up to 140 MN/m. 16mm and 12mm plate thickness models give almost the same plastic force in pure bending(Elastic resistance). Nevertheless, due to the max lateral deflection of plate 16mm is lower than the 12mm model. The stiffness of these two models is different. The 20mm plate thickness model has the largest R_0 or called R_{el} in Biggs chart. It is easy to find that the thinner plate model would have a more significant elastic displacement. These results are corresponding to common sense and the guess before the tests.
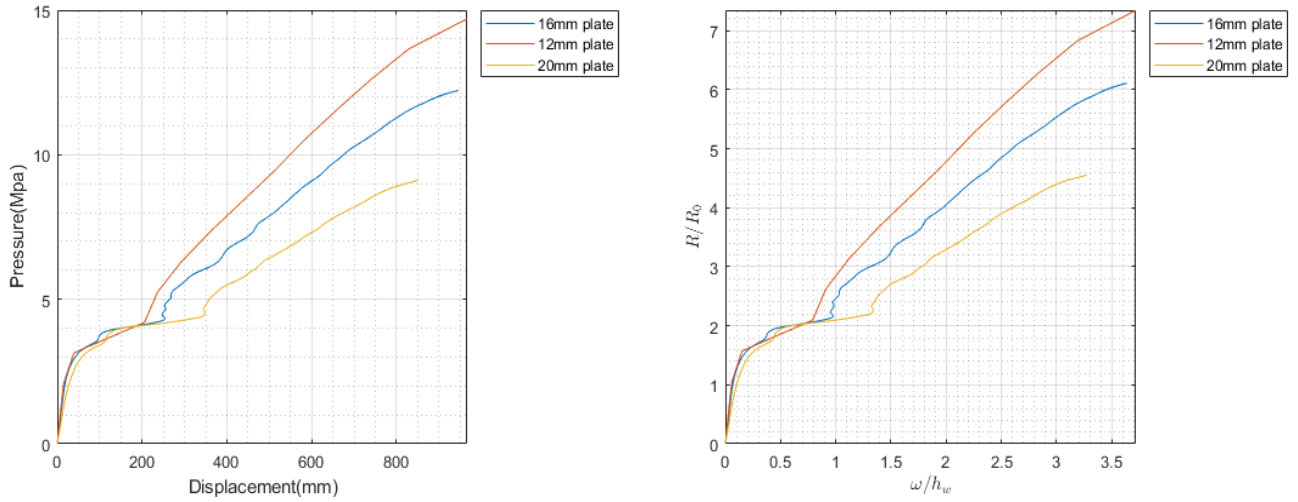
(a) Resistance curve comparison between three different plate thickness models

(b) Non-dimensional resistance curve comparison between three different plate thickness models

Figure 4.22: Comparison of resistance curve with different plate thickness

4.1.4 SDOF Method Parameters

SDOF method has been illustrated in the theory part. The objective of this section is to calculate the parameters and information preparing for calculating the response in Biggs chart method and Runge-Kutta time integration method.

1. SDOF Parameters

From the resistance curve above, SDOF parameters could be concluded in the table 4.12: K_1 is the stiffness in elastic range, the k_{ep} is the stiffness in elasto-plastic range.

Table 4.12: SDOF parameters from static analysis in LS-Dyna

Plate thickness	R_{el}	ω_{el}	k_1	k_{ep}
16mm	1.5 MN	12.5mm	120MN/m	11.2 MN/m
12mm	1.5 MN	17.5mm	85.7MN/m	9.01 MN/m
20mm	1.7 MN	13 mm	130MN/m	13.9 MN/m

2. Mass and Added Mass of the Equivalent Beam

Even if the whole structure is huge, which has the mass up to $187.35t$, the meaning of SDOF beam analogy is to simulate the response in a plate strip. This plate strip could be seen as a stiffener on the side plate with an effective plate flange. The evaluation of the equivalent

48

beam mass needs to be conducted in hand calculation. Before that, the effective plate flange width needs to be known. In the figure 4.23, l_0 is the total length of the stiffened plate, b is the stiffener spacing. The effective flange width could be calculated by the bC_e. In our case, the pressure is set locally, and most of the structural response also focuses on the loading area. Then choose the l_0 as the length of the loading area (5000mm) is reasonable. The spacing of the stiffener is around 625mm. The ratio in the figure 4.23 is 8. Then the calculated effective flange width is one stiffener spacing (625mm).
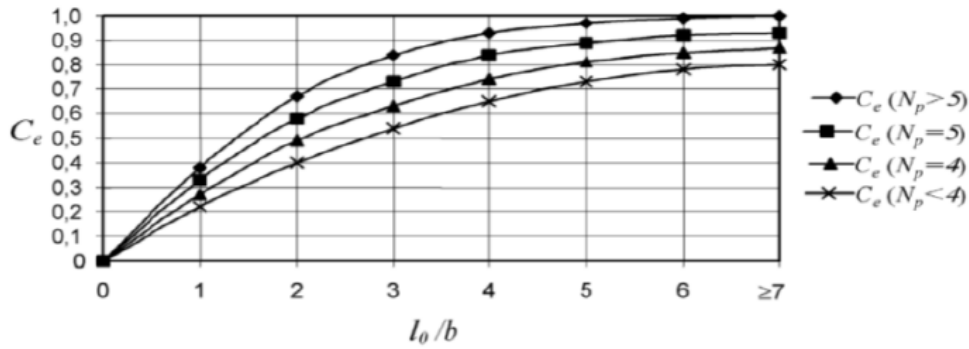
Figure 4.23: Coefficient for estimation of the effective flange (Referenced from [7])

The area of the side plate stiffener section profile is $3611mm^2$, and the plate flange area is $10000mm^2$ for 16mm side plate thickness. Totally the area of the cross-section of the equivalent beam is $1.36e4mm^2$. The length of the beam is 2100mm. The volume of the beam is $2.858e7mm^3$. With $7.8e-9t/mm^3$, the total mass of the equivalent beam is $0.223t$.

In the ALE calculation, the structure will be immersed into the water, and added mass could not be forgotten in that case. In order to compare the SDOF result with ALE calculation, added mass for the equivalent beam still need to be evaluated. Equation 2.39 could be used to calculate the added mass analytically. The total length of the loading area is 500mm corresponding with b in figure 2.9. The height of the loading area is around 2100mm, which is a in the same figure. $b/a = 2.38$. By interpolation from the table, added mass coefficient C_A is around 0.79. Then the added mass is around $0.176t$ by equation 2.39. Table 4.13 shows the mass properties of the equivalent beam in detail.

3. Parameters of the Equivalent Beam in SDOF Analysis

The parameters of the equivalent beam in all thickness are concluded in table 4.14. K_{lm} is the

Table 4.13: Mass properties of equivalent beam

Equivalent beam	Plate thickness	Mass in the air(M)	Added mass(M_a)	Mass in the water(M_t)
1	16mm	$0.223t$	$0.176t$	$0.399t$
2	12mm	$0.182t$	$0.144t$	$0.326t$
3	20mm	$0.264t$	$0.208t$	$0.472t$

load mass factor in figure B1 for a clamped beam subjected to uniform pressure load. By using $K_{lm} * M_t$, the generalized mass $\overline{M_t}$ could be obtained.

Table 4.14: Mass properties of equivalent beam strip

Material	Plate thickness	K_{lm}	$\overline{M_t}$	k
Elastic	16mm	0.77	$0.307t$	$120MN/m$
Elasto-plastic	16mm	$0.78t$	$0.311t$	$11.2MN/m$
Elastic	12mm	0.77	$0.251t$	$85.7MN/m$
Elasto-plastic	12mm	$0.78t$	$0.254t$	$13.9MN/m$
Elastic	20mm	0.77	$0.363t$	$140MN/m$
Elasto-plastic	20mm	$0.78t$	$0.368t$	$9.01MN/m$

4.1.5 Standard Tri-linearisation of Resistance Curve Comparison

In figure 4.24a,4.24b and 4.24c, the resistance curves of the corresponding structure in LS-Dyna are plotted with the standard tri-linearisation resistance curve with different k_3. k_3 is equal to 0.1 k_1, 0.2 k_1 and 0.5 k_1. k_1 is the elastic stiffness which could be found in table 4.14. From the figure 4.24a, the resistance curve for 16mm plate thickness structure is between the resistance curve of $k_3 = 0.1k_1$ and $k_3 = 0.2k_1$. But $k_3 = 0.1k_1$ is closer to the original resistance curve. For 12mm plate thickness structure 4.24b, the resistance curve is in the middle of $k_3 = 0.1k_1$ and $k_3 = 0.2k_1$. In figure 4.24c, 20mm plate structure resistance curve is similar with $k_3 = 0.1k_1$ than others.
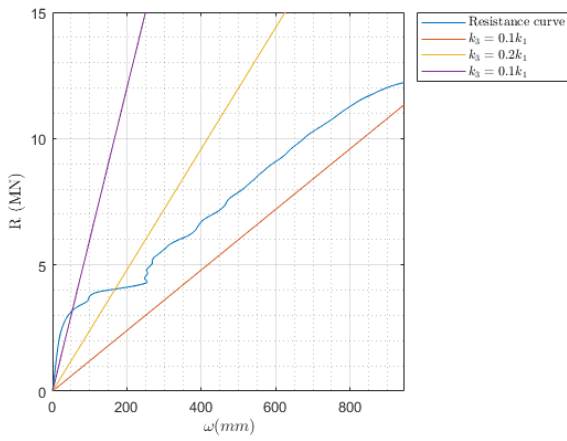
(a) Resistance curve of plate thickness 16mm model compared with a standard tri-linearisation of resistance curve with k_1 =120 N/m
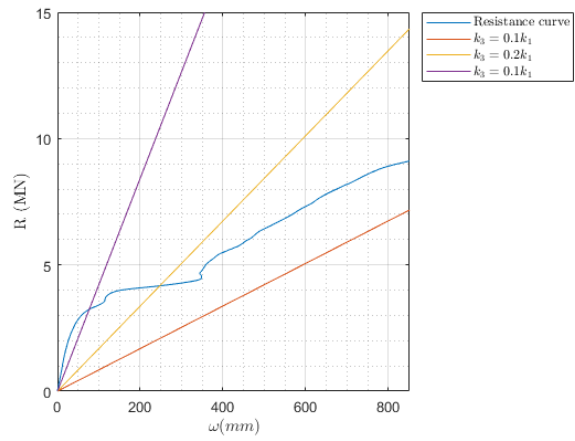
(b) Resistance curve of plate thickness 12mm model compared with a standard tri-linearisation of resistance curve with k_1 =85.7 N/m
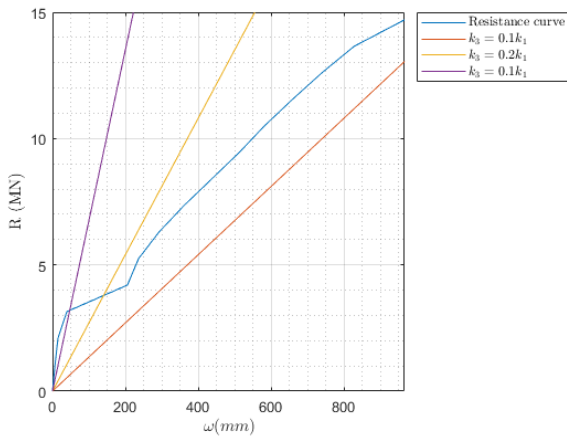
(c) Resistance curve of plate thickness 20mm model compared with a standard tri-linearisation of resistance curve with k_1 =130 N/m

Figure 4.24: Resistance comparison for the deck BC

4.2 Drop Test of Steel Column in ALE Method

The objective of the ALE drop tests in this thesis :

1. Analyse the process of the impact process in detail.

2. Parametric study to evaluate the effect of different parameters on the structural response.

3. Comparison of the structural response between SDOF method and ALE methods.

In this section, ALE drop tests are executed with different inputs to study the FSI interaction phenomenon. A typical case would be conducted in order to analyse the process of the whole slamming impact in detail. A parametric study following with different materials, velocities and plate thickness are also introduced. Finally, SDOF methods would show how to calculate the structural response without numerical methods.

4.2.1 Case Study

In this section, a detailed analysis of the deformation mode will be done. Characteristic of the displacement response times series and pressure plot would be introduced. The impact velocity of this test is $20m/s$. All geometry information has been introduced in the table 3.1. The side plate thickness uses 16mm as the default value in the analysis. Only material 2 in table 3.7 is adopted in this case study. The analytical model of the ALE test is provided by Zhaolong.Y for comparison reason, which is the same analytical model in paper [8] and [29].

1. Wet Eigen Period of the Structure

The wet eigen period T_n could be obtained from the oscillation period of upper strain in the longitudinal direction of the loading stiffened plate (y-direction), which is approximately 11 ms in 16mm pate thickness model.

2. Response Results

The figure 4.25 shows the characteristic of maximal lateral deformation of the plate in impact direction. The maximal deformation of the structure is 141.5 mm at 12 ms. The side plate deformed almost linearly in the first stage up to the max displacement. Later, there is a recovery of the deformation from the max to a constant plastic deformation, which is around 105mm.

After that, the structure starts to oscillate around the balanced position after 20 ms, which could be seen as elastic deformation. The natural period of this oscillation is about one wet natural period, even though it is hard to read the natural oscillation period from the plot accurately. The maximal Von-mises stress at the max displacement level is around 690 Mpa, which is a little higher than the proportional limit of this material. The material just enters into the elasto-plastic range. From the deformation plot, a non-linear curve around the peak could be seen correspondingly.
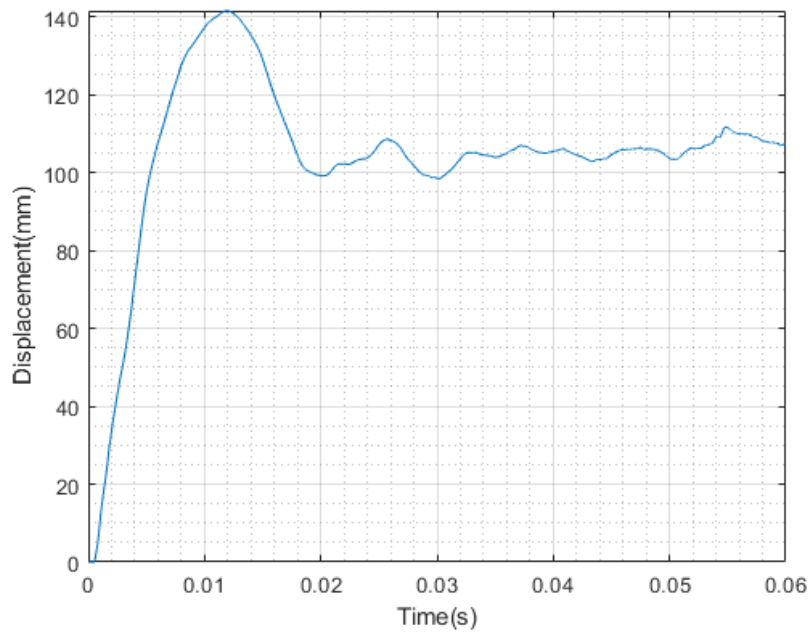
Figure 4.25: The displacement of the drop test (impact velocity:$20m/s$, plate thickness:16mm, material: 2)

3. Pressure Results

The pressure time series is visualised in figure 4.26. The zero part before the first peak is because the gap between the structure and water initially. At the first stage of slamming, the initial phase, the acoustic wave will develop with the sound speed. Analytically, the max pressure should be lower than acoustic pressure $p_a = \rho_w V_0 c_s = 30.7 Mpa$ in (eq: 2.13). In contrast, the calculated result in ALE calculation is much higher than the analytical result. The potential reason will be analysed in section 4.3. Actually, the peak pressure is tough to measure both in the numerical calculation and the experiment test. After the great peak, the pressure decreases very rapidly. From 2.3 ms to 14 ms, the pressure could be described by a rectangular impulse which has an average pressure level of 1.95 Mpa. The duration of the pressure impulse t_d is around 14 ms. From this point, the structure starts to osculate. $t_d/T_n = 1.273$ means the impulsive domain is in the dynamic domain [4] which is introduced in section 2.3.6. The response needs to be calculated numerically.
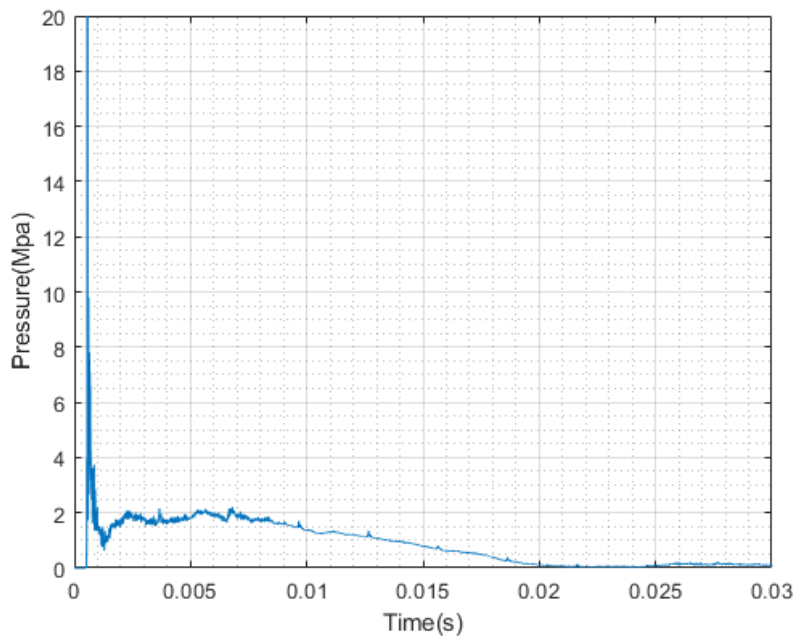

Figure 4.26: The pressure time variation of the drop test (impact velocity:$20m/s$, plate thickness:16mm, material: 2)

4. Description of Response Process

From the plot A1 in the Appendix, the lateral deformation pattern is visualised. At the start in figure A1a, the plate deforms between stiffeners. The maximal deformation occurs in the middle of the plate. With the increase of the pressure, the stiffener starts to deform and lose the support function for the plate—the stiffened plate responses as a whole structure. The deformation establishes to expand outside of the loading area. At the peak deformation points, t=14 ms A1e, the deformation spread out to the largest domain. After 20ms A1h, the structure starts to oscillate.

Figure A2 provides the section plot of the deformation pattern during the impact. t=1ms, the stiffener starts to deform in the figure A2b. All girders and the bulkhead keep straight in shape. From 6ms start A2d, the stiffener deforms as the sinusoid curve, the half-wave is equal to the girder spacing. Further, the bulkhead and the girders establish to deform. The bulkhead deforms more than the girders on the side plate. It is proved that the girder gives strong support for the plate and the stiffeners.

The relative volume fraction of the fluid is plotted in A3. In the initial stage, even if the peak pressure is very high, the water does not deform very heavily from figure A3b. That means the peak pressure for the slamming phenomenon is not very important, and the crucial thing is the total impulse and the duration of the impulse in the pressure time series.

5. Comparison of Displacement History Plot with Analytical Model Results

Figure 4.27 shows a comparison between the ALE drop test calculation and the analytical result in the maximal lateral deflection. The ALE calculation shows a very consistent result in the elastic range (before the maximal deflection). Nevertheless, it overestimates the maximal deflection compared with the analytical one. The max deflection for ALE test is about 141 mm, while the peak deformation in the analytical model is only 120mm. The relative error is up to 17.5 %.

4.2.2 Comparison of Different Materials in ALE Drop Test

In this section, all materials in section 3.2 are tested in ALE methods in LS-Dyna. The comparison would be made in three aspects: displacement, pressure and parameters at the peak
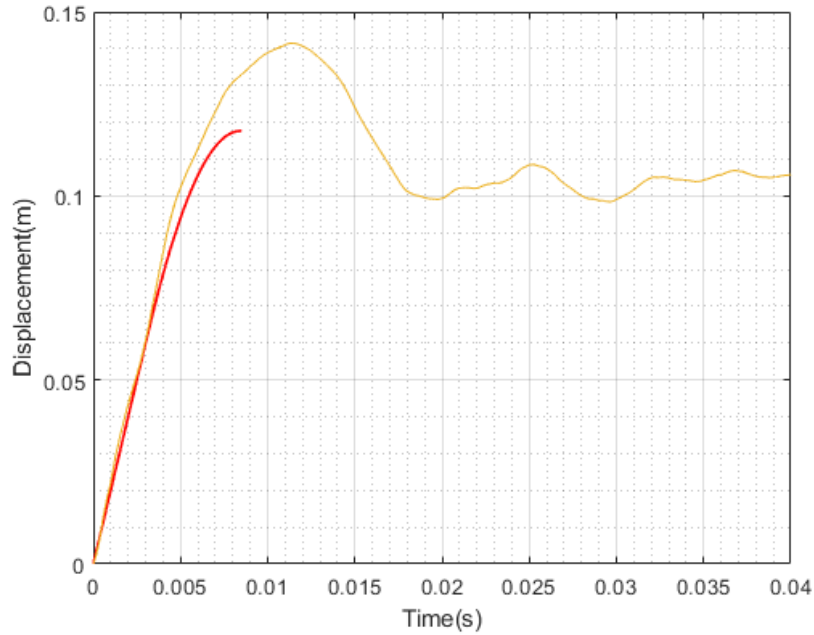
Figure 4.27: Comparison of maximal lateral deflection from LS-Dyna (impact velocity:$20m/s$, plate thickness:16mm, material: 2) and the analytical model [8]

deflection level.

Summary of all materials used in this section:

1. Mat-1: Elastic material.

2. Mat-2: Calibrated power-law model with the strain rate hardening effect.

3. Mat-3: Calibrated power-law model without the strain rate hardening effect.

4. Mat-4: Power-law model from [28].

5. Mat-5: Power law model from [18].

1. Displacement Comparison

All the deformation series follow three main stages in figure 4.28. The first stage is linearly increasing stage, where the loads start to develop simultaneously. The secondary stage is for the part they attain to the maximal lateral deflection. After that, it establishes to oscillate in a period around a constant displacement level decided by the properties of the material and the structure itself. Overall, Mat-4 and Mat-5 give similar results. The difference between Mat-2

and Mat-3 is the strain rate hardening. It is shown that the strain rate hardening is a very crucial parameter that may affect the results. Deformation series of elastic material Mat-1 has its own unique characteristic compared with other elasto-plastic cases. All of the curves have almost the same slope in the first development stage.

The effect of strain rate hardening is crucial, from the curve of Mat-2 and Mat-3, the material without strain rate hardening will give a relatively higher maximal lateral deflection during the impact.

The deformation of the elastic material drop test -Mat-1, as expected, oscillates around the zero displacement level. Due to the material in elastic range, all elastic deformation could be recovered due to the decreasing of the load. While other materials are all belongs to the elasto-plastic material domain, they can not recover to zero constant displacement level due to the plastic deformation which can not be eliminated with the loading decline as the elastic part of the displacement in Mat-1. Also, there will be several peaks in the high level of the domain, not one peak in other elasto-plastic materials.

Even if Mat-4 and Mat-5 have different parameters in the power-law model and strain rate hardening, they provide similar results in the drop test. The reasons may because the parameters of K and np counteract the effect of strain rate hardening.

The eigen period will not change among all the material types due to it is the inherent structural property. However, the displacement series may not oscillate in the natural period. Although it is hard to read the oscillation period from all the curves, the oscillation period for the Mat-1 elastic one is relatively smaller than other elasto-plastic cases. Mat4 and Mat-5 seem to have the most significant oscillation period. The elastic oscillation amplitudes for the two cases are lower than others. Mat-2 and Mat-3 give similar results in the oscillation period and amplitudes. It means the strain rate hardening will not affect the oscillation part of the deformation series.

2. Pressure Comparison

The common characteristics for all pressure series in figure 4.29 are they both have the initial stage with extremely high peak pressure, and an approximate rectangular impulse following. There is a significant difference between the elastic drop test pressure series (Mat-1) and other elasto-plastic cases. The peak pressure is not very meaningful to affect the response but be the
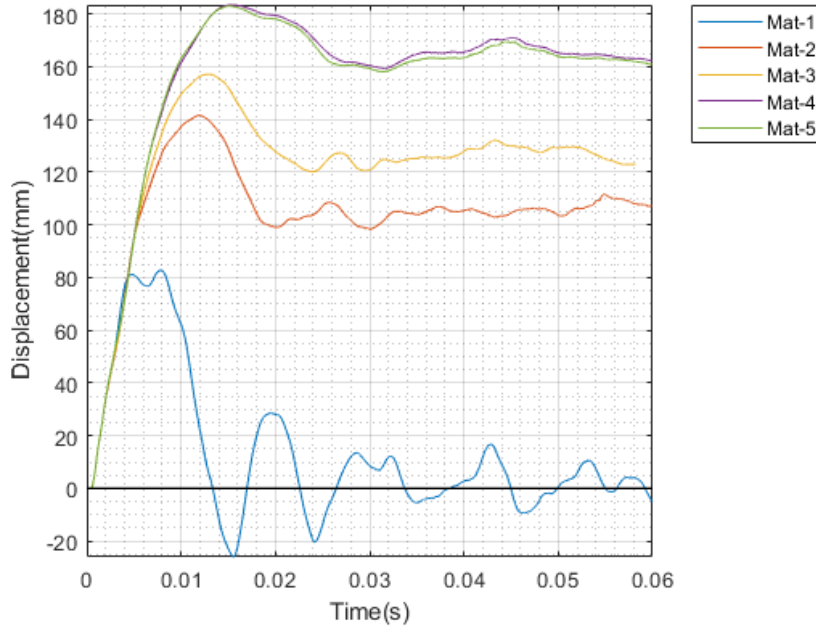
Figure 4.28: Comparison of the max lateral deflection with different materials in ALE calculation (impact velocity:$20m/s$, plate thickness:16mm, material: 1,2,3,4,5)

impulse.

The pressure series from Mat-1 has a focused rectangular impulse compared with other cases. All of the impulses concentrate in a relatively small range so that the duration time t_d would be lower than others. Among all elasto-plastic materials, Mat-2 has the largest amplitude of the rectangular impulse. The second-largest is the same power-law model without strain rate hardening. That means the strain rate hardening intends to make the structure have a higher impulse amplitude and lower impulse duration.

3. Comparison of Parameters of the Drop Test

From the table 4.15, the max Von-mises stress for the elastic material could be neglected due to the effective stress will continue increasing even it already passes the yield stress in the elastic numerical calculation, which is meaningless. From the max Von-mises stress value of other materials, at max lateral deflection, Mat-4 and Mat-5 are stronger than Mat-1 and Mat-2. The max deflections for Mat-4 and Mat-5 could be up to 180 mm, while displacements of the Mat-2 and Mat-3 are only around 150 mm. In such high displacement, the max von-mises stress of these two materials is lower than Mat-2 and Mat-3, which is explained Mat-4 and Mat-5 could
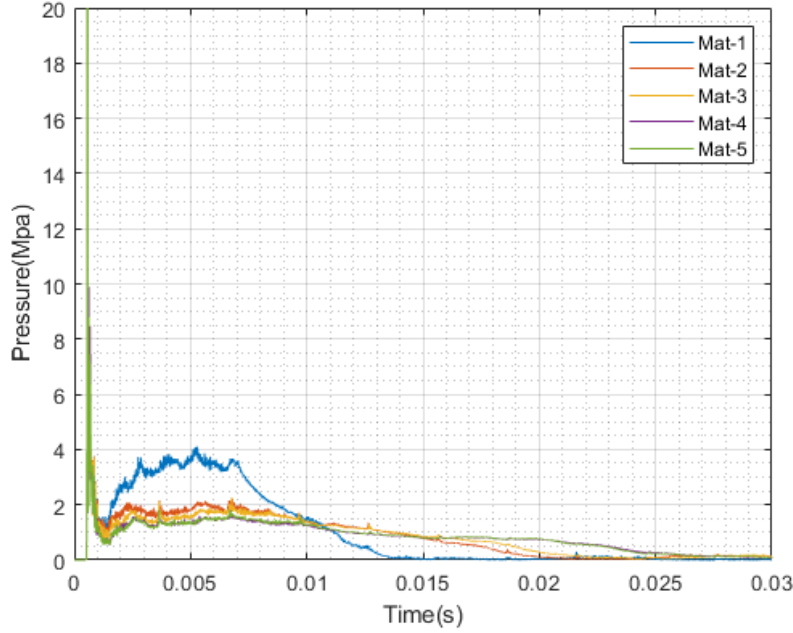
Figure 4.29: Comparison of the pressure series with different materials in ALE calculation (impact velocity:$20m/s$, plate thickness:16mm, material: 1,2,3,4,5)

take more load in the same displacement level. This difference has a relation with the power-law parameters. The maximal lateral displacement occurs later in Mat-4 and Mat-5 than Mat-2 and Mat-3. Furthermore, Mat-4 also has a longer duration. From t_d/T_n, all of the drop tests should be categorized into the dynamic domain $(0.3t_d/T_n < 3)$. The impulse values for all kinds of material are very close, which is proved only the impulse can have a huge effect on the structural response for the slamming events.

Table 4.15: Comparison of the Parameters at peak deflection level between different materials

Material	Max V-M stress	Max displacement	Time at ω_{max}	t_d	t_d/T_n	Impulse
1	2792 Mpa	82.8 mm	8 ms	13 ms	1.62	0.0333 Mpa s
2	690 Mpa	141.5 mm	12 ms	20.2 ms	1.84	0.0331 Mpa s
3	566 Mpa	157.1 mm	13 ms	22.1 ms	2.00	0.0332 Mpa s
4	507 Mpa	183.4 mm	15 ms	26.1 ms	2.37	0.0332 Mpa s
5	476 Mpa	183.0 mm	15 ms	26.1 ms	2.37	0.0333 Mpa s

4.2.3 Comparison of Different Impact Velocities in ALE Drop Test

In this section, ALE drop tests with three different impact velocities are conducted for the purpose to evaluate the effect of the impact velocity in slamming events.

1. Displacement Comparison

From figure 4.30, all of the displacement has a similar shape as the comparison for different materials. At the first stage, a higher impact velocity model owns a larger slop to increase linearly. Also, it is easy to see the more significant maximal lateral deflection occurs in a model with higher impact velocity. Further, this kind of increment in deflection seems linearly related to the increment of the impact velocity. The elastic oscillation domain is also very similar among all tests, included the oscillation period and the amplitude of the oscillation. Around 8ms, the displacement curve of impact velocity 20m/s model has two local maxima with the elastic model before. The response of 10m/s model is more close to the elastic domain, which leads to a similar shape with the response from the elastic model. In small displacement range (close to the elastic domain), the first elastic recovery must happen before the all elastic deformation is set free. The elastic recovery phenomenon occurs more than one time in this situation.
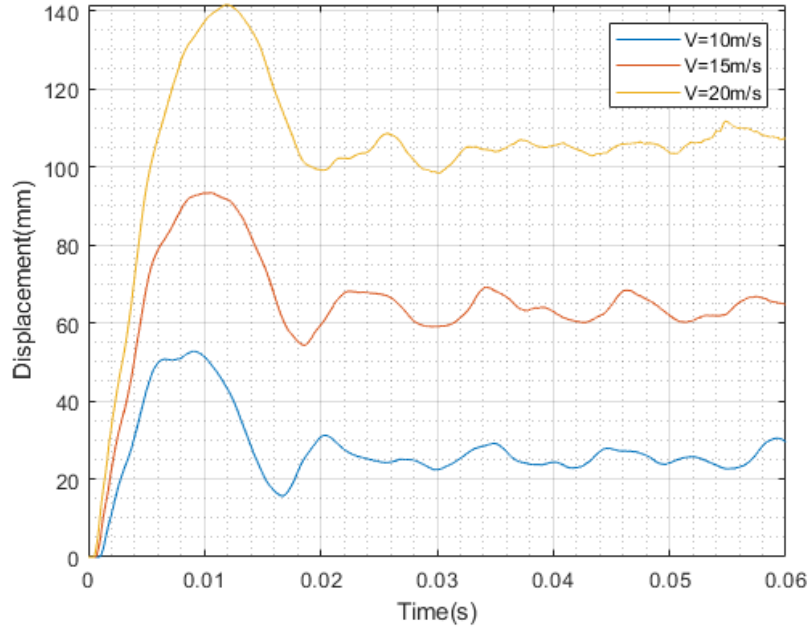
Figure 4.30: Comparison of the max lateral deflection with different impact velocities in ALE calculation (impact velocity:$20m/s$, $15m/s$, $10m/s$ plate thickness:16mm, material: 2)

2. Pressure Comparison

Due to the gap between the structure and the fluid, the pressure series of different velocities in figure 4.31 should be normalised to the same initial time for comparison. Higher velocity model will give a higher total impulse than other models which is represented with higher rectangular impulse amplitude and higher duration of the impact. Compared with other models, the model with 20m/s velocity has more fluctuations in the pressure amplitude than others. Due to the numbers of the data sets used in figure 4.31 is very high, more fluctuations of the pressure curve will be depicted as a thicker line. As we could see, the yellow line, which represents the 20m/s velocity model is very thick, especially in the initial stage.
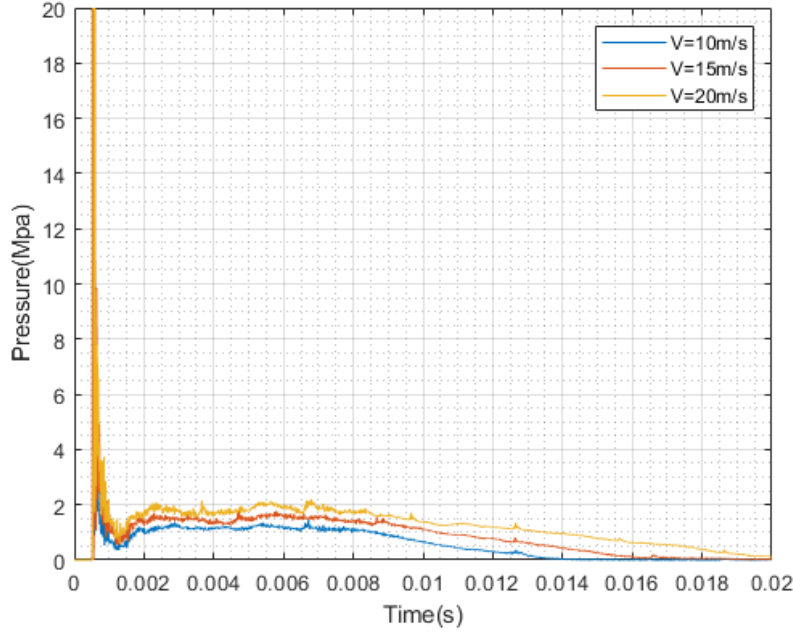
Figure 4.31: Comparison of the pressure series with different impact velocities in ALE calculation (impact velocity:$20m/s$, $15m/s$, $10m/s$ plate thickness:16mm, material: 2)

3. Comparison of Parameters of the Drop Test

From velocity 10 m/s to 15 m/s, the max Von-mises stress of the models at maximal lateral displacement keeps increasing from 633 Mpa to 703 Mpa. But in 20 m/s velocity model, the effective stress changes in another direction. Actually, from the contour plot of the result in all ALE models, the max effective stress always has the oscillation behaviour after it attains to the first constant level. After that, it will decrease to the second constant level and keep oscillating at this level. All the data in table 4.16 from max Von-mises stress represents the constant level for it to oscillate. The specific value is not important. Then it means the max Von-mises stress for these three models has not much difference. The maximal lateral displacement and the impulse almost increase linearly with the increase of velocity amplitude. Higher velocity model attains to the maximal displacement slowly than the low-velocity model. This has the relation with the duration and the impulse of the impact in pressure series.

Table 4.16: Comparison of the Parameters at peak deflection level between different velocities

Velocity	Max V-M stress	Max displacement	Time at ω_{max}	t_d	t_d/T_n	Impulse
$10m/s$	633 Mpa	52.7 mm	9 ms	13.4 ms	1.22	0.0133 Mpa s
$15m/s$	703 Mpa	93.3 mm	10ms	17.8 ms	1.62	0.0224 Mpa s
$20m/s$	690 Mpa	141.5 mm	12 ms	19.5 ms	1.77	0.0331 Mpa s

4.2.4 Comparison of Different Plate thickness models in ALE Drop Test

In this section, three plate thickness models are discussed in ALE calculation. The change of the plate thickness will modify the eigen period of the structure, which will be concluded following.

1. Displacement Comparison

The displacement curve in figure 4.32 of different plate thickness is very similar to the velocity comparison, especially the oscillation part. The first developing stage is separated into two sub-stages. In the developing linear sub-stage, it shows the same slope not three different slopes as the velocity comparison plot. In contrast, it diverges in the non-linear developing sub-stage. To some extent, this comparison curves are very like the comparison with different materials. Thicker the plate is, the larger the deformation we could find in the figure. Stronger structures always deform little than weak structures. As the change in plate thickness would change the mass of the total structure, following the inherent natural period would be modified as well. From this figure, the thicker plate thickness model has a longer natural period than the thin one.
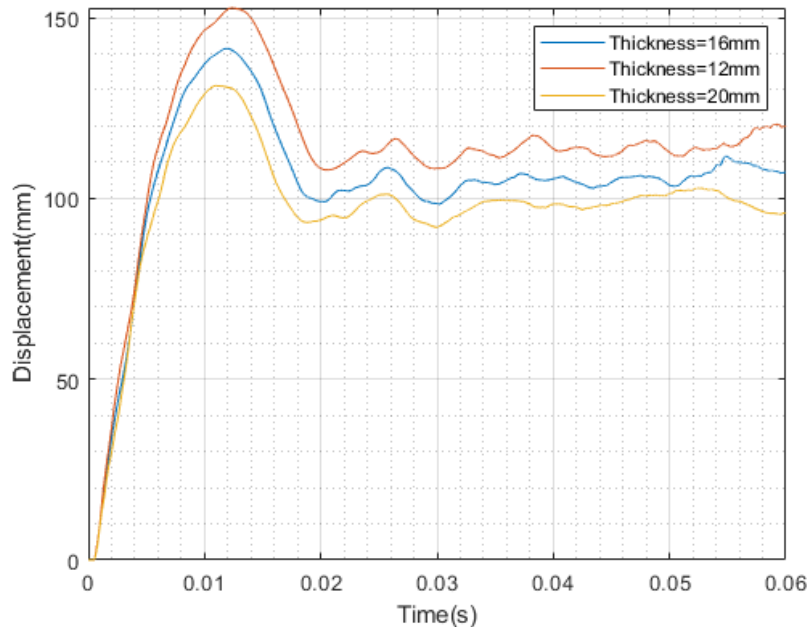

Figure 4.32: Comparison of the max lateral deflection with different plate thickness models in ALE calculation (impact velocity:$20m/s$ plate thickness:16mm, 12mm, 20mm material: 2)

2. Pressure Comparison

All three models of different thickness show consistent results in pressure series 4.33. As the comparison figure for different velocities, more local fluctuation of the pressure amplitude could be observed for all three models in the initial stage.
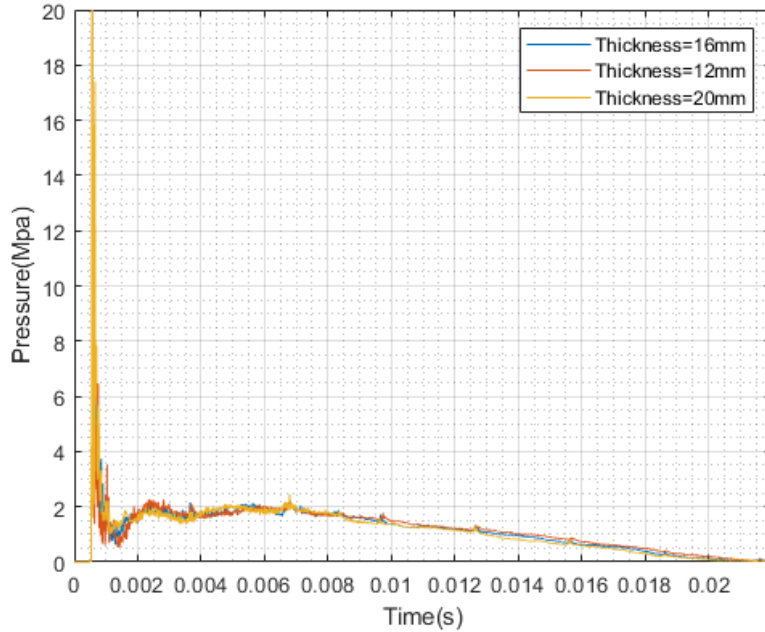

Figure 4.33: Comparison of the pressure series with different plate thickness models in ALE calculation (impact velocity:$20m/s$ plate thickness:16mm, 12mm, 20mm material: 2)

3. Comparison of Parameters of the Drop Test

The impulse and duration of impact could calculate F_{max}. In order to prepare for SDOF calculations, it is summarised in the table 4.17 . The meaning of the F_{max} is the amplitude of the equivalent triangular load without rising time. It could be used in the Biggs chart method to calculate the dynamic response by hand. The eigen period for the structure goes to the opposite way as the guessing before. The eigen period data comes from the upper Y directional strain oscillation period. The only explanation for this is that the thickness of the plate will change the stiffness and the mass together, which can not speculation only based on the mass change. For the impulse, thicker plate structure will have more impulse than the thinner one.

4.2.5 Comparison Between ALE Calculation and SDOF Analogy

In this section, two SDOF methods would be used to calculate the response of the structure. Both of the two methods assume the load is a triangular load without the rise time. Except this,

Table 4.17: Comparison of the Parameters at peak deflection level between different plate thickness models

Thickness	Max V-M stress	ω_{max}	$t_{\omega_{max}}$	t_d	T_n	t_d/T_n	F_{max}	Impulse
16mm	690 Mpa	141.5 mm	12 ms	19 ms	11 ms	1.73	1.83 MN	0.0331 Mpa s
12mm	710 Mpa	152.7 mm	11 ms	20 ms	13 ms	1.54	1.66 MN	0.0316 Mpa s
20mm	714 Mpa	131.1 mm	12.5 ms	20 ms	7ms	2.86	1.84 MN	0.035 Mpa s

the fourth-order Runge-Kutta method also assumes the sinusoid load profile. The equivalent load amplitude has already computed in the section before and shows in the table 4.17. The Biggs chart method is to check the standard chart in figure 4.34 to obtain the dynamic response in a specific loading. While the fourth-order Runge-Kutta Method is to use numerical integration method to calculate the dynamic response, the Matlab code for the fourth-order Runge-Kutta Method shows in Appendix.

1. Elasto-plastic Response Calculation by Biggs Charts

All the inputs information of Biggs chart are introduced in the table 4.18. Most data comes from the table 4.17 and some information e.g. k_3 is from table 4.12 and section 4.1.5. By using the parameter in the table 4.18 and check the chart 4.34, responses are marked with different colourful dot in the same chart. The results are shown in table 4.19.

Table 4.18: Inputs of Biggs chart calculation

Thickness	ω_{el}	R_{el}	F_{max}	R_{el}/F_{max}	k_3
16mm	12.5 mm	1.5 MN	1.83 MN	0.82	$k3 = 0.1k_1$
12mm	17.5 mm	1.5 MN	1.66 MN	0.90	$k3 = 0.1 - 0.2k_1$
20mm	15 mm	1.7 MN	1.84 MN	0.92	$k3 = 0.1k_1$

Table 4.19: Plate components dimensions in detail

Plate thickness	y_{max}/y_{el}	y_{el}	ω_{biggs}	ω_{FEA}	Marks in Biggs chart
16mm	11	12.5 mm	137.5 mm	141.5 mm	Red circle
12mm	10.5	17.5 mm	178.5 mm	152.7 mm	Green circle
20mm	10	15 mm	150 mm	131.1 mm	Yellow circle

The result from Biggs chart for 16mm plate thickness underestimate the max lateral deflection, while for the pate thickness 12mm and 20mmm, it overestimates the deformation results. The error is not such low. The potential reasons for the discrepancy are the data from the static
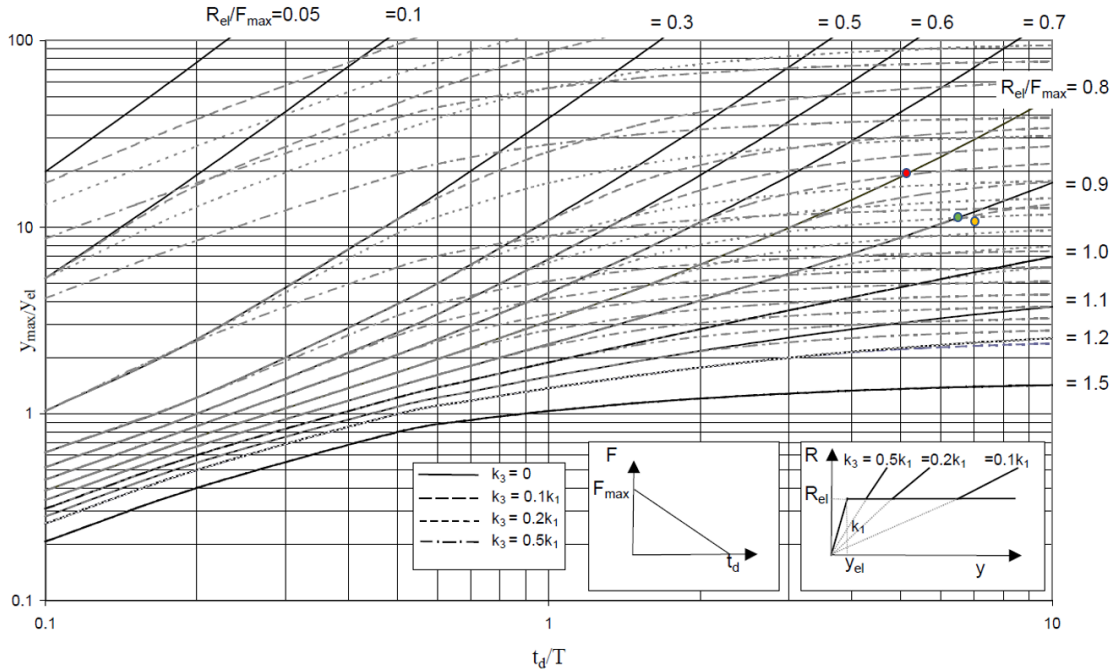
Figure 4.34: Biggs chart response calculation plot (Referenced from [3])

analysis has a higher level of error. Because the elastic deformation and the elastic load is observing by eye from the resistance curve, it may induce a significant error to some extent.

2. Elastic Response Calculation by Numerical Calculation in Fourth-order Runge-Kutta Method

In this section, the 4th order Runge-Kutta integration method would be used to calculate the dynamic response. The theory of this method is already introduced in section 2.3.9. The integration code is written by Matlab. The elastic max force could be calculated from the impulse in table 4.15. Also, the t_d is from the same table. Generalized mass and stiffness from table 4.13 and 4.14. t_{max} is equal to the calculation time in ALE calculation.

Figure 4.35 shows the two kinds of load profile with the same max load amplitude of F_{max}. Figure 4.36 shows the response compared with the ALE elastic drop test. The triangular load response has a more massive maximal displacement than the sinusoid load case. Nevertheless, both of them underestimate the maximal elastic deflection in ALE calculation. As for the natural period, both of the cases underestimate the natural period of the structure. These errors may come from the SDOF parameters calculation error. The sinusoid load shape simulates the natural period well than the triangular shape load. Both of them have a relatively accurate
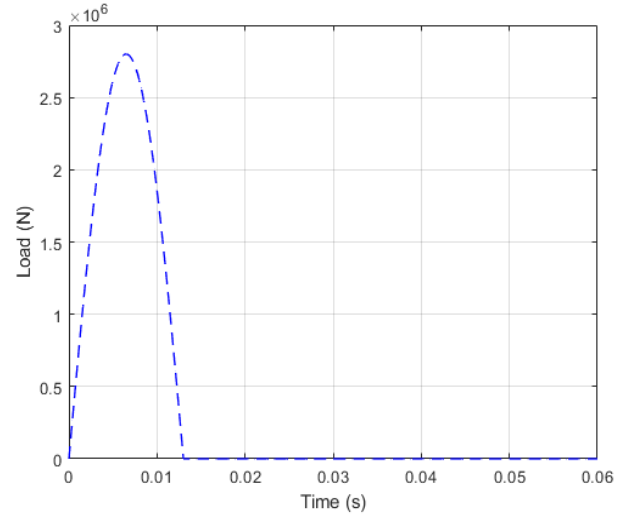
66

result in calculating the oscillation amplitude.

Table 4.20: Comparison between dynamic response from Biggs chart method and ALE drop tests

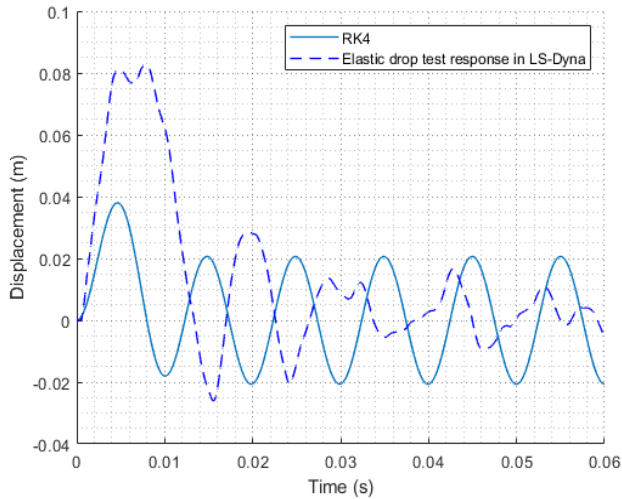| $\overline{m}$	$\overline{k}$	Step length(h)	F_{max}	t_d	Duration of analysis
0.307t	120 MN/m	1e-4 s	2.8 MN	13 ms	60 ms
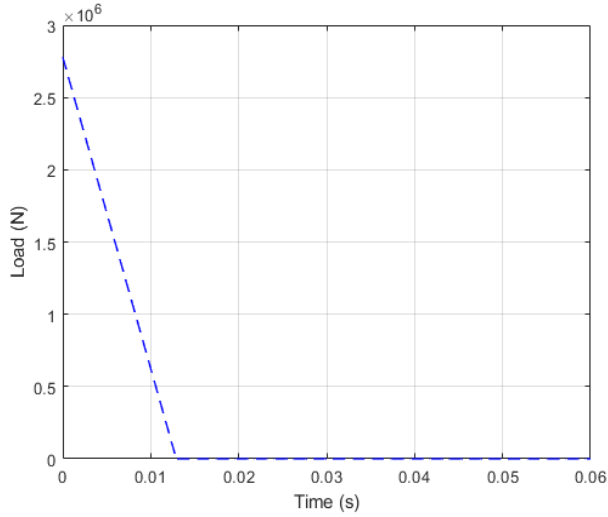
(a) Triangular load profile in 4th order R-K method
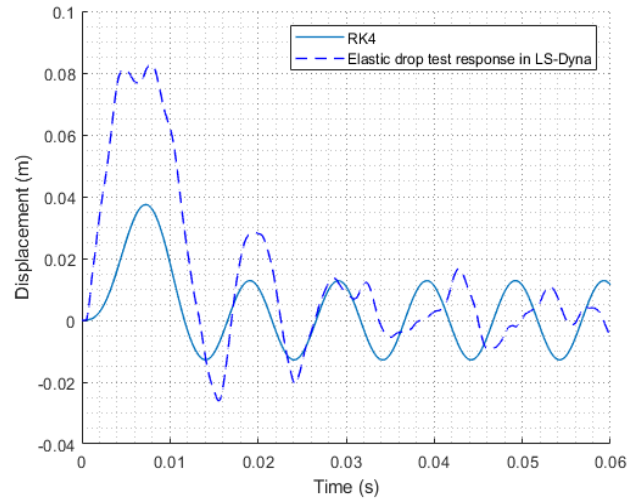

(b) Sinusoid load profile in 4th order R-K method

Figure 4.35: Loads profiles by using 4th order Runge-Kutta integration method

(a) Comparison between elastic response by using 4th order R-K method with triangular load and ALE drop test (impact velocity:$20m/s$, plate thickness:16mm, material: 1)

(b) Comparison between elastic response by using 4th order R-K method with triangular load and ALE drop test (impact velocity:$20m/s$, plate thickness:16mm, material: 1)

Figure 4.36: Responses by using 4th order Runge-Kutta integration method

67

4.3 ALE Test comparison for Different FSI Output Interval

During the calculation of the drop test, the extremely high initial peak pressure always occurs in the results. Efforts are made to find the reason of it in order to help other researchers to deal with the problem in the future, though the peak pressure is not very crucial for the structural response, and the high peak pressure may come from the numerical error in LS-Dyna.

A keyword in LS-Dyna called 'DATABASE_FSI' was found to have a relation with the peak pressure amplitude. This keyword is responsible for setting the output interval of the fluid-structure interaction information. This output interval is called DT in this thesis. Several drop tests with different DT in Mat-2, velocity=20m/s, plate thickness=16mm are made to evaluate the effect of this coefficient on the peak pressure. Figure 4.37 gives the pressure-time series in different DT. From the plot, the tests seem to show consistency results in all of time-domain globally except the initial stage—nevertheless, the local fluctuation which is hard to observe in detail from this plot. Integration has to be made to obtain the impulse of these tests.
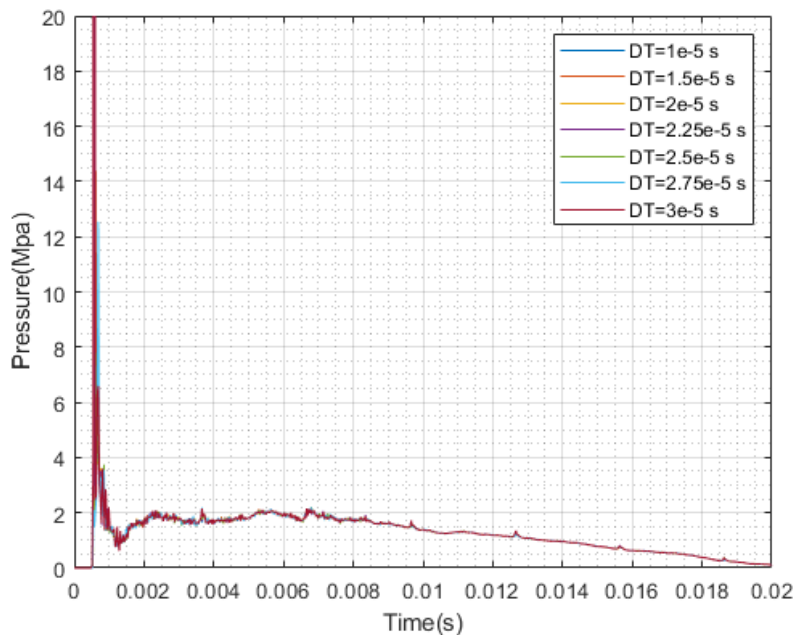

Figure 4.37: Pressure-time series of tests with different DT values

In figure 4.38, different impulses are plotted separately with different DTs. The series is divided into two parts. The first one is the peak part, which corresponds to the small triangular impulse in the initial stage in figure 4.37. The length of the right-angle side of this triangular is very long, which is equal to the peak pressure value. The impulse value in this triangular is not so

high, but can not be neglected. The other part is the constant impulse or rectangular impulse mentioned in the section before. The impulse value in this domain is relatively larger. This part will continue until the t_d. Figure 4.38 demonstrates the impulse value of two different divided parts in different DTs. Average and sum of impulse values are also calculated to show in the same figure. The results show that the rectangular impulse dominates the total impulse in the impact process. Tests with different DTs gives a relatively different impulse, but errors in the integration still need to be considered. It is proved that even the peak pressure is extremely high, the impulse for the first divided part is limited, and the sum of the total impulse is similar in different DT cases.
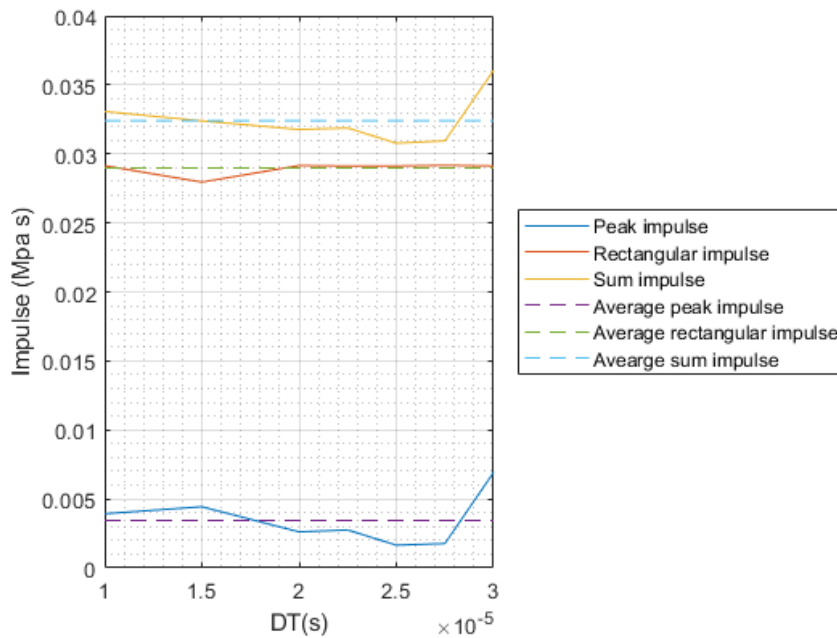

Figure 4.38: Impulse analysis of the tests with different DT values

Figure 4.39 gives the peak pressure of the tests with different DTs. The results show when DT is lower than 1.5e-5 s or higher than 2.75 e-s s, the peak pressure has no relation with this DT value and the pressure value itself could be up to 172 Mpa, which is far more extensive than the acoustic pressure. The acoustic pressure in the same test is around 30.7 Mpa, which is the theoretical maximal value for the presser peak. However, inside this DT range, a minimal value of peak pressure is found between 2.4e-5s and 2.6e-5s.
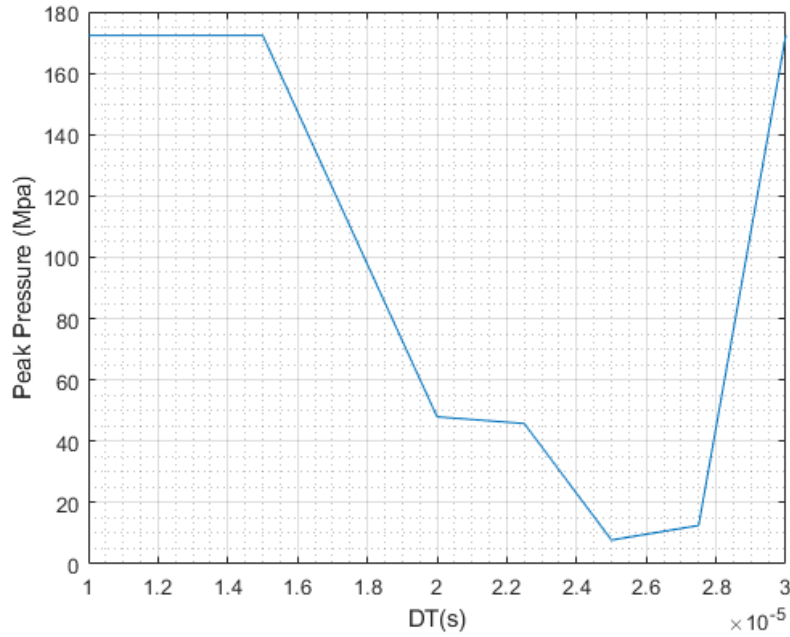
Figure 4.39: Peak pressure value of tests with different DT values

4.4 Dynamic Tests of Steel Column in Explicit Method

The objective of the dynamic analysis in this thesis :

1. Calculate the dynamic response of the structure under the pressure variation load from ALE drop tests.

2. Analyse the possibility to use the dynamic results from the impulse of ALE drop tests to approximate ALE drop test results.

In this section, several dynamic tests in LS-Dyna are conducted under the pressure loading outputted from ALE drop tests in different materials. Before that, a depiction of the pressure-time variation series from ALE drop tests needs to be done. Data fitting of the pressure curve in limited data points are done in Matlab in the purpose to input into LS-Dyna dynamic analysis program conveniently. Two main kinds of material, Mat-1 (elastic material) and Mat-2 (Elasto-plastic material) are used in the structure of dynamic analysis. Two kinds of pressure time variation series from the ALE drop tests in section 4.2.2 are also used. One of the pressure-time variation series is the elastic material ALE drop tests in figure 4.29 (impact velocity:$20m/s$, plate thickness:16mm, material: 1). The other pressure time variation series comes from the elasto-plastic material drop tests from the same figure (impact velocity:$20m/s$,

70

plate thickness:16mm, material: 2). Due to the convenience to use the elastic material in any kinds of the analysis, parameters related to the elasto-plastic material could be neglected. It is worthy of discussing the possibility to use the pressure variation series from elastic ALE drop test as load in the dynamic test of the same structure to approximate the results in elasto-plastic ALE drop test. The comparisons with ALE elasto-plastic drop test and analytical model are also plotted in figures below. Zhaolong. Yu provides the analytical model of the ALE test for comparison reason, which is the same analytical model in paper [8] and [29].

4.4.1 Data Fitting of the Pressure Variation Series from ALE Drop Tests

Data fitting is conducted in the Matlab. From the output of LS-Dyna, a pressure time variation series has at least 5000 sets of data totally. It is hard to input all the data points into the LS-Dyna again to conduct the dynamic analysis. A code in Matlab is created to choose one data from a group of continuous data as representative. Then the data number of the pressure-time variation series decreases from 5000 to round 50. Figure 4.40 illustrates the fitting pressure series and the true pressure series together. The red line represents the fitting data series, and the blue line is the original true pressure data series. The difference between the impulse of the fitting series and the true series is minimal, which explains the fitting data series could replace the true series as an input for the following dynamic analysis.
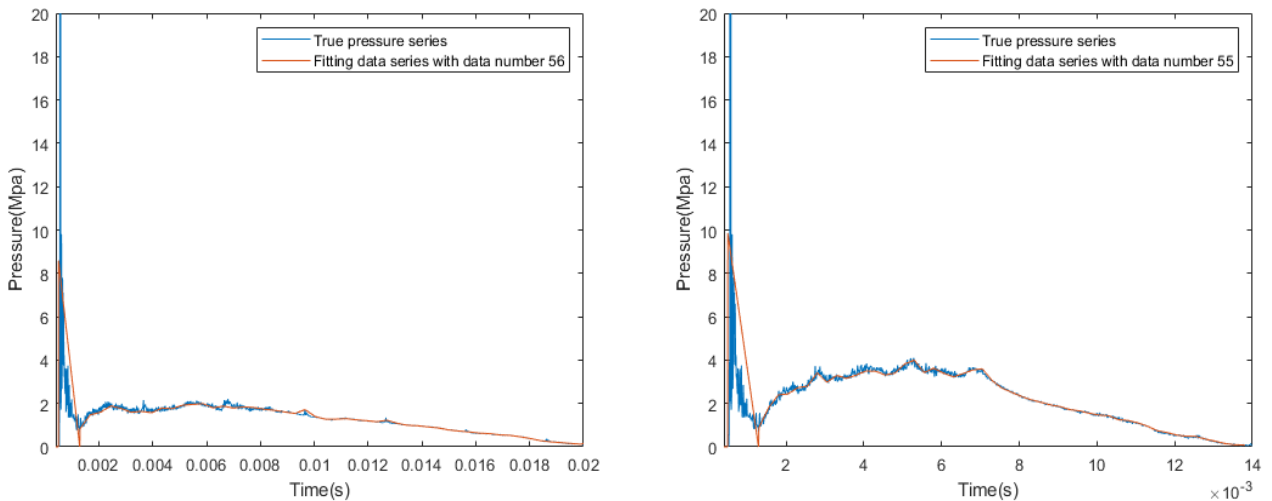
(a) Pressure comparison between true pressure series in elasto-plastic drop test and fitting data series

(b) Pressure comparison between true pressure series in elastic drop test and fitting data series

Figure 4.40: Pressure comparison between true pressure series and fitting data series

71

4.4.2   Elasto-plastic Material Dynamic Test

Figure 4.41 shows all the dynamic analysis results of elasto-plastic material (Mat-2) with different pressure inputs.

A. Input from Pressure Time Series of Elasto-plastic ALE Calculation

In the figure 4.41a, the dynamic results under the pressure in figure 4.40a is shown. Table 4.24 makes a detailed conclusion of the information on the plots. All three results show good consistency in the displacement developing stage. Because the pressure-time variation series also comes from the elasto-plastic ALE drop test. Analytically, it should have the same displacement curve in both the dynamic test and the ALE drop tests. Due to the displacement from the ALE drop test is caused by the pressure time series of the same test, and the dynamic test uses the same pressure-time variation series as load. Also, the structure is elasto-plastic as well. Both the ALE drop test and the dynamic test give the dynamic response under a given load. So it should get the same response. However, the displacement in dynamic test attains to the peak earlier than the ALE drop test. This phenomenon probably because of the interaction between the fluid and the structure. Also, in the oscillation domain, the dynamic test results own a longer oscillation period than the ALE test. No added mass is considered in the dynamic test. This result explains that the added mass is a kind of pressure interacting with the structure. In dynamic tests, no added mass is needed if a pressure variation series is applied and this series comes from ALE tests. The oscillation amplitude in the ALE test is more than the dynamic test. The reason may also come from the fluid interaction problem.

Table 4.21: Comparison of the Parameters between the Dynamic Analysis and ALE drop Test (Case A)

Analysis	Max displacement	$t_{\omega max}$	Oscillation average level	Oscillation period	Oscillation amplitude
Dynamic test	137 mm	9 ms	100 mm	12 ms	5mm
ALE drop test	141.5 mm	12 ms	105 mm	8 ms	10mm

B. Input from the pressure time series of elastic ALE calculation

From the figure 4.41b, the dynamic results under the pressure in figure 4.40b is visualized. Table 4.25 makes a detailed conclusion of the information on the plots. When the elastic pressure time series as input, the dynamic test will give a total divergence from the ALE drop test. The maximal lateral deflection and the average oscillation level are extremely high in the results

of the dynamic tests, which may because when the structure interacts with the fluid in the ALE drop test, the part of the energy absorbed by the fluid is different from the energy in elasto-plastic ALE dro tests. In the dynamic test, no fluid takes part in the calculation. However, all of the FSI information contains in the pressure series. Different material properties would change the structural response of the structure with time. At the same time, the structural response would have an interaction with the fluid and try to alter the pressure field itself. That also explains why different material tests own different oscillation periods. The pressure from the ALE test could store much information between the structure and the fluid. If we directly load it on the elasto-plastic structure with elastic pressure series, all elastic FSI would be subjected to the structure which finally changes the response from the ALE elasto-plastic tests. This idea could also explain a longer oscillation period in results of dynamic tests. The oscillation amplitude is like the stored elastic energy. Dynamic test from elastic pressure series shows a larger oscillation amplitude than ALE drop test, which means the structure has to sustain the difference of FSI state between elasto-plastic material -fluid and elastic material-fluid cases. From the pressure aspect, as mentioned before, the pressure series of elastic ALE drop test has a higher rectangular pressure level and lower duration time of the impact than elasto-plastic ALE case. Focused pressure load would lead to higher max lateral deflection in dynamic result in figure 4.41b than dynamic result in figure 4.41a.

Table 4.22: Comparison of the parameters between the dynamic analysis and the ALE drop test (Case B)

Analysis	Max displacement	$t_{\omega max}$	Oscillation average level	Oscillation period	Oscillation amplitude
Dynamic test	283 mm	13 ms	220 mm	14 ms	40mm
ALE drop test	141.5 mm	12 ms	105 mm	8 ms	10mm

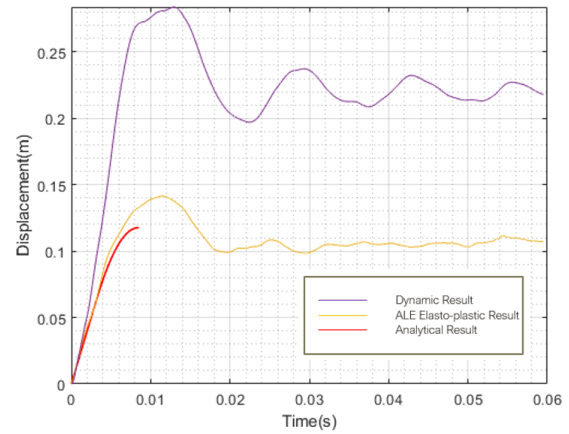## C. Input from Pressure Time Series of Elastic ALE Calculation (3 times density in dynamic test)

Figure 4.41c and table 4.23 give a detailed observation for the dynamic results under the pressure in figure 4.40b. The difference from the 4.41b is to add two times density in the dynamic test to account for the added mass in the ALE drop test. However, this procedure has been proved not valid even if it has a relatively good approximation of the deflection in the oscillation domain. The oscillation period is even longer than in the first two cases.

Table 4.23: Comparison of the Parameters between the Dynamic Analysis and ALE drop Test (Case C)
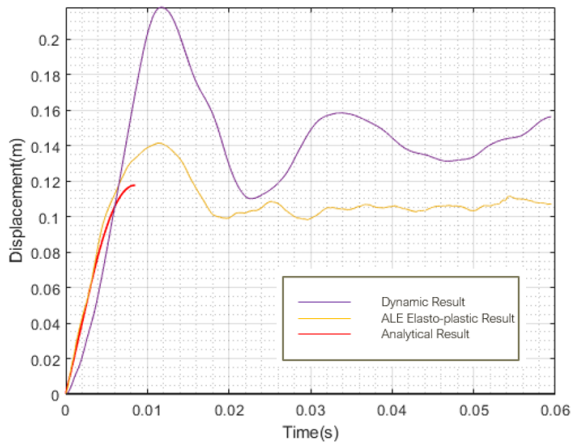
Analysis	Max displacement	$t_{\omega max}$	Oscillation average level	Oscillation period	Oscillation amplitude
Dynamic test	218 mm	12 ms	140 mm	15 ms	50mm
ALE drop test	141.5 mm	12 ms	105 mm	8 ms	10mm
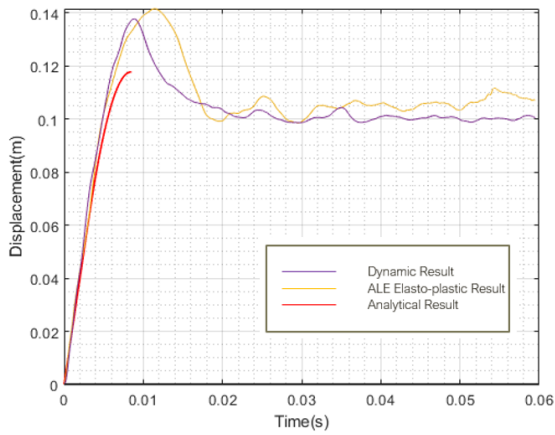
(a) Input from pressure time series of elasto-plastic ALE calculation

(b) Input from pressure time series of elastic ALE calculation

(c) Input from pressure time series of elastic ALE calculation (3 times density in dynamic test)

Figure 4.41: Elasto-plastic material dynamic tests

4.4.3 Elastic Material Dynamic Test

Figure 4.42 shows all the dynamic analysis results of elastic material (Mat-1) with different pressure inputs. All dynamic tests of elastic material give a displacement curve that would

finally oscillate along with the zero level deflection, even if the pressure loads are from the elasto-plastic ALE drop tests. This phenomenon could be easily seen in figure 4.42a. None of the elastic material dynamic test could approximate the elasto-plastic ALE drop tests in oscillation domain. Nevertheless, case E compared with other cases could approximate the ALE elasto-plastic test results more accurately in the first deflection developing stage.

D. Input from Pressure Time Series of Elasto-plastic ALE Calculation

Table 4.24: Comparison of the Parameters between the dynamic analysis and ALE drop test (Case D)

| Analysis	Max displacement	$t_{\omega max}$	Oscillation average level	Oscillation period	Oscillation amplitude
Dynamic test	60mm	4 ms	0 mm	4 ms	17mm
ALE drop test	141.5 mm	12 ms	105 mm	8 ms	10mm

E. Input from Pressure Time Series of Elastic ALE Calculation

Table 4.25: Comparison of the parameters between the dynamic analysis and ALE drop test (Case E)

Analysis	Max displacement	$t_{\omega max}$	Oscillation average level	Oscillation period	Oscillation amplitude
Dynamic test	95 mm	5 ms	0 mm	6 ms	12mm
ALE drop test	141.5 mm	12 ms	105 mm	8 ms	10mm
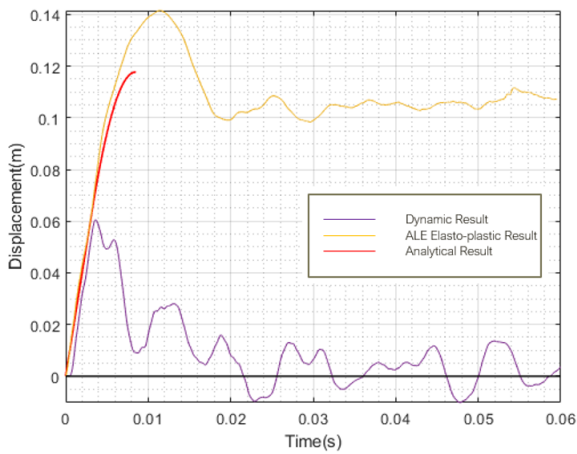
(a) Input from pressure time series of elasto-plastic ALE calculation
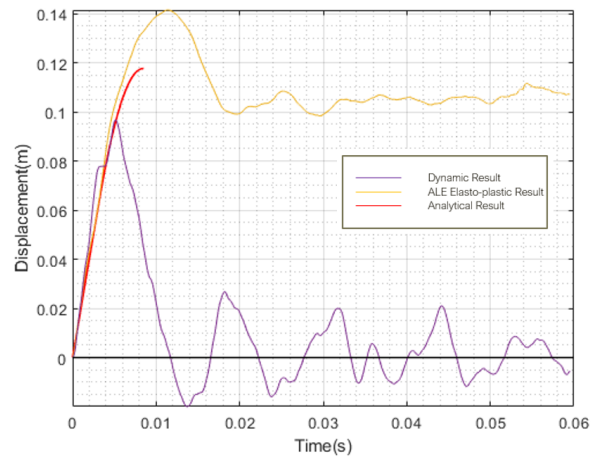
(b) Input from pressure time series of elastic ALE calculation

Figure 4.42: Elastic material dynamic testS

5   Discussion

Several impressive results are of worth to be discussed in detail to find the fundamental reasons and possibilities. Finally, six topics are picked out to be explained further.

5.1   BCs Effects on the Structure

As indicated in section 4.1.1, boundary conditions on the rear end is not crucial for the resistance of the steel column. However, the resistance curve is plotted with the max displacement against the external load. We can not say the static response of the whole structure would be same in different BCs. Actually, the distribution of stress and strain is very different among BCs. When the external pressure is up to 1.1 Mpa (the structure enters into fully plastic range), the max von-mises stress could be smaller for the deck boundary with fixed all rotational dofs and translational dofs in x and y direction than the free deck boundary or fix z-direction dof. The difference is huge. Nevertheless, these difference is smaller when the structure is subjected to the load in the elastic range. The utilisation of the side plate is also different between the two kinds of BCs in the elastic range. It seems the structure with rotational deck BCs and translational BCs in x and y direction could distribute the load evenly on the whole stiffened side plate than without this BCs. To some extent, that is the reason why the structure with this strong BCs on deck could take more external loads and have smaller Von-mises stress in the same external load level. In contrast, in the longitudinal BCs, the opposite results will get. Within the elastic range, the free end or BCs only set z-direction dof on the longitudinal end will lead to lower Von-mises stress and seem to exploit the plate better. However, free the longitudinal end is not a good idea, which will also cause an extremely high effective stress in the plastic domain.

The boundary conditions in the ALE calculation is slightly different from the dynamic analysis and the static analysis. The reasons are that the impact type is different. Usually, the pressure load will be set on the side plate in static and dynamic analysis in order to simulate the slamming water impact. While in ALE calculation, the structure has to move to give an impact of the fluid, which means we can not set any BCs on the impact direction (z-direction in this thesis). Nevertheless, even if the BCs on the rear end is not important for the resistance curve, it will affect the stress-strain distribution in the structure. Setting the z-direction translational BC on the longitudinal end of the structure would increase the structure capability to some extent.

5.2 Effects Material Model on Structural Response

In section 4.2.2, strain rate hardening effect is discussed by observing the figure 4.28. The model with strain rate hardening (Mat-2) has a relatively higher peak than the case without strain hardening (Mat-3). It explains that the strain rate hardening effect would strengthen the structure stiffness. The maximal lateral deflection is 141.5 mm for Mat-2 and 156 mm for Mat-3. In [27], the resistance curves of different materials are calculated, which draws a similar conclusion. Material with strain rate hardening would give a larger elasto-plastic stiffness than the same material without strain rate hardening effects. By comparison with the analytical model, the ALE test for Mat-2 in figure 4.27 overestimate the maximal deflection than the analytical one. The analytical model gives 120 mm as the peak displacement. Strain hardening effects shall be considered in material properties in ALE drop tests in order to give a similar result as the analytical model. In the same comparison plot with various of materials, Mat-4 and Mat-5 give very consistent results of the max lateral deflection curves, while the two materials are different in both the power-law parameters and the strain rate hardening effects. The most possible explanation is this two kinds parameters counteract the effect of each other. Further, the difference between different elasto-plastic material is huge, even if the difference of the material model parameters are small. These results mention the researchers to choose the right material model type and always calibrate the material model parameters before doing the simulation.

5.3 Elastic Recovery Phenomenon during the Impact

In section 4.2.1, a description of the process for the max lateral deflection to develop is introduced with figure 4.25. In this figure, the deflection would decrease to a constant level and starts to oscillate after it attains to the peak value. In this thesis, this phenomenon is called elastic recovery. Obviously, due to the elasto-plastic material properties, the constant oscillation level is referred to as the permanent plastic deflection. Plastic deflection could not be set free in the whole slamming impact process, and it would always accumulate as long as the external load keeps increasing. This kind of resilience could be only caused by the recovery of elastic energy. The time for this recovery in the same displacement plot is from 11 ms to 20 ms. In 4.26, the external pressure starts to decrease from 7 ms, which is much earlier than 11 ms. However,

after around 20 ms, it indeed goes to the zero pressure level, which also explains the plastic deflection will not change after 20 ms. The peak deflection is obtained at time 11 ms when the pressure already falls halfway to zero. The same conclusion could also be found in the elastic material. In figure 4.28, the blue curve has a peak of around 8 ms, which corresponds to the middle point of the decreasing blue line in pressure plot 4.29. Nevertheless, at this time point, the maximal impulse is not attained. The only explanation is from the impact start, the system would absorb energy to transform the external energy from the pressure to the plastic and elastic energy inside. The recovery phenomenon occurs at every time in the whole impact process. When the speed of recovery is equal to the speed of the input energy, the maximal deflection will attain. After that, the recovery speed would be larger than the input, then the displacement decrease until all of the elastic energy is set free.

5.4 Error Source in SDOF method

In section 4.2.5, two SDOF methods are used for predicting the dynamic response of the structure with the simplified load profile. The difference of maximal lateral deflection between the ALE drop test and Biggs chart method is relatively considerable. Mostly, the Biggs chart method overestimates the peak deflection for elasto-plastic material 4.20. While by using fourth-order Runge- Kutta method, calculated elastic dynamic response underestimates both the response and oscillation period in ALE drop tests 4.36. The input for the SDOF method comes from the impulse ALE drop test. This error may come from the calibration of the elastic stiffness in static resistance curve plot and the formula to calculate added mass analytically. The resistance curve of the structure is calculated by the explicit method in LS-Dyna. Some local oscillations could be found in the resistance curve. These oscillations may be from the step length is too high in the explicit method. Commonly, the implicit method should be adopted for the resistance curves. The explicit method would introduce some numerical error accordingly. Also, the calculation of the max load by using the impulse and duration of impact would also induce some errors. It is difficult to define how long the impact would last, due to there is always a small level of pressure exist through all of the calculation time. Especially for the elasto-plastic case, the pressure would decrease with such a gentle slope that the impulse of the drop test is hard to calculated by the numerical integration accurately. An unavoidable numerical error would take part in as well.

5.5   Characteristic of Maximal Von-mises Stress in Drop Tests

In all of the parametric study in the result chapter, the maximal Von-mises stress at the max displacement time point is summarised by the table for each drop tests. It is worthy of knowing what would happen with the maximal Von-mises stress when the structure attains to the maximal deflection. An interesting result is the maximal Von-Mises stress would also oscillate in both the linear developing stage and the oscillation stage of the displacement curve. It is reasonable to some extent because the maximal Von-mises stress would always change the position in the structure. The maximal displacement is only a history plot for just one point. If the Von-mises stress is plotted with the time only at one point of the structure, the same results as the displacement curve will get. This change of position of the maximal phenomenon is more like a strategy for the structure to adapt to different loadings. From the description of the response process, different components would play the primary role when resist the external load at different time points. At the start of the impact, maybe the plates are the most vulnerable components in the structure. The stiffeners, girders and bulkhead would give the plate full support in the initial stage. When the plates deform to a certain extent, the stiffeners and bulkhead will take part in to deform together, which would play the most crucial role in sustaining the pressure. Then it is very reasonable to get the maximal Von-mises stress at a different location. Furthermore, the oscillation may come from the recovery of the elastic deformation mentioned before.

5.6   Possibility Using Dynamic Tests to Approximate the Results in Elasto-plastic ALE Drop Test

In the last section of the result chapter, dynamic analysis has been conducted in order to find the possibility of using the elastic information to approximate the result in the elasto-plastic ALE drop test. The analysis proved the application of extra added mass is meaningless in the dynamic analysis when the input comes from the pressure-time variation series. The reasons are explained very shortly in the result prat. However, it needs to be analysed in detail here. Due to the fluid is simulated to have an impact on the structure in the ALE test, the interaction between fluid and structure would occur, which lead to the deformation of the structures when we apply the outputted pressure variation series from the ALE drop test. A higher oscillation

period than the ALE test would be observed, which shows the pressure series already contains the information of the added mass. The added mass is indeed a pressure field related to FSI phenomenon. The name is just because it has the same phase with the acceleration of the object. If someone wants to use pressure series from ALE elastic test as load in dynamic analysis to approximate the elasto-plastic FSI results. One thing that needs to declare first is the meaning of the pressure. From figure 4.41, the dynamic tests always give out a higher displacement level than ALE drop test if the elastic pressure series is adopted. The elastic pressure series contains the information of the added mass and the deformation of the elastic structure in ALE model implicitly. When this information enters into the elasto-plastic dynamic test, correction shall be made with the pressure theory in order to obtain a consistent result with the ALE elasto-plastic drop tests. The recommended work would be introduced in the next section.

6 Conclusion and Recommendations for Further Work

6.1 Conclusion

In this thesis, a steel column model is established to prepare for the numerical analysis in LS-Dyna. Static analysis is conducted first to evaluate the boundary effects on the resistance curve of the steel column. It is proved that the rear end boundary condition does not affect the resistance curve of the steel column. Then different resistance curves of different plate thickness model are plotted to find SDOF parameters, e.g. elastic stiffness, added mass.

By applying the ALE drop test, the whole process of slamming events have been analysed with a typical case. The displacement curve of the typical case shows very good consistency with the analytical model, which proved the validity of the model and the method. Through the whole impact process, the stiffeners deform first and the bulkhead following, the side plate girders give the plate and stiffeners strong support and almost unreformed during the whole impact process.

Three group parametric studies have been made to evaluate the effect of material properties, velocities, and plate thickness on the response of the structures. SDOF method is also established by using the parameters from static analysis. Comparison between the SDOF method and ALE methods shows a feasible approximation by using the SDOF method to predict ALE drop test results.

Finally, dynamic tests are made trying to find the possibility to use the elastic material result to predict the response of elasto-plastic material. It is proved the pressure series from elastic ALE drop test need to be corrected from elastic FSI information to elasto-plastic information for the dynamic test to get a good prediction of the elasto-plastic ALE tests.

6.2 Recommendations for Further Work

There are several aspects in the thesis could be improved to make a deeper investigation for the procedure of prediction for the slamming response, methods to avoid numerical errors in LS-Dyna, and the possibility to use the elastic analysis information as input to approximation elasto-plastic analysis.

6.2.1 Static Analysis of Implicit Method in LS-Dyna

In this thesis, the explicit method is used for the static analysis. The advantage of this method is undeniable. For short time analysis, the explicit method could avoid the converge problem in the implicit method to speed up the calculation and prevent the failure of calculation because of the same problem. However, the disadvantage is it can not ensure all the time step is in the equilibrium. The local oscillation from the resistance curve in section 4.1 may come from this. In order to overcome this, an implicit static analysis could be tried in static analysis. Even if it takes time to adjust the parameters in LS-Dyna implicit method environment, this work is worthy of being done.

6.2.2 Reasons for the Effect of DT on the Peak Pressure

In section 4.3, the effect of DT on the peak pressure is analysed. However, the reasons are still unknown clearly. DT must have a relation with the FSI data transformation in the ALE method, which would influence the peak pressure. Getting knowing this is a good start point to correct the ALE method for a more accurate prediction.

6.2.3 Methods using Elastic Analysis Information as Input to Predict Elasto-plastic Response

Many discussion in the thesis to argue the method using elastic analysis information as input to approximate elasto-plastic material results in both section 4.4 and section 5.6. However, the work in this thesis related to this part still confines inside discussing. In figure 4.29, the pressure plot shape for all the elasto-plastic materials have a similar shape different from the elastic one. More drop tests need to be done and try to find the relation between the elasto-plastic material pressure series and elastic material pressure series in different structures. The steel column is so massive for this to investigate. 2D plate strip or 3D stiffened plate could be used as the structure in the analysis. The parametric study also needs to be done to evaluate the effects of some factors on the shape of pressure. AI algorithm could be used to establish the connection between the shape of pressure and the material properties. Once the correction could be realized, it would be possible to use the elastic analysis information as input to predict the elasto-plastic response.

References

[1] M. Greco, "Tmr 4215: Sea loads lecture notes." 2019.

[2] O. M. Faltinsen, "Hydrodynamics of high-speed marine vehicles." 2006.

[3] DNV, "Design against accidental loads,dnv-rp-c204." 2010.

[4] N-004, "Design of steel structures." 2004.

[5] AkerSolutions, "Slade input semi hull column design rev03." 2020.

[6] G. Z.-M. Du Y, "Application of the non-contact video gauge on the mechanical properties test for steel cable at elevated temperature." *Applied Sciences*, vol. 9, no. 8, p. 1670, 2019.

[7] DNV, "Design of offshore steel structure, dnv-os-c101." 2015.

[8] M. G. H. X. Zhaolong Yu, Jørgen Amdahl, "Hydro-plastic response of beams and stiffened panels subjected to extreme water slamming at small impact angles, part 1: an analytical solution." *Marine Structures*, 2019.

[9] T. Von Karman, "The impact on seaplane floats during landing." *Technical report*, 1929.

[10] "Über stoß-und gleitvorgänge an der oberfläche von flüssigkeiten."

[11] O. M. Faltinsen, "Water entry of a wedge by hydroelastic orthotropic plate theory." *Journal of Ship Research*, 1999.

[12] DNV, "Prediction of air gap for column stabilised units, dnvgl-otg-13." 2016.

[13] ——, "Horizontal wave impact loads for column stabilised units, dnvgl-otg-14." 2016.

[14] O. M. Faltinsen, "Sea loads on ships and offshore structures." 1944.

[15] J. Newman, "Marine hydrodynamics." *Cambridge(Mass.): MIT Press*, 1977.

[16] J. Chakrabarty, "Theory of plasticity." 2005.

[17] M. Storheim and J. Amdahl, "On the sensitivity to work hardening and strain-rate effects in nonlinear fem analysis of ship collisions." *Ships and Offshore Structures*, 2015.

[18] DNV, "Determination of structural capacity by non-linear fe analysis methods, dnv-rp-c208."

2013.

[19] L. Pakiding, "Design criteria for high strength steel joints." 2007.

[20] J. Cowper and P. Symonds, "Strain-hardening and strain-rate effects in the impact loading of cantilever beams." *Technical report28,Division of Applied Mathematics,Brown University*, 1957.

[21] T. M. Hadi K.K.Amlashi, "Ultimate strength analysis of a bulk carrier hull girder under alternate hold loading condition – a case study: Part 1: Nonlinear finite element modelling and ultimate hull girder capacityk." *Marine structures*, 2008.

[22] S. Sævik, "Course: tmr4305."

[23] C. Larsen, "Tmr4180 marin dynamikk." *Akademika*, 2014.

[24] J.-P. J.Donea, Antonio Huerta and A.Rodriguez-Ferran, "Arbitrary lagrangian-eulerian methods." 2004.

[25] J. P.Kjellgren, "An arbitrary lagrangian-eulerian finite element method." 1998.

[26] LSTC, "Ls-dyna support," *http://www.dynasupport.com/tutorial.*, 2001.

[27] L. Rolland, "Fluid structure interaction analysis of abnormal wave slamming events." *Master's thesis*, 2018.

[28] Y. S. Zhaolong Yu, Jørgen Amdahl, "Large inelastic deformation resistance of stiffened panels subjected to lateral loading." *Marine Structures*, 2018.

[29] M. G. H. X. Zhaolong Yu, Jørgen Amdahl, "Hydro-plastic response of beams and stiffened panels subjected to extreme water slamming at small impact angles, part 2: Numerical verification and analysis." *Marine Structures*, 2019.

Appendix A   Deformation Patterns and Relative Volume Fraction Patterns
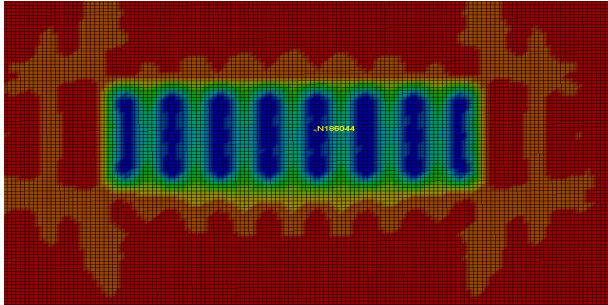
(a) t=3ms
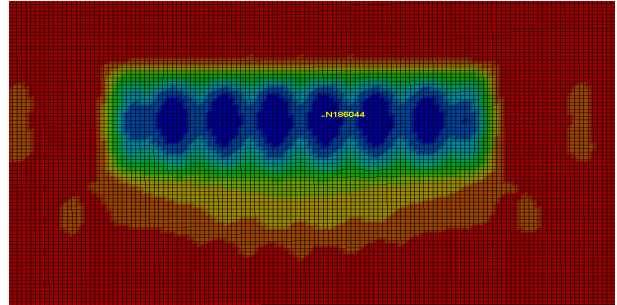
(b) t=4ms
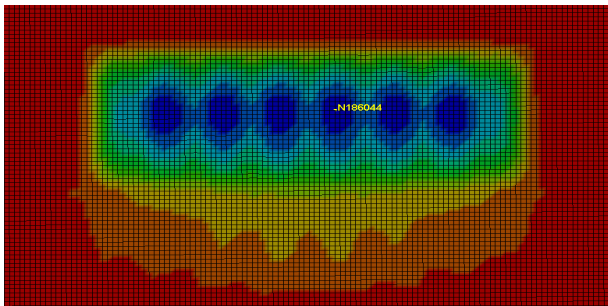
(c) t=5ms
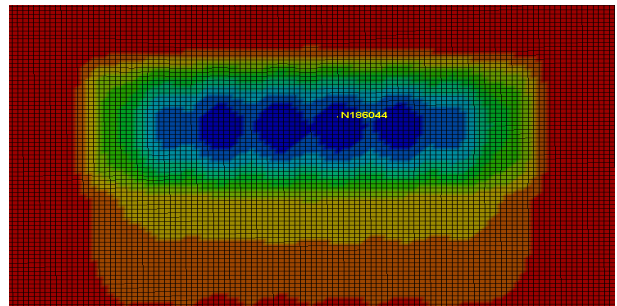
(d) t=10ms
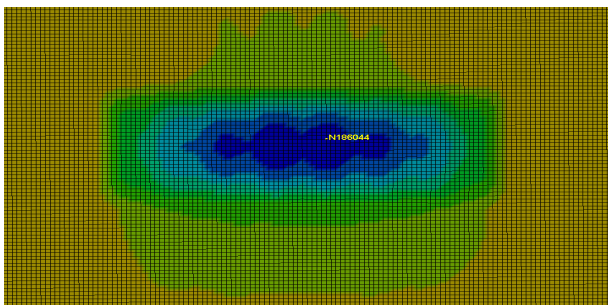
(e) t=13ms
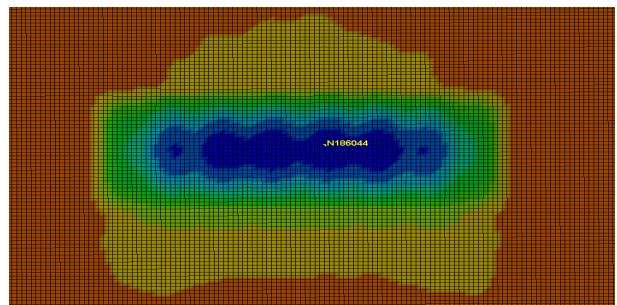
(f) t=17ms
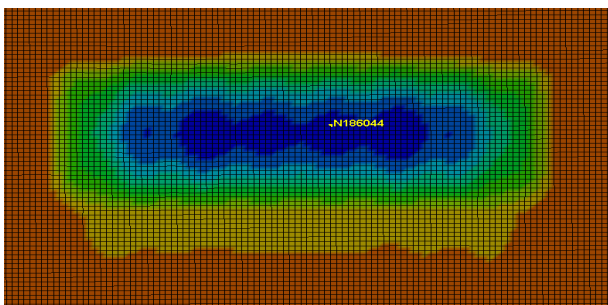
(g) t=18ms
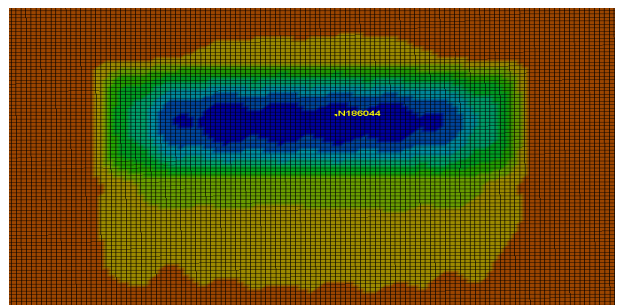
(h) t=20ms

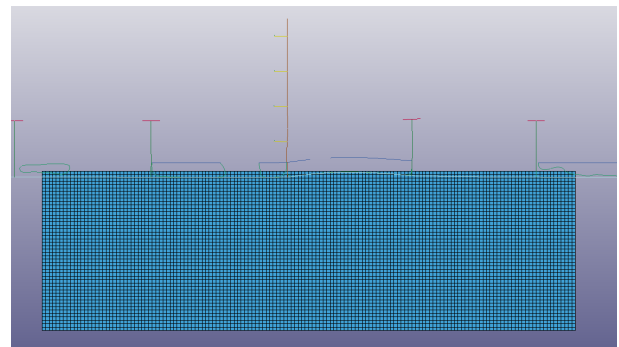Figure A1: Lateral deformation pattern (impact velocity:$20m/s$, plate thickness:16mm, material: 2)
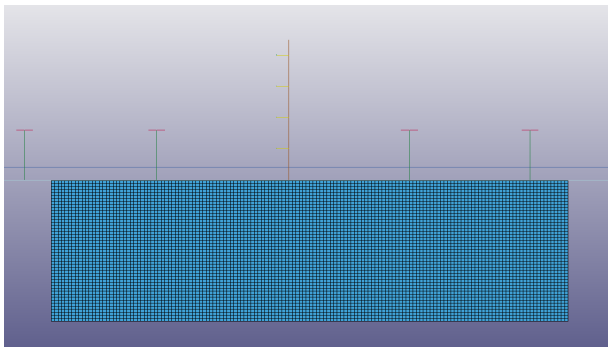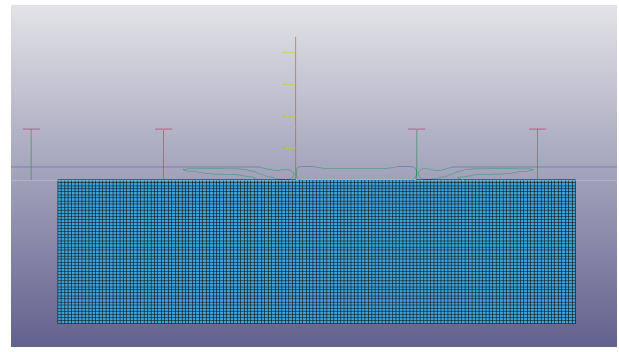
(a) t=0ms

(b) t=1ms
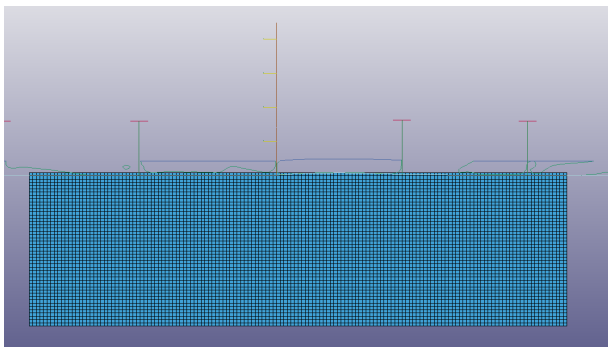
(c) t=3ms

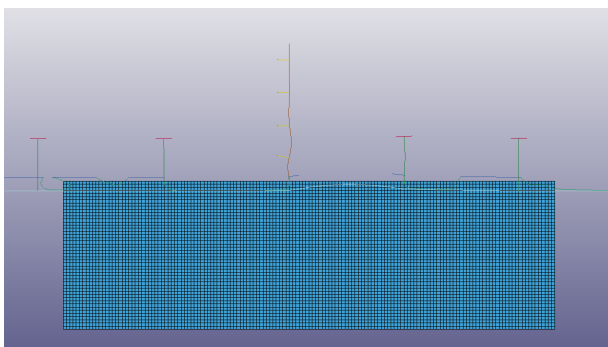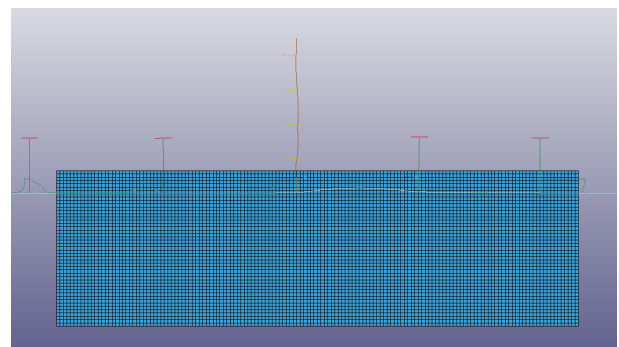(d) t=6ms

(e) t=10ms
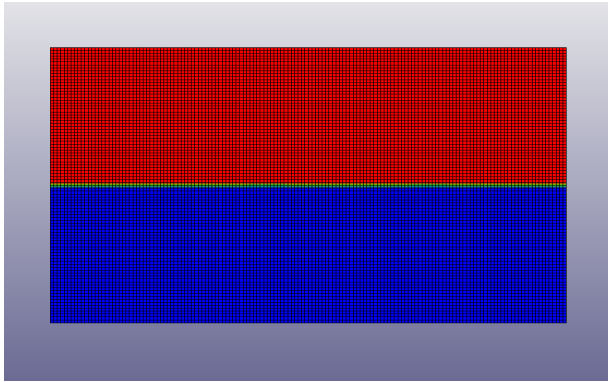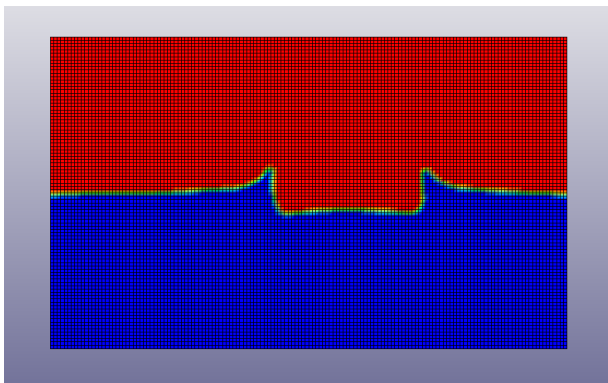
(f) t=21ms
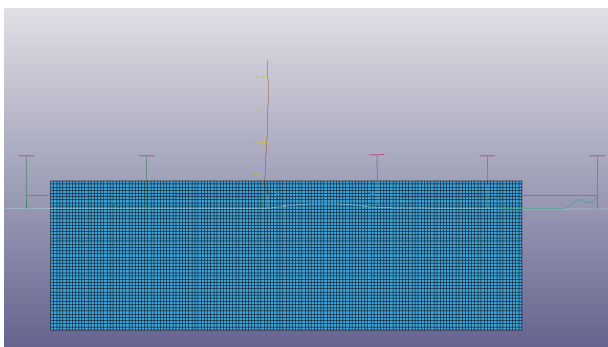
(g) t=27ms
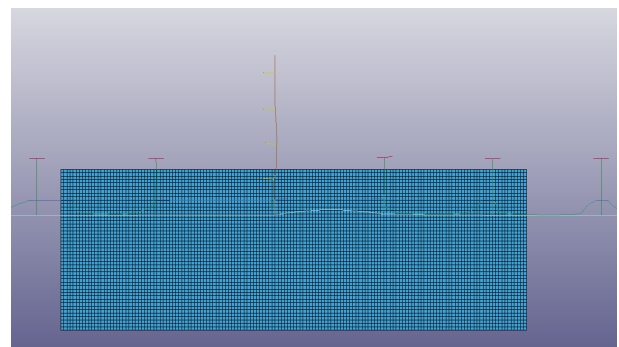
(h) t=41ms

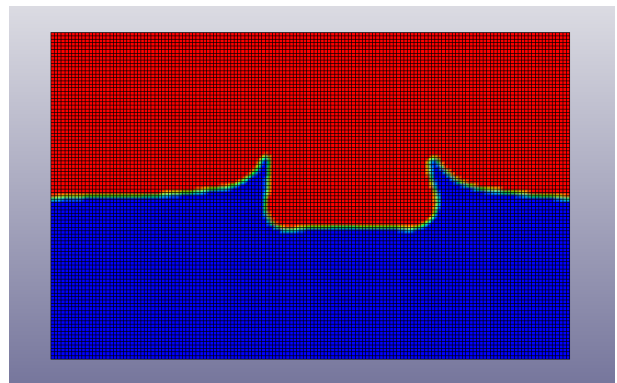Figure A2: Section of deformation pattern (impact velocity:$20m/s$, plate thickness:16mm, material: 2)
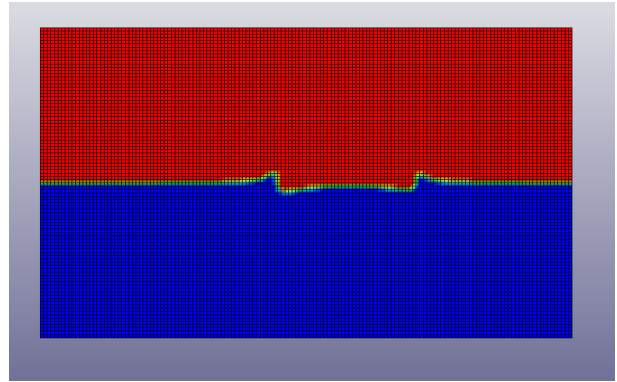
(a) t=0ms   (b) t=10ms

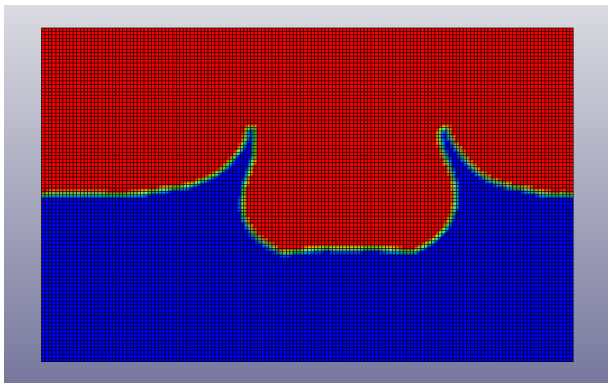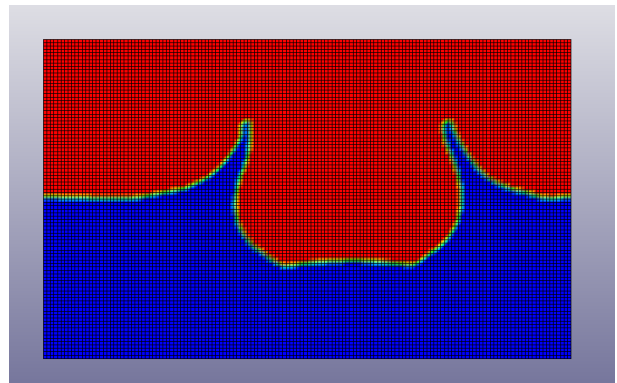(c) t=20ms   (d) t=30ms

(e) t=50ms   (f) t=60ms

Figure A3: Relative volume fraction of the fluid upon impact (impact velocity:$20m/s$, plate thickness:16mm, material: 2)
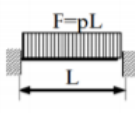
Appendix B Transformation Factor For Beams

Load case	Resist-ance domain	Load Fac-tor K_l	Mass factor K_m		Load-mass factor K_{lm}		Maximum resistance R_{el}	Linear stiffness k_l	Equiva-lent lin-ear stiffness k_e	Dynamic reaction V
			Concen-trated mass	Uniform mass	Con-cen-trated mass	Uniform mass				
F=pL (L)	Elastic	0.53		0.41		0.77	$\frac{12 M_{pn}}{L}$	$\frac{384 EI}{L^3}$	$\left(\frac{307\,EI}{L^3}\right)\cdot m_l$	$0.36R + 0.14F$
	Elasto-plastic bending	0.64		0.50		0.78	$\frac{8(M_{pn}+M_{pm})}{L}$	$\frac{384 EI}{5L^3}$		$0.39R_{el}+0.11F$
	Plastic bending	0.50		0.33		0.66	$\frac{8(M_{pn}+M_{pm})}{L}$	0		$0.38R_{el}+0.12F$
	Plastic mem-brane	0.50		0.33		0.66		$\frac{4N_P}{L}$		$\frac{2N_{p}y_{max}}{L}$

Figure B1: Transformation factors for a clamped beam in SDOF system (Referenced from [3]

Appendix C   Code

1. The Matlab Code of 4th order Runge-Kutta integration method for sinusoid load shape

```
close all
clear all
clc
mdisp5=load('1.txt');
bcdisp5=mdisp5(:,1)*20000;
disp5=(bcdisp5-mdisp5)/1000;



m = 0.307e3;
k = 120e6;
PERIOD=2*pi*sqrt(m/k)



h = 1e-4;
Pmax = 2.8e6;
t1 = 0.013;
% integration parameters
tmax = 0.06;
omega = 2*pi/(2*t1);
T0=2*pi/omega;
t = (0:h:tmax).';
P = zeros(length(t),1);
indt1 = sum(t<=t1);
P(1:indt1) = Pmax*sin(omega*t(1:indt1));
% P(1:indt1) = Pmax-(Pmax/0.013)*(1:indt1)/10000;
```

```
[urk,t]= runge_kutta4(m,k,c,P,t);


figure(1)
ax= gca;
ax.GridLineStyle = ':';
ax.GridAlpha = 0.5;
ax.XGrid = 'on';
ax.YGrid = 'on';
grid minor;
plot(t,P,'b--','LineWidth',1)
xlabel('Time (s)');
ylabel('Load (N)');
xlim([0, 0.06]);
grid on


figure(2)
hold on
ax= gca;
ax.GridLineStyle = ':';
ax.GridAlpha = 0.5;
ax.XGrid = 'on';
ax.YGrid = 'on';
grid minor;

plot(t,urk,mdisp5(:,1),disp5(:,2),'b--','LineWidth',1)
xlabel('Time (s)');
legend('RK4','Elastic drop test response in LS--Dyna','Location', 'NorthEast')
ylabel('Displacement (m)');
xlim([0, 0.06]);
```

grid on

2. The Matlab Code of 4th order Runge-Kutta integration method for triangular load shape

```
close all
clear all
clc
mdisp5=load('1.txt');
bcdisp5=mdisp5(:,1)*20000;
disp5=(bcdisp5-mdisp5)/1000;


m = 0.307e3;
k = 120e6;
PERIOD=2*pi*sqrt(m/k)
h = 1e-4;
Pmax = 2.8e6;
t1 = 0.013;

tmax = 0.06;
omega = 2*pi/(2*t1);
T0=2*pi/omega;
t = (0:h:tmax).';
P = zeros(length(t),1);
indt1 = sum(t<=t1);
% P(1:indt1) = Pmax*sin(omega*t(1:indt1));
P(1:indt1) = Pmax-(Pmax/0.013)*(1:indt1)/10000;


[urk,t]= runge_kutta4(m,k,c,P,t);


figure(1)
```

```matlab
ax= gca;
ax.GridLineStyle = ':';
ax.GridAlpha = 0.5;
ax.XGrid = 'on';
ax.YGrid = 'on';
grid minor;
plot(t,P,'b--','LineWidth',1)
xlabel('Time (s)');
ylabel('Load (N)');
xlim([0, 0.06]);
grid on


figure(2)
hold on
ax= gca;
ax.GridLineStyle = ':';
ax.GridAlpha = 0.5;
ax.XGrid = 'on';
ax.YGrid = 'on';
grid minor;

plot(t,urk,mdisp5(:,1),disp5(:,2),'b--','LineWidth',1)
xlabel('Time (s)');
legend('RK4','Elastic drop test response in LS-Dyna','Location', 'NorthEast')
ylabel('Displacement (m)');
xlim([0, 0.06]);
grid on
```

3. The function of Runge-Kutta integration method

```
function [urk,t] = runge_kutta4(m,k,c,P,t)
h=1e-4;
tt=(1:0.5:length(t));
PP= interp1(P,tt);
A=[0,1;-k/m,-c/m];
I=[0;0];


Load=[zeros(1,length(PP));PP/m];


X=zeros(size(A,1),length(t));


for ii=1:1:size(A,1)
for jj=1:1:size(A,2)
X(ii,1)=I(ii,1);
AA(ii,jj)=A(ii,jj);
end
end


for i=1:(length(t)-1)
Coe=zeros(size(A,1),4);


Coe(:,1)=AA*X(:,i)+Load(:,i*2-1);
Coe(:,2)=AA*(X(:,i)+[h/2*Coe(1,1);h/2*Coe(2,1)])+Load(:,i*2);
Coe(:,3)=AA*(X(:,i)+[h/2*Coe(1,2);h/2*Coe(2,2)])+Load(:,i*2);
Coe(:,4)=AA*(X(:,i)+[h*Coe(1,3);h*Coe(2,3)])+Load(:,(i+1)*2-1);


X(:,i+1)=X(:,i)+h/6*(Coe(:,1)+2*Coe(:,2)+2*Coe(:,3)+Coe(:,4));
urk=X(1,:);
```

```
udrk=X( 2 ,: ) ;
end
```